Supersymmetry Phenomenology in IIB String Theory

by

Kevin Mitchell Givens

B.S., Vanderbilt University, 2006

A thesis submitted to the

Faculty of the Graduate School of the

University of Colorado in partial fulfillment

of the requirements for the degree of

Doctor of Philosophy

Department of Physics

2012

This thesis entitled:
Supersymmetry Phenomenology in IIB String Theory
written by Kevin Mitchell Givens
has been approved for the Department of Physics

Senarath P. de Alwis

Prof. William T. Ford

Prof. Oliver DeWolfe

Prof. K. T. Manhanthappa

Prof. J. Michael Shull

Date

The final copy of this thesis has been examined by the signatories, and we find that both the content and the form meet acceptable presentation standards of scholarly work in the above mentioned discipline.

Givens, Kevin Mitchell (Ph.D., Physics)

Supersymmetry Phenomenology in IIB String Theory

Thesis directed by Prof. Senarath P. de Alwis

IIB string theory represents one of the most promising realizations of string theory studied to date because it successfully handles a variety of phenomenological issues. These issues include mechanisms for stabilizing all relevant moduli fields, generating a small cosmological constant and breaking supersymmetry on a low scale. In this dissertation we examine these issues and describe the phenomenological consequences of a class of realistic IIB models that have the potential to effect both LHC physics and cosmology. In addition, we explore ways to embed interesting physical models, such as the QCD axion, within this class of IIB models.

Dedication

First, I would like to express my sincerest appreciation to my advisor, Shanta de Alwis, for his steadfast support and encouragement throughout the entire course of my dissertation. His wisdom, compassion and genial nature are truly outstanding human traits, traits I can only hope to emulate in my own life.

Second, I would like to thank my parents, Stan and Joyce Givens, for their love and encouragement throughout my entire education. They have gone to great lengths to ensure that all of their children receive excellent educations. These educations rightly deserve to be my parents' greatest legacy.

Finally, I would like to thank my girlfriend Rocio Vargas for her love and support during my years as a graduate student. She has stood by me and helped me to overcome many challenges along the way. Without her love and humor I'm not sure I would have succeeded as a graduate student. Any success I achieve in life belongs to her.

Acknowledgements

- This work was supported in part by the United States Department of Energy under grant DE-FG02-91-ER-40672.
- Most of the papers that constitute this dissertation were directly of indirectly affected by the research of Prof. Howie Baer at the University of Oklahoma. Prof. Baer coauthored papers (chapters) 1 and 2 as well as provided invaluable assistance in papers 3 and 5.
- For paper 2 we thank Yuri Gershtein of Rutgers University for discussions.
- For paper 4 we thank James Gray of the Arnold Sommerfield Center for Theoretical Physics for correspondence concerning the STRINGVACUA program.

Contents

Tables

Table

Figures

Figure

Chapter 1

Introduction

1.1 String Theory Generalities

For more than four decades, string theory has captured the imagination of a large section of the theoretical physics community. The undeniable allure of the string theory lies in its promise to unify the Standard Model with gravity in a UV complete theory. Over the course of these decades, physicists' beliefs about the ultimate meaning of string theory have been significantly altered by several paradigm-shifting revolutions. In the wake of each of these revolutions, their presuppositions about string theory have proven incomplete and a deeper and less obvious picture of string theory's ultimate interpretation has emerged.

The most important of these major revolutions came in realizing that each consistent, low energy construction of string theory was related to all other constructions via transformations known as *dualities*. No longer were there several different string theories, only several weakly coupled limits of the same theory. These limits are related to each other via the so-called "web of duality" (see Figure 1.1). Each corner of this web represents a different string construction that contains different content and interactions. Accordingly, each construction has different virtues and drawbacks. However, the web of duality enables one to focus on a specific string construction and work out its consequences without worrying about what form the ultimate version of string theory will take. For the time being, we are content to live on a corner of the web of duality until the day comes when the web's center (M Theory) can be elucidated.

In Table 1.1 we provide some basic information about each string construction. The essential

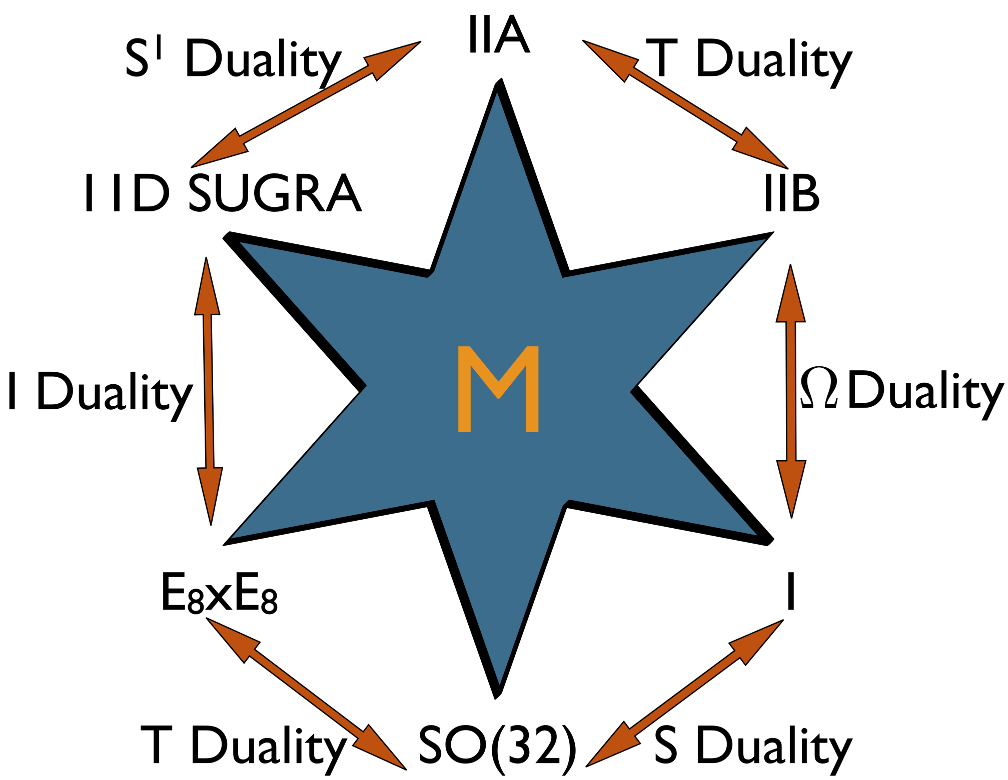

Figure 1.1: String theory web of duality

differences between constructions comes from how the left and right propagating string modes are handled.

Name	Comments
Type I	Contains unoriented open and closed strings Preserves $\mathcal{N} = 1$ SUSY
Type IIA	Left and right moving string modes have opposite chirality Odd Dimensional D-branes and O-planes Preserves $\mathcal{N} = 2$ SUSY
Type IIB	Left and right moving string modes have same chirality Even Dimensional D-branes and O-planes Preserves $\mathcal{N} = 2$ SUSY
Heterotic E **(**$E_8 \times E_8$**)**	Left and right moving string modes are independent Preserves $\mathcal{N} = 1$ SUSY, gauge group is $E_8 \times E_8$
Heterotic O **(**$SO(32)$**)**	Left and right moving string modes are independent Preserves $\mathcal{N} = 1$, gauge group is $SO(32)$

Table 1.1: Basic information about various 10D superstring constructions.

Another major theoretical revolution came in understanding the vacuum state of string theory. Naively, one might assume that there exists a single, unique vacuum state of string theory. In this picture, most (if not all) of the free parameters of the Standard Model are direct consequences of this vacuum state. The job of a string theorist would be to identify this state and hence uniquely reproduce the Standard Model. However, at least two intrinsic features of string theory prevent this from happening. One is the above mentioned web of duality. The other, as we shall see, comes from a fundamental freedom in choosing other parameters in string theory. This freedom is irreducible and leads to an enormous vacuum degeneracy that can be envisioned to be parameterized by an unknown potential function known as the *landscape*. For some time, the landscape was thought to be an intractable bug within string theory. However, like many persistent bugs, it eventually became a feature. We will see why this is the case later on.

While readily accepting the elegance and simplicity of string theory, one is forced to contend with several necessary additional features that, at first blush, seem non-obvious. The first of these features is the fact that string theory is a ten dimensional theory. Like any higher dimensional theory, these extra dimensions have to be compactified to a small internal volume that lives at each point in spacetime, as in Kaluza Klein models. In string theory, the internal space is parameterized by scalar fields, known as moduli. The fields must be stabilized in order to recover a four dimensional theory. This category of research is known as *moduli stabilization*, and it represents a significant portion of this dissertation.

Another non-obvious feature of string theory that will play a crucial role in our discussion is the presence of p-dimensional extended objects known as branes. In type II string theory, an important type of brane is referred to as D-branes. These objects can be viewed as hyperplanes upon which strings can end. Additionally branes act as sources for higher dimensional generalizations of field strengths, known as *fluxes*. As we shall see, branes are essential for realizing both chiral matter and gauge fields in certain string constructions. In addition, the fluxes sourced by these branes will enable us to successfully stabilize some the moduli fields. As extended objects, p-branes can wrap around homology cycles inside the compactified volume, providing a potential energy that stabilizes some of the moduli fields.

A final feature of string theory that turns out to be enormously beneficial is the presence of supersymmetry (SUSY). Supersymmetry enters into string theory in a fundamental way, namely it can be viewed as a symmetry transformation on the string worldsheet exchanging bosonic coordinates with fermionic coordinates. This symmetry is necessary for removing a tachyon from the bosonic sector. Additionally, supersymmetry reduces the number of dimensions of string theory from 26 down to 10. In fact, the need to preserve the simplest version of supersymmetry, ($\mathcal{N} = 1$ SUSY in 4D), plays a crucial role in identifying the class of manifolds of which the compactified volume is a member.

The low energy limit of string theory is a local version of supersymmetry known as supergravity (SUGRA). As the name implies, this symmetry includes the spin-3/2 supersymmetric partner of the graviton, namely the *gravitino*. The mass of the gravitino is denoted $m_{3/2}$ and it plays the role of something like an order parameter for the supergravity models considered in this dissertation, in that is sets the mass scale of all the other SUSY particles. It can be demonstrated that all generic models of supergravity can be summarized by three specific functions. Some basic information about these functions is given below:

- **Kähler Potential**, $K(\overline{\Phi}, \Phi)$, This is a real function that parameterizes the kinetic terms. It is corrected perturbatively to all orders as well as non-perturbatively.

- **Superpotential**, $W(\Phi)$, This is a holomorphic function that parameterizes potential terms. It is only corrected non-perturbatively.

- **Gauge Kinetic Function**, $f(\Phi)$, This is a holomorphic function that parameterizes gauge coupling. It is perturbatively corrected at 1-loop as well as non-perturbatively.

The minimum of the SUGRA scalar potential constitutes a cosmological constant, Λ, and could explain the observed acceleration of the expansion of the universe in the form of dark energy. The SUGRA scalar potential is given by

$$V_{SUGRA} = e^K \left[K^{N\overline{M}} D_N W \overline{D_M W} - 3|W|^2 \right] \tag{1.1}$$

Here, $D_N W$ represents the Kähler covariant-derivative of the superpotential, W, with respect to a superfield, N, that is $D_N W = \partial_N W + K_N W$. It can be shown that supersymmetry is broken if $D_N W \neq 0$.

The basic approach of much the following work is to first consider a string theory construction that can be summarized by an effective supergravity action by specifying K, W and f. We then examine the scalar potential, eq. (1.1), and search for a minimum of this potential. If the moduli fields satisfy the equation $D_N W = 0$ at the minimum of the potential then they preserve supersymmetry, otherwise they break it spontaneously. The value of the scalar potential at its minimum corresponds to the cosmological constant. So, in principle, we want this value to be extremely small and positive, ($V_{min} \sim 10^{-120}\,\mathrm{M_P^4}$). As one might imagine, arriving at such situation is non-trivial.

To close this section we reiterate some of the well known phenomenological consequences of supersymmetry. The list of contemporary theoretical challenges potentially resolved by supersymmetry include the following:

- Resolving the Hierarchy Problem by stabilizing the Higgs mass near the weak scale.

- Driving electroweak symmetry breaking.
- Providing a dark matter candidate in the Lightest Supersymmetric Partner (LSP).
- Providing a source for dark energy and the cosmological constant in the vacuum energy density of the SUSY fields.
- Allowing for improved gauge coupling unification around 10^{16} GeV.

As one can see from this list, if broken supersymmetry is realized in Nature, many of the outstanding challenges of theoretical physics have the potential to be resolved. String theory enables an efficient study of supersymmetry breaking for several reasons. Principle among these is the fact that it reduces the enormous parameter space that accompanies the simplest realizations of supersymmetry breaking. For instance, if one adds supersymmetric partners to the Standard Model and allows each one of these partners to break SUSY by aqcuiring a mass, one arrives at the Minimal Supersymmetric Standard Model (MSSM). The most generic soft MSSM Lagrangian is given in eq. (1.2)

$$\begin{aligned}\mathcal{L}_{soft}^{MSSM} \;=\;& -\frac{1}{2}\left(M_3\tilde{G}\tilde{G}+M_2\tilde{W}\tilde{W}+M_1\tilde{B}\tilde{B}\right)-\left(\tilde{\bar{u}}\mathbf{A_u}\tilde{Q}H_u+\tilde{\bar{d}}\mathbf{A_d}\tilde{Q}H_d+\tilde{\bar{e}}\mathbf{A_e}\tilde{L}H_d\right)+h.c.\\ & -\tilde{Q}^*\mathbf{m_Q^2}\tilde{Q}-\tilde{L}^*\mathbf{m_L^2}\tilde{L}-\tilde{\bar{u}}^*\mathbf{m_u^2}\tilde{\bar{u}}-\tilde{\bar{d}}^*\mathbf{m_d^2}\tilde{\bar{d}}-\tilde{\bar{e}}^*\mathbf{m_e^2}\tilde{\bar{e}}-m_{H_u}^2H_u^*H_u-m_{H_d}^2H_d^*H_d\\ & -\left(\mu H_uH_d+h.c.\right)\end{aligned} \tag{1.2}$$

This Lagrangian introduces 105 new free parameters. As we will see in the text, IIB string theory allows us to reduce this parameter space to two continuous parameters and one sign. It turns out that this is the fewest number of free parameters of any phenomenological model of supersymmetry.

1.2 IIB String Theory

As stated earlier, in this dissertation we are exclusively focused on examining the phenomenological consequences of a particular string construction, namely IIB string theory. Let us now review some facts about IIB string theory. The essential ingredients of this theory are

- Open and closed strings whose massless modes (hopefully) correspond to various bosonic and fermionic particles in the Standard Model as well as other massless fields.
- D3/7 branes and O3/7 planes.
- Two types of fluxes, RR and NSNS.
- A Calabi Yau Orientifold representing the compactified volume.

In 10 dimensions, IIB string theory possesses an extended version of supersymmetry ($\mathcal{N} = 2$). For phenomenological reasons, namely the presence of chiral fermions, this supersymmetry needs to be reduced to $\mathcal{N} = 1$ in four dimensions. This can be achieved if the internal volume is taken to be a so-called "Calabi Yau" manifold with an orientifold projection. This is often referred to as Calabi Yau Orientifold (CYO). Fluxations of this manifolds metric that preserve the the Calabi Yau nature of the manifold correspond to massless scalars in the four dimensional theory. These fields are known as moduli. For IIB string theory, the moduli fields are

- **Kähler Moduli**, T, These fields determine the size of internal manifold via $\mathcal{V} = k_{ijk}t^i t^j t^k$, ($\Re T^i = \frac{\partial \mathcal{V}}{\partial t^i}$). The number of these fields is given by $h_{11} \sim \mathcal{O}(1)$.
- **Complex Structure Moduli**, z, These fields determine the "shape" of internal manifold. The number of these fields is given by $h_{21} \sim \mathcal{O}(100)$.
- **axio-Dilaton**, S, This field determines gauge couplings after it is stabilized.

These massless scalars need to be stabilized, otherwise they may give rise to 5th-forces via gravitational interactions with Standard Model particles. In addition, the moduli fields need to break the remaining supersymmetry $\mathcal{N} = 1$ down to nothing. In a seminal work Giddings et. al. [1], it was shown that both the complex structure moduli as well as the axio-Dilaton can be stabilized when fluxes are turned on the internal manifold. Specifically, the RR 3-form flux, F_3, and the NSNS 3-form flux, H_3, have to satisfy integral cohomology conditions. These can be viewed has higher dimensional generalizations of Dirac quantization.

$$\frac{1}{(2\pi)^2\alpha'}\int_\gamma F = n_F \in \mathbb{Z} \quad \frac{1}{(2\pi)^2\alpha'}\int_\gamma H = n_H \in \mathbb{Z} \tag{1.3}$$

Where γ is a three cycle (akin to a donut hole). In [1], it was shown that fluxes conditions, eq (1.3) can be chosen in such a way that the complex structure moduli, z_i, as well as the axio-Dilaton, S, can be stabilized at supersymmetric points in field space. That is

$$D_{z^i}W = D_S W = 0 \tag{1.4}$$

With a Minkowski minimum for the scalar potential. This leaves the remaining Kähler moduli unfixed, and hence this model is known as "no-scale".

The remaining Kähler moduli need to be stabilized in such a way that supersymmetry is broken spontaneously and a near-zero cosmological constant is achieved. This first model to successfully achieve these requirement is referred to as the Large Volume Scenario (LVS) [2]. In this model the authors considered a Calabi Yau Orientifold with one large Kähler modulus and several small Kähler moduli. The overall volume of this space is computed from subtracting out the volumes of the smaller volumes from the large volume, must like piece of swiss cheese. For this reason this class of CYO's is referred to as a "Swiss Cheese" Manifold. A humorous yet informative picture of this manifold is given in figure 1.2

In LVS, the presence of these smaller volumes is crucial for stabilizing the Kähler moduli and breaking supersymmetry. It can shown that non-perturbative effects such as gaugino condensation from a condensing gauge group on a stack of D branes or string instantons are necessary for stabilizing the Kähler moduli. However, once they are stabilized, the resulting four dimensional theory has many promising features. Namely, it is non-supersymmetric and it can have a nearly zero cosmological constant in such a way that the resulting scales of the SUSY particles is not strongly dependent upon how $V \sim 0$ is achieved.

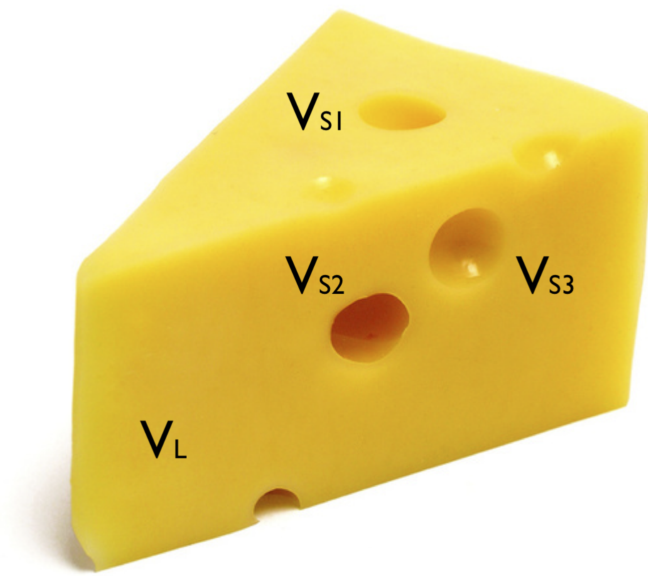

Figure 1.2: Swiss Cheese Manifold with $\mathcal{V} = V_L - \sum_i V_{Si}$.

1.3 Summary of Work

The work presented in this thesis can be separated into three categories, all related to examining the phenomenology of IIB string theory. These are

- **inoAMSB Trilogy** - Chapters 2, 3 and 4 are based on papers [3] [4] [5]. These chapters examine the phenomenological consequences of a type of supersymmetry breaking and mediation known as inoAMSB. This model comes directly from IIB string theory and the Large Volume Scenario in particular. In this series of papers we discuss the theoretical and phenomenological predictions for both LHC physics as well as modern cosmology.

- **Single Kähler Modulus Stabilization** - Chapter 5 is based on paper [6]. In this chapter, we return to the issue of moduli stabilization and examine a class of string models whose moduli can be stabilized along the lines of the Large Volume Scenario. We work out various phenomenological consequence for this class of models.

- **QCD Axion in LVS** - Chapter 6 is based on paper (to be published). In this chapter, we analyze the potential for realizing a QCD axion with the Large Volume Scenario. We make consistent assumptions about the types of fields and interactions that can be constructed with IIB string theory and we examine the phenomenological constraints on a model that reproduces the QCD axion.

Chapter 2

Gaugino Anomaly Mediated SUSY Breaking: phenomenology and prospects for the LHC

Chapter Summary

In this chapter, examine the supersymmetry phenomenology of a novel scenario of supersymmetry (SUSY) breaking which we call Gaugino Anomaly Mediation, or inoAMSB. This is suggested by recent work on the phenomenology of flux compactified type IIB string theory. The essential features of this scenario are that the gaugino masses are of the anomaly-mediated SUSY breaking (AMSB) form, while scalar and trilinear soft SUSY breaking terms are highly suppressed. Renormalization group effects yield an allowable sparticle mass spectrum, while at the same time avoiding charged LSPs; the latter are common in models with negligible soft scalar masses, such as no-scale or gaugino mediation models. Since scalar and trilinear soft terms are highly suppressed, the SUSY induced flavor and CP-violating processes are also suppressed. The lightest SUSY particle is the neutral wino, while the heaviest is the gluino. In this model, there should be a strong multi-jet $+E_T^{\rm miss}$ signal from squark pair production at the LHC. We find a 100 fb^{-1} reach of LHC out to $m_{3/2} \sim 118$ TeV, corresponding to a gluino mass of ~ 2.6 TeV. A double mass edge from the opposite-sign/same flavor dilepton invariant mass distribution should be visible at LHC; this, along with the presence of short– but visible– highly ionizing tracks from quasi-stable charginos, should provide a smoking gun signature for inoAMSB.

2.1 Introduction

String theory is very attractive in that it allows for a consistent quantum mechanical treatment of gravitation, while at the same time including all the necessary ingredients for containing the well-known gauge theories which comprise the Standard Model of particle physics. Phenomenologically viable versions of string theory require the stabilization of all moduli fields as well as weak to intermediate scale supersymmetry breaking. Models satisfying these criteria were first developed in the context of type IIB string theory using flux compactifications and non-perturbative effects on Calabi Yau orientifolds (CYO's) (for reviews see [7] [8]). The low energy limit of type-IIB string theory after compactification on a CYO is expected to be $N = 1$ supergravity (SUGRA).

Two classes of the above models which yield an interesting supersymmetry breaking scenario have been studied:

a) Those with only a single Kähler modulus (SKM models). These are essentially of the KKLT type [9] but with uplift coming from one-loop quantum effects.

b) Large Volume Scenario (LVS) [2] models which require at least two moduli.

In both of these types of models, the moduli fields are stabilized using a combination of fluxes and non-perturbative effects. Additionally, supersymmetry is broken by the moduli fields acquiring non-zero F-terms and interacting gravitationally with the MSSM. For both models, the gauginos acquire mass predominately through a Weyl anomaly effect while the classical contribution to the scalar masses and trilinear coupling constants are naturally suppressed.

Generically in a string model there are three types of contributions to the soft SUSY breaking terms:

(1) Terms generated by classical string theory effects.

(2) Terms generated by quantum effects (effectively string loop corrections).

(3) Weyl anomaly (AMSB) contributions [10] to the gaugino masses.

In this class of models, the MSSM may be located on D3 branes at a singularity or on D7 branes wrapping a collapsing four cycle in the CYO. The string theory calculations are expected to give boundary conditions at (or near) the string scale M_{string}, which may range (almost) up to the GUT scale or as low as some intermediate scale $\ll M_{GUT}$. In both cases, the classical string theory as well as 1-loop quantum contributions to the soft SUSY breaking terms are suppressed relative to the weak scale. For gaugino masses, it has been shown that these will gain contributions from the Weyl anomaly, and therefore assume the usual form as expected in models with anomaly-mediated SUSY breaking:

$$M_i = \frac{b_i g_i^2}{16\pi^2} m_{3/2}. \tag{2.1}$$

Here i labels the gauge group, g_i is the associated gauge coupling, $m_{3/2}$ is the gravitino mass, and b_i is the co-efficient of the gauge group beta function: $b_i = (33/5, 1, -3)$. Meanwhile, soft SUSY breaking scalar masses will have generically suppressed classical string masses and 1-loop contributions, and receive *no contribution* from Weyl anomalies [11].

To good approximation, we can set in this class of models,

$$m_0 = A_0 = 0, \tag{2.2}$$

where m_0 is the common soft SUSY breaking scalar mass at M_{string} and A_0 is the trilinear soft SUSY breaking (SSB) term.

In addition, the bilinear SSB mass B and the superpotential μ term would be zero at the classical (AdS) minimum. However these can acquire non-zero values once uplift terms that correct the value of the cosmological constant are turned on. Here, we will feign ignorance as to the origin of these terms, and instead adopt a phenomenological approach which determines their values by finding an appropriate minimum of the electroweak scalar potential. The minimization procedure allows one to trade the B parameter for the ratio of Higgs field vevs, $\tan\beta$, and to require the value of $|\mu|$ which is needed in order to specify the correct mass of the Z boson [12]. In this case, the SKM and LVS models would both be well-described by the following parameter space

$$m_{3/2},\ \tan\beta,\ sign(\mu), \tag{2.3}$$

where in addition we take $m_0 = A_0 = 0$. While the SSB scalar and trilinear terms are small at M_{string}, they can become large at $Q = M_{weak}$ due to renormalization group (RG) running.

In fact, these sort of RG boundary conditions are similar to those of no-scale supergravity models (NS) [13], and also gaugino-mediated SUSY breaking (inoMSB) models [14]. However, in both NS and inoMSB models, it is expected that the gaugino masses unify to a common gaugino mass $m_{1/2}$ at the string scale. The fact that both scalar and trilinear soft SUSY breaking terms have only small contributions at the high scale (compactification scale M_c, M_P or M_{GUT}) is highly desirable for solving the SUSY flavor and CP problems. In the general MSSM, unconstrained off-diagonal terms in the scalar and trilinear sector lead to large contributions to flavor changing and CP violating processes, for which there are tight limits [15]. Under renormalization group evolution, the off-diagonal terms remain small, while diagonal terms receive significant contributions due to gauge interactions and the large gaugino masses.

Using the NS or inoMSB boundary conditions, it is well known that one gains a sparticle mass spectrum with τ sleptons as the lightest SUSY particle (LSP)[1] . In models with R-parity conservation, the $\tilde{\tau}_1$ would be absolutely stable, thus violating constraints coming from search experiments for long lived, stable charged relics from the Big Bang. One way around this dilemma has been suggested by Schmaltz and Skiba [16]: adopting $M_{string} > M_{GUT}$, so that above-the-GUT-scale running lifts the value of m_0 above zero at the GUT scale. Another possibility is to allow for unconstrained, or a less-constrained, form of *non-universal* gaugino masses [17].

We find here that the $m_0 \sim A_0 \sim 0$ boundary conditions– along with the AMSB form for gaugino masses– in fact leads to viable sparticle mass spectra across most of parameter space, without the need for above-the-GUT-scale running, or a less-constrained form for gaugino masses, or an artifically light gravitino mass. While these boundary conditions seem to emerge naturally in type IIB string models with flux compactifications, we may also consider such boundary conditions by themselves as being perhaps more general, and well-motivated by their desirable low energy

[1] One way out is to hypothesize the gravitino as LSP. In our case, we will find that the gravitino mass is always in the multi-TeV range.

features. For this reason, we will hereafter refer to the class of models leading to the above boundary conditions as gaugino anomaly mediated SUSY breaking, or *inoAMSB* models, since only the gaugino masses receive contributions of the AMSB form, and the other soft parameters are similar to those as generated in gaugino mediation.

The remainder of this chapter is organized as follows. In Sec. 2.2, we review some of the string theoretic supergravity model details that motivate us to consider the inoAMSB form of boundary conditions. In Sec. 2.3, we plot out the spectra of superpartners that is expected in the inoAMSB model. While some features are similar to what is known as "minimal" AMSB (mAMSB), some crucial differences exist that may allow one to distinguish inoAMSB from mAMSB and also "hypercharged" anomaly-mediation (HCAMSB) [18]. We also examine what happens if the string scale is taken to be some intermediate value, or if some small universal scalar mass is adopted. We also plot out low energy constraints from $BF(b \to s\gamma)$ and $(g-2)_\mu$. In Sec. 2.4, we examine the sort of signatures expected from the inoAMSB model at the CERN LHC. Since squark masses are always lighter than gluinos, we expect a large rate for $\tilde{q}\tilde{q}$ and $\tilde{q}\tilde{g}$ production, leading to a large rate for multi-jet+$E_T^{\rm miss}$ events. Since the lightest SUSY particle is a neutral wino, as in most AMSB-type models, we expect a nearly mass degenerate, quasi-stable chargino, which can lead to short but observable highly ionizing tracks in a collider detector. In addition, squarks cascade decay to neutralinos, followed by neutralino decay to lepton plus either left- or right-slepton states. The unique cascade decay pattern leads to a distinct double mass edge in the same-flavor/opposite-sign dilepton invariant mass distribution, which distinguishes inoAMSB from mAMSB or HCAMSB. In Sec. 3.5, we present our conclusions.

2.2 Effective supergravity from IIB strings: Overview of Models

2.2.1 Effective Supergravity Theory

The low energy limit of IIB string theory, after compactification on a Calabi-Yao orientifold, yields $\mathcal{N} = 1$ supergravity. The (superspace) action then has the generic form (see for example

[19, 20])

$$S = -3\int d^8z\mathbf{E}\exp[-\frac{1}{3}K(\Phi,\bar{\Phi};C,\bar{C}e^{2V})] + \left(\int d^6z2\mathcal{E}[W(\Phi,C)+\frac{1}{4}f_a(\Phi)\mathcal{W}^a\mathcal{W}^a]+h.c.\right), \quad (2.4)$$

where we have set $M_P = (8\pi G_N)^{-1/2} = 2.4\times 10^{18}GeV = 1$. Here $K-$ the Kähler potential– is a real superfield as is the gauge pre-potential V. $W-$ the superpotential– is a holomorphic field, as is the gauge coupling function f_a and the (fermionic) gauge (super) field strength $\mathcal{W}(V)$. $\mathbf{E}d^8z$ is the full superspace measure and $\mathcal{E}d^6z$ is the chiral superspace measure. Ignoring the D-terms, which are zero at the minimum of the potential in the class of models considered here, the SUGRA potential takes the standard form (after going to the Einstein frame)

$$V(\Phi) = F^AF^{\bar{B}}K_{A\bar{B}} - 3|m_{3/2}(\Phi)|^2. \quad (2.5)$$

Here $F^A = e^{K/2}K^{A\bar{B}}D_{\bar{B}}W$, $D_AW \equiv \partial_AW + K_AW$ where $K_A = \partial_AK$, $K_{A\bar{B}} = \partial_A\partial_{\bar{B}}K$ and $|m_{3/2}|^2 \equiv e^K|W|^2$ becomes the squared gravitino mass when evaluated at the minimum of the potential.

We separate the chiral superfields of the theory into moduli fields (which come from string theory and describe the internal geometry of the CY manifold) and the dilaton (which are collectively called Φ) and the MSSM fields (which we have called C). Expanding K and W in powers of the MSSM fields we have:

$$W = \hat{W}(\Phi) + \mu(\Phi)H_dH_u + \frac{1}{6}Y_{\alpha\beta\gamma}(\Phi)C^\alpha C^\beta C^\gamma + \ldots, \quad (2.6)$$

$$K = \hat{K}(\Phi,\bar{\Phi}) + \tilde{K}_{\alpha\bar{\beta}}(\Phi,\bar{\Phi})C^\alpha C^{\bar{\beta}} + [Z(\Phi,\bar{\Phi})H_dH_u + h.c.] + \ldots \quad (2.7)$$

$$f_a = f_a(\Phi). \quad (2.8)$$

Here we have separated the two Higgs superfield multiplets ($H_{d,u}$). The moduli fields essentially play the role of spurion fields that break supersymmetry, once they are stabilized and acquire a definite vacuum expectation value such that one or more of them also has a non-zero F-term.

Also

$$\hat{K} = -2\ln\left(\mathcal{V}+\frac{\hat{\xi}}{2}\right) - \ln\left(i\int \Omega\wedge\bar{\Omega}(U,\bar{U})\right) - \ln(S+\bar{S}), \quad \text{and} \tag{2.9}$$

$$\hat{W} = \int G_3\wedge\Omega + \sum_i A_i e^{-a_i T^i}. \tag{2.10}$$

Here $\mathcal{V}$ is the volume of the CYO and is a function of the Kähler moduli superfields T^i (with $i = 1, \cdots, h_{11}$), and $\hat{\xi}$ is a stringy (α') correction that is an $O(1)$ number depending on the Euler character of the CYO and the real part of the dilaton superfield S. Ω is the holomorphic three form on the CYO and is a function of the complex structure moduli superfields U_r (with $r = 1, \cdots, h_{21}$).

2.2.2 Single Kähler modulus scenario

In this construction, type IIB string theory is compactified on a CYO and the MSSM lives on a stack of D3 branes. We take a CYO with just one Kähler modulus, T, (i.e. $h_{11} = 1$) but with a number $\sim 10^2$ of complex moduli, U_r. These moduli, along with the axio-dilaton, S, are then stabilized using internal fluxes and non-perturbative effects. Classically, we can find a minimum of this potential with the F-term of T being $\sim m_{3/2}$ with the other moduli F-terms being suppressed. The cosmological constant would be negative but suppressed. The soft terms are also highly suppressed. This solution of course receives quantum mechanical corrections starting at 1-loop. In terms of an effective field theory description, they would depend on a string scale cutoff Λ. These can serve to uplift the cosmological constant and to generate the soft SUSY breaking masses, proportional to $\frac{\Lambda}{4\pi}m_{3/2}$. The cutoff Λ is essentially the string scale and in this class of models may be taken as large as $10^{-2}M_P$ so that a GUT scenario could be accommodated. This class of models is discussed in [21].

2.2.3 Large Volume Scenario (LVS)

In this class of models [2], we again compactify IIB string theory on a CYO. However, we now consider more than one Kähler modulus, $T^i (i = 1, \cdots, h_{11})$. In particular– in the simplest such situation– we have a large modulus, τ_b, and small moduli, (τ_s, τ_a), controlling the overall size of the CYO and the volume of two small 4-cycles respectively. The total volume is then given by

$$\mathcal{V} = \tau_b^{3/2} - \tau_s^{3/2} - \tau_a^{3/2}. \tag{2.11}$$

This is referred to as a "Swiss Cheese" model. Again the MSSM may be located on D3 branes at a singularity. Alternatively, we could have it on a stack of D7 branes wrapping a four cycle (taken to be the one labelled by the index a). In this case, it has been argued [22, 23] that the necessity of having chiral fermions on this brane prevents this cycle from being stabilized by non-perturbative effects and it shrinks below the string scale. Effectively, this means that the physics is the same as in the D3 brane case.

Extremizing the potential leads to an exponentially large volume [2] $\mathcal{V} \sim e^{a\tau_s}$, $\tau_s \sim \hat{\xi}$. It turns out that the suppression of FCNC effects lead to $\mathcal{V} \gtrsim 10^5 l_P^6$ [24] (where l_P is the Planck length), so the string scale is $M_{string} \lesssim M_P/\sqrt{\mathcal{V}} \sim 10^{15.5}$GeV. The minimum of the potential (CC) is given by $V_0 \sim -\frac{m_{3/2}^2 M_P^2}{\ln m_{3/2}\mathcal{V}}$. This minimum can be uplifted to zero when S and U_r acquire (squared) F-terms of the order $\frac{m_{3/2}^2 M_P^2}{\ln m_{3/2}\mathcal{V}}$. Classical contributions to the scalar and slepton masses are also of this same order. With the above lower bound on the volume, this means that even for $m_{3/2} \sim 100$ TeV, the classical soft terms are $\lesssim 100$ GeV. Of course if one wants to avoid fine-tuning of the flux superpotential, we would need to take even larger values of $\mathcal{V}$ corresponding to a string scale of 10^{12} GeV. In this case the classical soft terms are completely negligible (for $m_{3/2} \sim 100$ TeV) but the (classical) μ-term is also strongly suppressed.

In the rest of this section we will call the holomorphic variable associated with the large modulus τ_b, T.

2.2.4 Gaugino Masses - Weyl Anomaly Effects

For a generic version of supergravity, the gaugino masses satisfy the following relation at the classical level:

$$\frac{M_a}{g_a^2} = \frac{1}{2} F^A \partial_A f_a(\Phi). \tag{2.12}$$

For both the single Kähler modulus model and LVS cases, the leading contribution to the gauge coupling function $f_a(\Phi)$ comes from the axio-dilaton S, so at a classical minimum where the SUSY breaking is expected to be in the T modulus direction, the string theoretic contribution to the gaugino mass is highly suppressed.

However, there is an additional contribution to the gaugino mass due to the (super) Weyl anomaly. This comes from the expression for the effective gauge coupling superfield that has been derived by Kaplunovsky and Louis [26] (KL)[2] . For the gaugino masses, the relevant contribution comes from taking the F-term of

$$H_a(\Phi, \tau, \tau_Z) = f_a(\Phi) - \frac{3c_a}{8\pi^2}\ln\phi - \frac{T_a(r)}{4\pi^2}\phi_Z. \tag{2.13}$$

Here, the first term on the RHS is the classical term; the second comes from the anomaly associated with rotating to the Einstein-Kähler frame. $c_a = T(G_a) - \sum_r T_a(r)$ is the anomaly coefficient and the last term comes from the anomaly associated with the transformation to canonical kinetic terms for the MSSM fields. Also note that we have ignored the gauge kinetic term normalization anomaly [11, 27] which is a higher order effect. The chiral superfields ϕ, ϕ_r that generate these transformations are given by,

$$\ln\phi + \ln\bar{\phi} = \frac{1}{3}K|_{\text{Harm}}, \tag{2.14}$$

$$\phi_r + \bar{\phi}_r = \ln\det\tilde{K}^{(r)}_{\alpha\bar{\beta}}. \tag{2.15}$$

The instruction on the RHS of the first equation is to take the sum of the chiral and anti-chiral (i.e. harmonic) part of the expression. After projecting the appropriate F terms we arrive at the following expression:

$$\frac{2M_a}{g_a^2} = F^A\partial_A f_a - \frac{c_i}{8\pi^2}F^A K_A - \sum_r \frac{T_i(r)}{4\pi^2}F^A\partial_A \ln\det\tilde{K}^{(r)}_{\alpha\bar{\beta}}. \tag{2.16}$$

As pointed out earlier, the first (classical) term is greatly suppressed relative to $m_{3/2}$. The dominant contribution therefore comes from the last two (Weyl anomaly) contributions. It turns out that

[2] As explained in [11], the usual formulae for AMSB [10], [25] need modification in the light of [26].

(after using the formulae $F^T = -(T+\bar{T})m_{3/2}$, $K_T = -3/(T+\bar{T})$ and $\tilde{K}_{\alpha\bar{\beta}} = k_{\alpha\beta}/(T+\bar{T})$ which are valid up to volume suppressed corrections), this yields[3] ,

$$M_a = \frac{b_a g_a^2}{16\pi^2} m_{3/2}, \tag{2.17}$$

where $b_a = -3T(G_a) + \sum_r T_a(r)$ is the beta function coefficient.

2.2.5 Scalar Masses, Trilinear Couplings, μ and $B\mu$ terms

Here we summarize the results from this class of string theory models for the values of the soft parameters at the UV scale, *i.e.* $\Lambda \sim M_{string} \sim M_P/\sqrt{\mathcal{V}}$. These values should be the initial conditions for the RG evolution of these parameters. In the LVS case, it was estimated [24] that the lower bound on the CYO volume was $\mathcal{V} > 10^5$. Also, we will choose typical values $h_{21} \sim O(10^2)$ for the number of complex structure moduli. We will also take the gravitino mass $m_{3/2} \sim |W|M_P/\mathcal{V} \sim 50$ TeV. Such a large value of $m_{3/2}$ allows us to avoid the SUGRA gravitino problem, which leads to a disruption of Big Bang nucleosynthesis if $m_{3/2} \lesssim 5$ TeV and $T_R \gtrsim 10^5$ GeV [28].

Unlike the gaugino masses, scalar masses and trilinear soft terms do not acquire corrections from the Weyl anomaly. They are essentially given at the UV scale by their classical string theory value plus one loop string/effective field theory corrections. In the $h_{11} = 1$ case, the classical soft terms are essentially zero while in the LVS case

$$m_0 \sim O\left(\frac{m_{3/2}}{\sqrt{\ln m_{3/2}\mathcal{V}}}\right),\ \mu \sim \frac{B\mu}{\mu} \lesssim \sqrt{h_{21}} m_0,\ A_0 \ll m_0. \tag{2.18}$$

After adding quantum corrections at the UV scale both cases give similar values for the soft terms. As an example, we illustrate for two values for the CYO volume:

- $\mathcal{V} \sim 10^5, M_{string} \sim \Lambda \sim 10^{-2.5} M_P \sim 10^{15.5}$ GeV. Then,

$$\mu \sim \frac{B\mu}{\mu} \lesssim 250 \text{ GeV},\ m_0 \sim 25 \text{ GeV},\ A_0 \ll m_0. \tag{2.19}$$

[3] Note that we expect the Weyl anomaly expressions for the gaugino masses given below to be valid only because of the particular (extended no-scale) features of this class of string theory models. It so happens that these are exactly the same as the expressions given in what is usually called AMSB: but that is an accident due entirely to the fact that in these extended no-scale models the relationship $F^A K_A \simeq 3m_{3/2}$ is true.

- $\mathcal{V} \sim 10^{12},\ M_{string} \sim \Lambda \sim 10^{-6} M_P \sim 10^{12}$ GeV. Then,

$$\mu \sim \frac{B\mu}{\mu} \lesssim 10^{-1}\ \text{GeV},\ m_0 \sim 10^{-2}\ \text{GeV},\ A_0 \ll m_0. \tag{2.20}$$

  The second very large volume case can be accessed only in the LVS model.

The first case is at the lower bound for the volume. This gives the largest allowable string scale. This is still somewhat below the apparent unification scale, but it is close enough that (allowing for undetermined $O(1)$ factors) we may use the GUT scale as the point at which to impose the boundary conditions. This is useful for the purpose of comparing with other models of SUSY mediation where it is conventional to use the GUT scale.

The second case above corresponds to choosing generic values of the flux superpotential, while the first needs a fine tuned set of fluxes to get $|W| \sim 10^{-8}$, in order to have a gravitino mass of $\sim 10^2$ TeV, though in type IIB string theory general arguments show that there exist a large number of solutions which allow this. The most significant problem with the second case (apart from the fact that there is no hope of getting a GUT scenario) is the extremely low upper bound on the μ term. In other words, there is a serious μ- problem. The first case also may have a μ term problem, but again since these estimates are accurate only to $O(1)$ numbers, it is possible to envisage that the problem can be resolved within the context of this model.

In any case, as we discussed in the introduction, we are going to take an approach where the string theory input is used to suggest a class of phenomenological models. Given that in both the GUT scale model and the intermediate scale model, the soft scalar mass and A term are suppressed well below the weak scale, we will input the value zero for these at the UV scale, while the gaugino masses at this scale are given by (2.17).

We also discuss the case when the input scalar mass m_0 is non-negligible. This would be the case for instance in the SKM model with smaller volumes and/or larger values of h_{21}, and also in the case of LVS with the volume at the lower bound but with larger values of h_{21}.

2.3 Mass spectra, parameter space and constraints for the inoAMSB model

2.3.1 Sparticle mass spectra and parameter space

We begin our discussion by examining the sort of sparticle mass spectra that is expected from the inoAMSB boundary conditions: $m_0 = A_0 = 0$ but with $M_i = \frac{b_i g_i^2}{16\pi^2} m_{3/2}$. We compute the sparticle mass spectra using the Isasugra subprogram of the event generator Isajet [29], along with the option of non-universal gaugino masses. The parameter space is that of Eq. 3.1.

After input of the above parameter set, Isasugra implements an iterative procedure of solving the MSSM RGEs for the 26 coupled renormalization group equations, taking the weak scale measured gauge couplings and third generation Yukawa couplings as inputs, as well as the above-listed GUT scale SSB terms. Isasugra implements full 2-loop RG running in the $\overline{DR}$ scheme, and minimizes the RG-improved 1-loop effective potential at an optimized scale choice $Q = \sqrt{m_{\tilde{t}_L} m_{\tilde{t}_R}}$ (which accounts for leading two-loop terms) [30] to determine the magnitude of μ and the value of m_A. All physical sparticle masses are computed with complete 1-loop corrections, and 1-loop weak scale threshold corrections are implemented for the t, b and τ Yukawa couplings [31]. The off-set of the weak scale boundary conditions due to threshold corrections (which depend on the entire superparticle mass spectrum), necessitates an iterative up-down RG running solution. The resulting superparticle mass spectrum is typically in close accord with other sparticle spectrum generators [32].

We begin by examining a single point in inoAMSB parameter space, where $m_{3/2} = 50$ TeV, and $\tan\beta = 10$, with $\mu > 0$ as suggested by the $(g-2)_\mu$ anomaly [33, 34]. In Fig. 2.1, we plot in frame *a*). the running gaugino masses, and in frame *b*). the running third generation and Higgs soft SUSY breaking scalar masses. We actually plot here $sign(m_i^2) \times \sqrt{|m_i^2|}$, in order to show the possible running to negative squared masses, while at the same time showing the true scale of the soft terms in GeV units. Frame *a*). is as expected in most AMSB masses *i.e.* where $M_1 \gg |M_3| \gg M_2$ at $Q = M_{string}$, where here we take $M_{string} = M_{GUT}$. The RG running of the gaugino masses leads to $-M_3 \gg M_1$ at $Q = M_{weak}$, while M_2 remains the lightest of gaugino masses at the weak scale, leading to a wino-like lightest neutralino $\widetilde{Z}_1$, which might also be the lightest SUSY particle (LSP). In frame b)., we see that the SSB scalar masses, beginning with negligible GUT scale values, are initially pulled up to positive values, mainly by the influence of the large value of M_1 at the GUT scale. In fact, the right-slepton mass $m_{E_3}^2$ initially evolves to the highest values, since it has the largest hypercharge quantum number $Y = 2$. The disparate Y values between E_3 and the doublet L_3 lead ultimately to a large splitting between left- and right- slepton SSB masses in the inoAMSB case, while these masses tend to be quite degenerate in mAMSB [35]. As the scale Q moves to values $\ll M_{GUT}$, QCD effects pull the squarks to much higher masses: in this case around the TeV scale, while sleptons, which receive no QCD contribution, remain in the 200-400 GeV range. The value of $m_{H_u}^2$ is driven as usual to negative squared values, resulting in a radiative breakdown of electroweak symmetry (REWSB). Since $M_2 < \sqrt{m_{L_3}^2}$, we generically find a wino-like neutralino as the LSP, and there is no problem with a charged LSP (as in NS/inoMSB models) or tachyonic sleptons (as in AMSB).

Once the weak scale SSB terms are computed, then the physical mass eigenstates and mixings may be computed, and one-loop mass corrections added. The resulting physical mass spectrum is listed schematically in Fig. 2.2a). and in Table 2.1, column 3. We adopt this inoAMSB model as a benchmark case, labeled inoAMSB1. In Table 2.1, we also show for comparison two related cases with $m_{3/2} = 50$ TeV and $\tan\beta = 10$: for mAMSB supersymmetry in column 1, with $m_0 = 300$ GeV, and in HCAMSB [18], column 2, with mixing parameter $\alpha = 0.025$.[4] While the first three cases listed in Table 2.1 have similar values of $m_{\tilde{g}}$ and $m_{\widetilde{W}_1, \widetilde{Z}_1}$ (due to the same input value of $m_{3/2}$), we see that inoAMSB1 has the previously noted large $\tilde{e}_L$-$\tilde{e}_R$ splitting, with $m_{\tilde{e}_L} < m_{\tilde{e}_R}$, while mAMSB has nearly degenerate $\tilde{e}_L$ and $\tilde{e}_R$, with $m_{\tilde{e}_R} < m_{\tilde{e}_L}$. However, the left-right slepton splitting in inoAMSB1 is not as severe as that shown in HCAMSB1, from Ref. [18], where an even larger value of M_1 at M_{GUT} is expected. In the HCAMSB1 case, the $\widetilde{Z}_4$ state tends to be nearly pure bino-like, whereas in inoAMSB1, it is instead higgsino-like.

[4] In the HCAMSB model, while most of the MSSM resides on a visible brane, $U(1)$ gauginos propagate in the bulk. Thus, the SSB boundary conditions, taken at the GUT scale, are those of AMSB, but with an additional contribution to the hypercharge gaugino mass, proportional to the mixing parameter α.

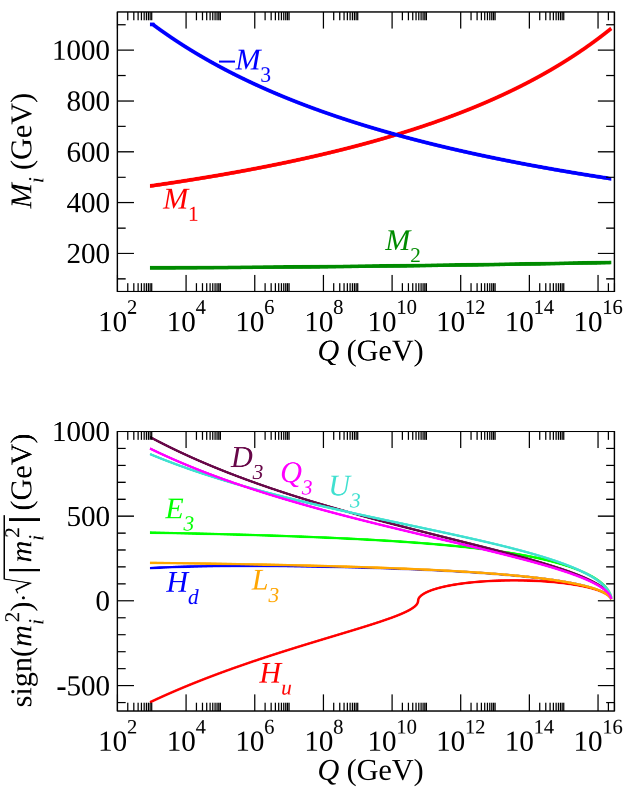

Figure 2.1: Running of soft SUSY breaking parameters as a function of energy scale Q for $m_{3/2} = 50$ TeV, $\tan\beta = 10$ and $\mu > 0$ in the inoAMSB model, with $M_{string} = M_{GUT}$.

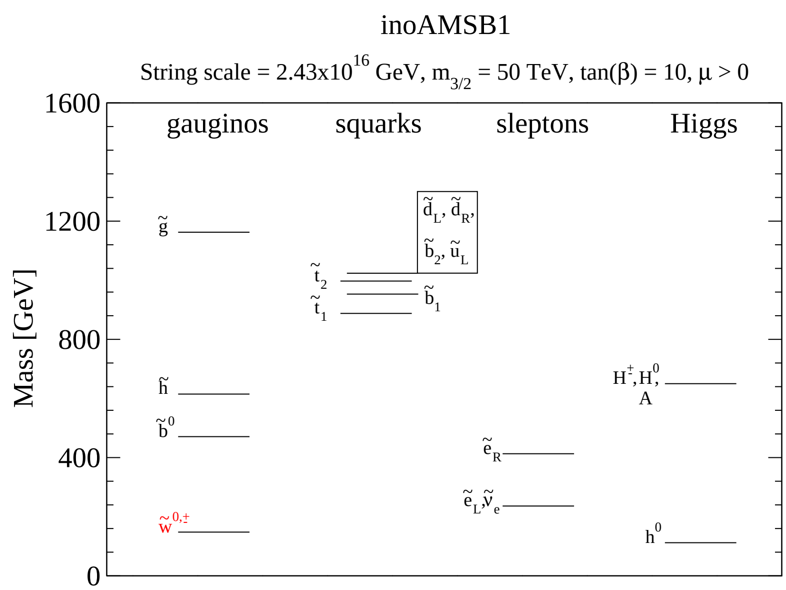

Figure 2.2: Plot of sparticle masses for the inoAMSB1 case study with $m_{3/2} = 50$ TeV, $\tan\beta = 10$ and $\mu > 0$.

parameter	mAMSB	HCAMSB1	inoAMSB1	inoAMSB2
α	—	0.025	—	—
m_0	300	—	—	—
$m_{3/2}$	50 TeV	50 TeV	50 TeV	100 TeV
$\tan\beta$	10	10	10	10
M_1	460.3	997.7	465.5	956.1
M_2	140.0	139.5	143.8	287.9
μ	872.8	841.8	607.8	1127.5
$m_{\tilde{g}}$	1109.2	1107.6	1151.0	2186.1
$m_{\tilde{u}_L}$	1078.2	1041.3	1011.7	1908.7
$m_{\tilde{u}_R}$	1086.2	1160.3	1045.1	1975.7
$m_{\tilde{t}_1}$	774.9	840.9	878.8	1691.8
$m_{\tilde{t}_2}$	985.3	983.3	988.4	1814.8
$m_{\tilde{b}_1}$	944.4	902.6	943.9	1779.5
$m_{\tilde{b}_2}$	1076.7	1065.7	1013.7	1908.3
$m_{\tilde{e}_L}$	226.9	326.3	233.7	457.8
$m_{\tilde{e}_R}$	204.6	732.3	408.6	809.5
$m_{\widetilde{W}_2}$	879.2	849.4	621.2	1129.8
$m_{\widetilde{W}_1}$	143.9	143.5	145.4	299.7
$m_{\widetilde{Z}_4}$	878.7	993.7	624.7	1143.2
$m_{\widetilde{Z}_3}$	875.3	845.5	614.4	1135.8
$m_{\widetilde{Z}_2}$	451.1	839.2	452.6	936.8
$m_{\widetilde{Z}_1}$	143.7	143.3	145.1	299.4
m_A	878.1	879.6	642.9	1208.9
m_h	113.8	113.4	112.0	116.0
$\Omega_{\widetilde{Z}_1}h^2$	0.0016	0.0015	0.0016	0.007
σ [fb]	7.7×10^3	7.4×10^3	7.5×10^3	439
$\tilde{g},\tilde{q}$ pairs	15.0%	15.5%	19.1%	3%
EW − ino pairs	79.7%	81.9%	75.6%	93%
slep. pairs	3.7%	0.8%	3.1%	3%
$\tilde{t}_1\bar{\tilde{t}}_1$	0.4%	0.2%	0.1%	0%

Table 2.1: Masses and parameters in GeV units for four case study points mAMSB1, HCAMSB1, inoAMSB1 and inoAMSB2 using Isajet 7.80 with $m_t = 172.6$ GeV and $\mu > 0$. We also list the total tree level sparticle production cross section in fb at the LHC.

Next, we investigate the effect of varying $m_{3/2}$ on the sparticle mass spectrum. We plot in Fig. 2.3 the mass spectra of various sparticles versus $m_{3/2}$ in the inoAMSB model while taking $\tan\beta = 10$, $\mu > 0$ and $m_t = 172.6$ GeV. The lowest value of $m_{3/2}$ which is allowed is $m_{3/2} = 32.96$ TeV. Below this value, $m_{\widetilde{W}_1} < 91.9$ GeV, which is excluded by LEP2 searches for charginos from AMSB models [36]. We see from Fig. 2.3 that there is a characteristic mass hierarchy in the inoAMSB model, where $m_{\widetilde{Z}_1,\widetilde{W}_1} < m_{\tilde{e}_L,\tilde{\nu}_{eL}} < m_{\tilde{e}_R} < |\mu| < m_{\tilde{q}} < m_{\tilde{g}}$. As $m_{3/2}$ increases, all these masses grow, but the relative hierarchy is maintained. For such a spectrum with $m_{\tilde{q}} < m_{\tilde{g}}$ and with relatively light sleptons, we would thus expect LHC collider events which are dominated by squark pair production, followed by squark cascade decays $\tilde{q} \to q\widetilde{Z}_i \to q\tilde{\ell}^{\pm}\ell^{\mp}$, which would lead to events with two hard jets (plus additional softer jets) and rich in isolated leptons coming from cascade decay produced sleptons.

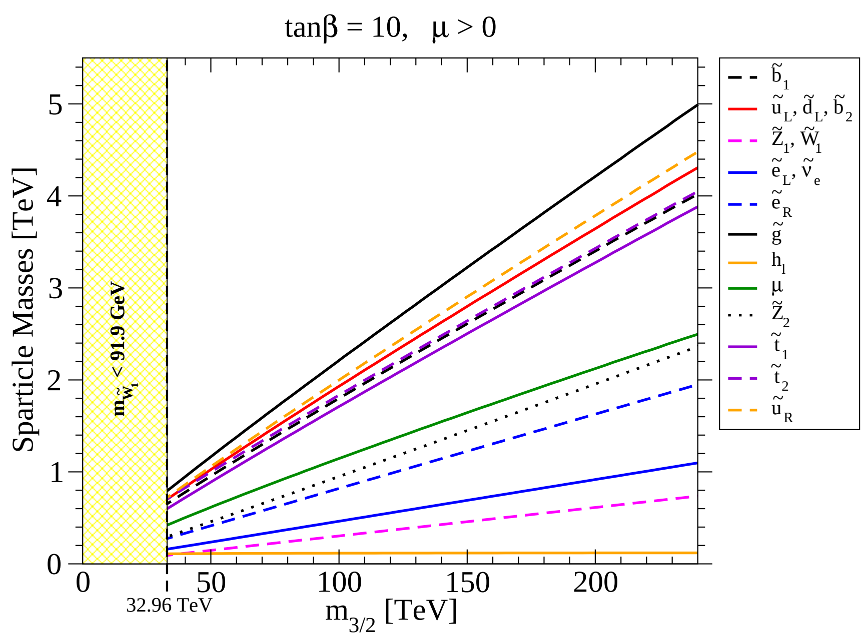

Figure 2.3: Sparticle mass spectrum versus $m_{3/2}$ in the inoAMSB with $M_{string} = M_{GUT}$, $\tan\beta = 10$, with $\mu > 0$ and $m_t = 172.6$ GeV.

In Fig. 2.4, we show the variation in sparticle masses against $\tan\beta$ with $m_{3/2}$ fixed at 50 TeV. As $\tan\beta$ increases, the b and τ Yukawa couplings both increase. These act to suppress the sbottom and stau SSB mass terms, and also give larger left-right mixing to the mass eigenstates. In addition, the value of $m_{H_d}^2$ is pushed to negative values by the large b and τ Yukawa couplings. The value of m_A is given approximately from the EWSB minimization conditions as $m_A^2 \sim m_{H_d}^2 - m_{H_u}^2$. Since the mass gap between $m_{H_u}^2$ and $m_{H_d}^2$ drops as $\tan\beta$ increases, the value of m_A also drops sharply with increasing $\tan\beta$. The point at which m_A drops below limits from LEP2 searches (and shortly thereafter REWSB no longer occurs in a valid fashion) provides the high $\tan\beta$ boundary to the parameter space.

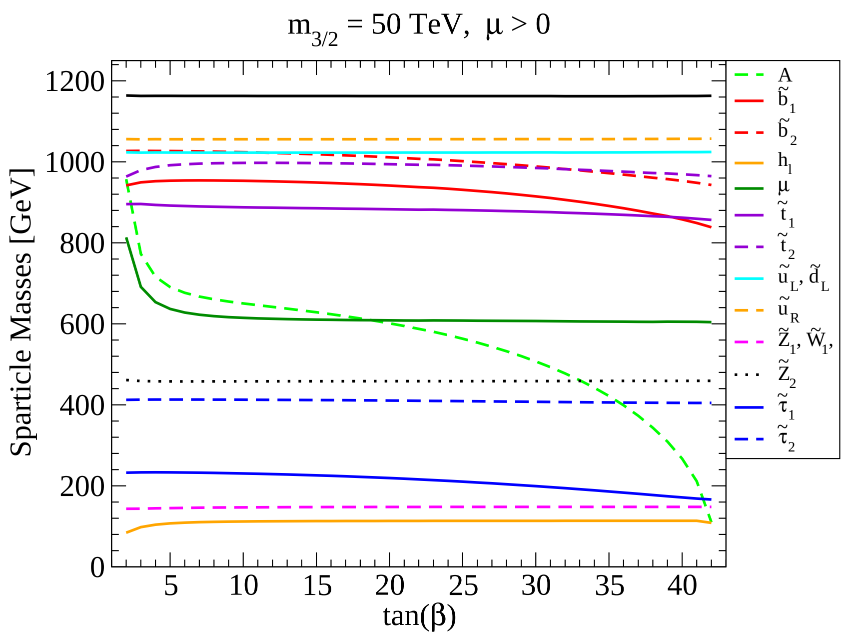

Figure 2.4: Sparticle mass spectrum versus $\tan\beta$ for $m_{3/2} = 50$ TeV in the inoAMSB with $M_{string} = M_{GUT}$ and with $\mu > 0$.

In Fig. 2.5, we show the entire parameter space for the inoAMSB model in the $m_{3/2}$ vs. $\tan\beta$ plane for $\mu > 0$ with $m_t = 172.6$ GeV. The gray shaded region gives allowable sparticle mass spectra. The orange region gives chargino masses below the LEP2 limit, and so is experimentally excluded. The brown shaded region for $\tan\beta \gtrsim 42$ is excluded because REWSB no longer occurs in an appropriate fashion. The brown shaded region at very low $\tan\beta$ gives too light a value of m_h: here we require $m_h > 111$ GeV (even though LEP2 requires $m_h > 114.4$ GeV), due to a projected $\sim \pm 3$ GeV theory error on our lightest Higgs mass calculation. We also show contours of $m_{\tilde{g}}$ ranging from 1-5 TeV. The $m_{\tilde{g}} \sim 5$ TeV range will surely be beyond the reach of LHC.

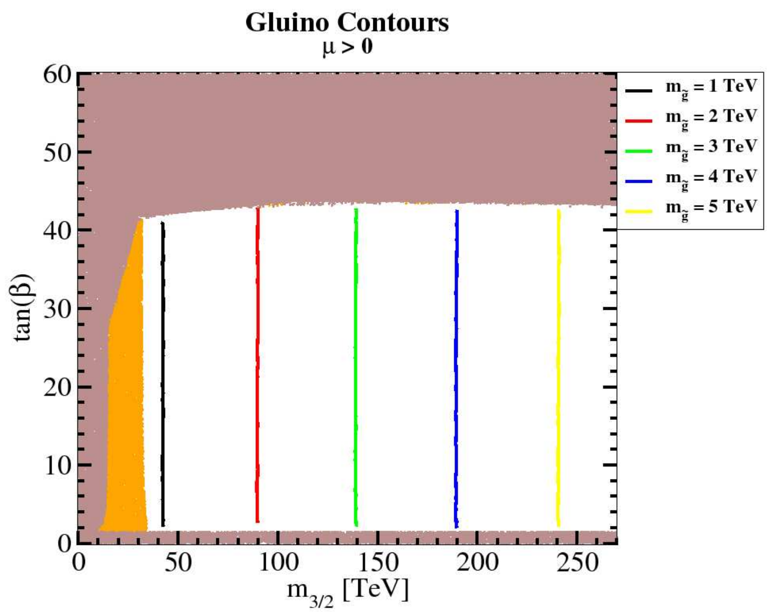

Figure 2.5: Allowed parameter space of the inoAMSB models in the $m_{3/2}$ vs. $\tan\beta$ plane with $\mu > 0$. We plot also contours of $m_{\tilde{g}}$.

As noted in Sec. 2.2, in the inoAMSB model the string scale M_{string} need not be equal to M_{GUT}. If it is not, then it can have significant effects on the sparticle mass spectrum. The sparticle mass spectrum versus variable M_{string} is shown in Fig. 2.6 for the case where $m_{3/2} = 50$ TeV, $\tan\beta = 10$ and $\mu > 0$. Here, we see that the sparticle mass spectrum spreads out as M_{string} varies from M_{GUT} down to 10^{11} GeV. In addition, some important level crossings occur. Most important of these is that for $M_s \lesssim 5 \times 10^{13}$ GeV, the $\tilde{\nu}_\tau$ state becomes the lightest MSSM particle, and for even lower M_s values, $m_{\tilde{\nu}_e}$ and $m_{\tilde{\nu}_\mu}$ drop below $m_{\widetilde{Z}_1}$. There already exist severe limits on stable sneutrino dark matter [37], which discourage this type of scenario. If we insist upon a neutralino as LSP, then we must take not too low a value of M_s.

Finally, we note that in the inoAMSB model, scalar masses and A-parameters are expected to be suppressed, but they are not expected to be exactly zero. In Fig. 2.7, we show the mass

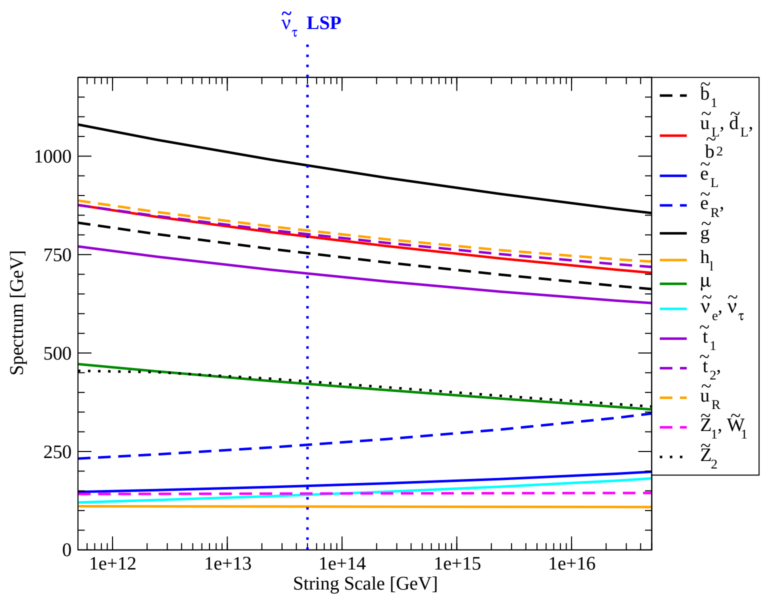

Figure 2.6: Plot of sparticle masses for the inoAMSB1 case study with $m_{3/2} = 50$ TeV, $\tan\beta = 10$ and $\mu > 0$, but with variable value of M_{string}.

spectra from inoAMSB models where we add an additional universal mass contribution m_0 to all scalars. We adopt values $m_{3/2} = 50$ TeV and $\tan\beta = 10$ for this plot. As m_0 increases beyond zero, it is seen that the spectra change little so long as $m_0 \lesssim 100$ GeV, and also the mass orderings remain intact. For larger values of m_0, the left- and right- slepton masses begin to increase, with first $m_{\tilde{e}_R}$ surpassing $m_{\widetilde{Z}_2}$, and later even $m_{\tilde{e}_L}$ surpasses $m_{\widetilde{Z}_2}$. At these high values of m_0, decay modes such as $\widetilde{Z}_2 \to \ell^{\pm}\tilde{\ell}^{\mp}$ would become kinematically closed, thus greatly altering the collider signatures. However, generically in this class of models, we would not expect such large additional contributions to scalar masses.

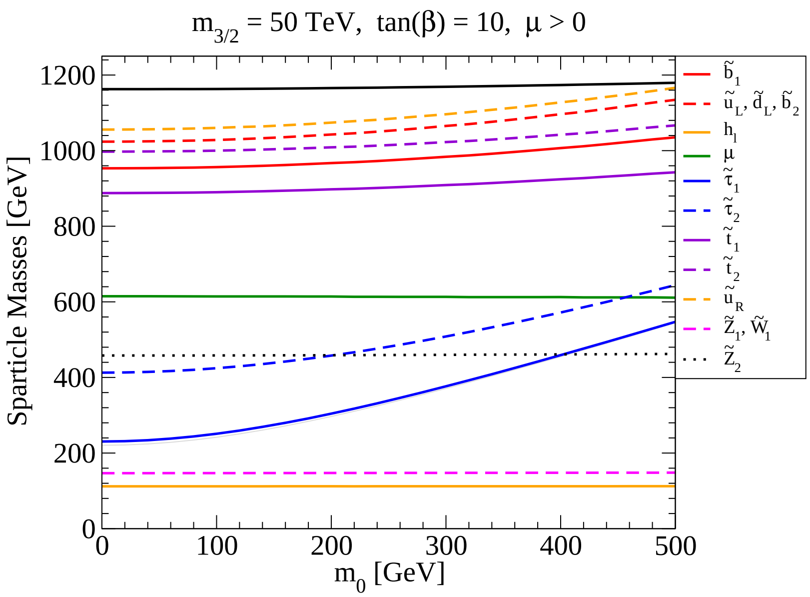

Figure 2.7: Plot of sparticle masses for the inoAMSB with $m_{3/2} = 50$ TeV, $\tan\beta = 10$ and $\mu > 0$, but with an additional universal contribution m_0 added to all scalar masses.

2.3.2 $BF(b \to s\gamma)$ and $(g-2)_\mu$ in inoAMSB

Along with experimental constraints on the inoAMSB models from LEP2 limits on m_h and $m_{\widetilde{W}_1}$, there also exist indirect limits on model parameter space from comparing measured values of $BF(b \to s\gamma)$ and $\Delta a_\mu \equiv (g-2)_\mu/2$ against SUSY model predictions.

2.3.2.1 $BF(b \to s\gamma)$

As an example, we show in Fig. 2.8 regions of the branching fraction for $BF(b \to s\gamma)$ in the inoAMSB model versus $m_{3/2}$ and $\tan\beta$ variation, calculated using the Isatools subroutine ISABSG [38]. The red-shaded region corresponds to branching fraction values within the SM theoretically predicted region $BF(b \to s\gamma)_{SM} = (3.15 \pm 0.23) \times 10^{-4}$, by a recent evaluation by Misiak [39]). The blue-shaded region corresponds to branching fraction values within the experimentally allowed region [40]: here, the branching fraction $BF(b \to s\gamma)$ has been measured by the CLEO, Belle and BABAR collaborations; a combined analysis [40] finds the branching fraction to be $BF(b \to s\gamma) = (3.55 \pm 0.26) \times 10^{-4}$. The gray shaded region gives too large a value of $BF(b \to s\gamma)$. This region occurs for low $m_{3/2}$, where rather light $\tilde{t}_1$ and $\widetilde{W}_1$ lead to large branching fractions, or large $\tan\beta$, where also the SUSY loop contributions are enhanced [41].

2.3.2.2 $(g-2)_\mu/2$

In Fig. 2.9, we plot the SUSY contribution to Δa_μ: Δa_μ^{SUSY} (using ISAAMU from Isatools [34]). The contribution is large when $m_{3/2}$ is small; in this case, rather light $\tilde{\mu}_L$ and $\tilde{\nu}_{\mu L}$ masses lead to large deviations from the SM prediction. The SUSY contributions to Δa_μ^{SUSY} also increase with $\tan\beta$. It is well-known that there is a discrepancy between the SM predictions for Δa_μ, where τ decay data, used to estimate the hadronic vacuum polarization contribution to Δa_μ, gives rough accord with the SM, while use of $e^+e^- \to hadrons$ data at very low energy leads to a roughly 3σ discrepancy. The measured Δa_μ anomaly, given as $(4.3 \pm 1.6) \times 10^{-9}$ by the Muon $g-2$ Collaboration [33], is shown by the black dotted region.

2.3.2.3 Dark matter in inoAMSB

Finally, we remark upon the relic density of dark matter in the inoAMSB model. If thermal production of the lightest neutralino is assumed to give the dominant DM in the universe, then all over parameter space, the predicted neutralino abundance $\Omega_{\widetilde{Z}_1}h^2$ is far below the WMAP measured value of $\Omega_{CDM}h^2 = 0.1126 \pm 0.0036$ [42]. Some sample calculated values are listed in Table 2.1.

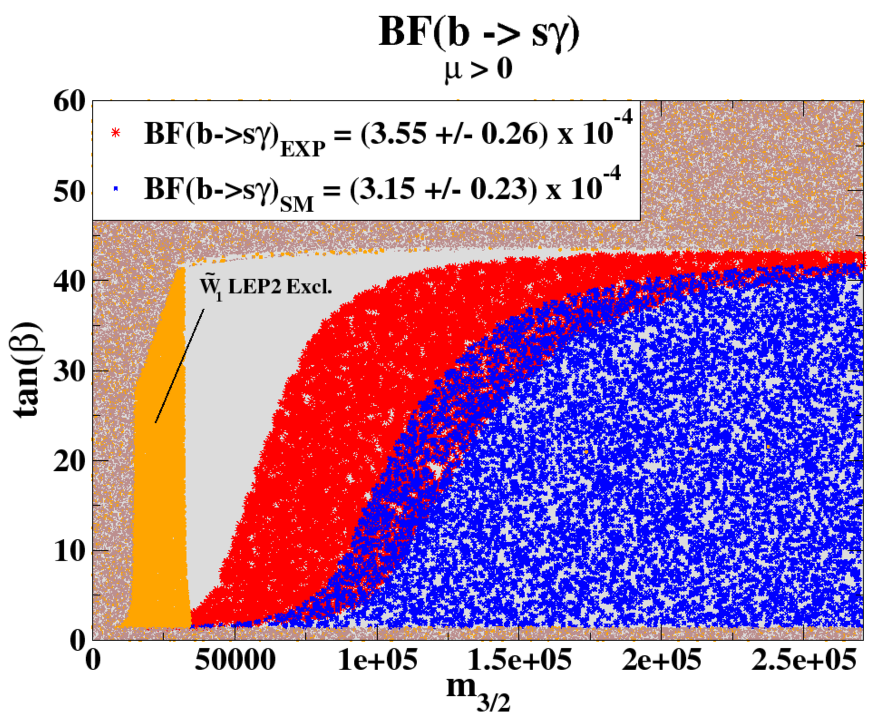

Figure 2.8: Branching fraction for $b \to s\gamma$ versus $m_{3/2}$ and $\tan\beta$ variation in the inoAMSB model with $M_{string} = M_{GUT}$.

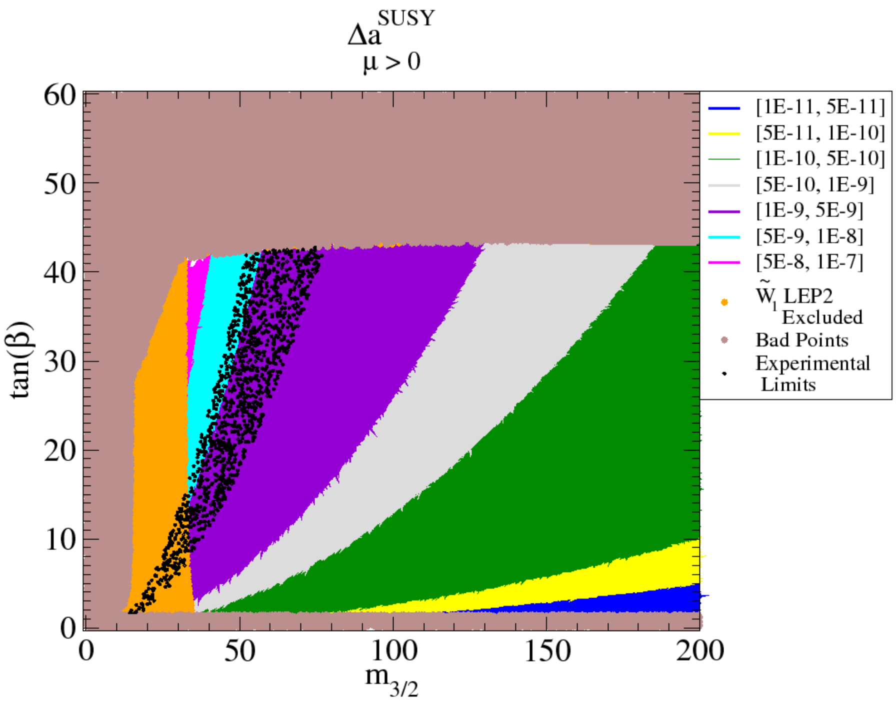

Figure 2.9: SUSY contribution to Δa_μ versus $m_{3/2}$ and $\tan\beta$ variation in the inoAMSB model with $M_{string} = M_{GUT}$. We also take $\mu > 0$ and $m_t = 172.6$ GeV.

It has been suggested in Ref. [43] that production and decay of moduli fields or other processes can also contribute to the DM abundance. Decay of moduli fields in the early universe could then account for the discrepancy between the measured DM abundance and the predicted thermal abundance in inoAMSB models.

As an alternative, if the strong CP problem is solved via the Peccei-Quinn mechanism, then a superfield containing the axion/axino multiplet should occur. In this case, a mixture of axions [44] and axinos [45], rather than wino-like neutralinos, could constitute the DM abundance [46]. The exact abundance will depend on the axino mass $m_{\tilde{a}}$, the Peccei-Quinn breaking scale f_a, and the re-heat temperature T_R after inflation.

In light of these two alternative DM mechanisms, we regard the inoAMSB parameter space as essentially unconstrained by the measured abundance of DM in the universe.

2.4 The inoAMSB model and the LHC

2.4.1 Sparticle production at LHC

In the inoAMSB model, for benchmark point inoAMSB1, we list several sparticle production cross sections in Table 2.1. We see that for this case, the dominant sparticle production consists of electroweak-ino pair production: mainly $pp \to \widetilde{W}_1^+\widetilde{W}_1^-$ and $\widetilde{W}_1^\pm\widetilde{Z}_1$ reactions. Since $\widetilde{Z}_1$ is stable (or quasi-stable in the event of light axino dark matter), and mainly $\widetilde{W}_1^\pm \to \pi^\pm\widetilde{Z}_1$ (where the $\pi^\pm$ is very soft), these reactions do not provide enough visible energy to meet detector trigger requirements (unless there is substantial initial state radiation).

The major visible production reactions consist of $pp \to \tilde{g}\tilde{g}$, $\tilde{g}\tilde{q}$ and $\tilde{q}\tilde{q}$ production (here, we take $\tilde{q}$ to represent generic species of both squarks and anti-squarks). In the case of inoAMSB models, we expect $m_{\tilde{q}} \sim 0.9 m_{\tilde{g}}$. Strongly interacting sparticle production cross sections (at NLO using Prospino [71]) are shown versus $m_{3/2}$ in Fig. 3.2 for $\tan\beta = 10$, $\mu > 0$ and $M_s = M_{GUT}$. We see that the reactions $pp \to \tilde{q}\tilde{q}$ and $\tilde{q}\tilde{g}$ are roughly comparable, with $\tilde{q}\tilde{g}$ production dominating for $m_{3/2} \lesssim 65$ TeV, and $\tilde{q}\tilde{q}$ pair production dominating for higher $m_{3/2}$ values. The $pp \to \tilde{g}\tilde{g}$

production cross section always occurs at much lower rates. For $m_{\tilde{g}} \sim 3$ TeV, corresponding to $m_{3/2} \sim 150$ TeV, the total hadronic SUSY cross section is around 0.1 fb, which should be around the upper limit of LHC reach given 100 fb^{-1} of integrated luminosity.

Since sleptons are much lighter than squarks in inoAMSB models, we also expect possibly observable rates for slepton pair production. Pair production rates for $pp \to \tilde{e}_L^+\tilde{e}_L^-$, $\tilde{e}_R^+\tilde{e}_R^-$ and $\tilde{\nu}_{eL}\tilde{e}_L$ are also shown in Fig. 3.2. Typically, the LHC reach for direct slepton pair production ranges up to $m_{\tilde{\ell}} \sim 350$ GeV for 10 fb^{-1} [48], corresponding to a $m_{3/2}$ value of ~ 75 TeV. Thus, LHC reach should be much higher in the hadronic SUSY production channels.

2.4.2 Sparticle decays in inoAMSB models

Since $m_{\tilde{g}} > m_{\tilde{q}}$ in inoAMSB models, we will have $\tilde{g} \to q\tilde{q}$, nearly democratically to all squark species. The left-squarks will dominantly decay to $wino + q$, and we find $\tilde{q}_L \to q\widetilde{W}_1$ at $\sim 67\%$, while $\tilde{q}_L \to q\widetilde{Z}_1$ at $\sim 33\%$, all over parameter space. The right-squark decays are simpler. The $\tilde{q}_R$ decays mainly to $bino + q$, so that in the inoAMSB model line, we obtain $\tilde{q}_R \to \widetilde{Z}_2 q$ at $\sim 97\%$ over almost all parameter space, since in this case $\widetilde{Z}_2$ is nearly pure bino-like.

For the sleptons, the left-sleptons dominantly decay to $wino + lepton$, so we find $\tilde{\ell}_L \to \ell\widetilde{Z}_1$ at $\sim 33\%$, and $\tilde{\ell}_L \to \widetilde{W}_1\nu_{\ell L}$ at $\sim 67\%$ all over parameter space. The latter decay mode should be nearly invisible, unless the highly ionizing $\widetilde{W}_1$ track is found in the micro-vertex detector. The sneutrino decays as $\tilde{\nu}_{\ell L} \to \widetilde{Z}_1\nu_\ell$ at $\sim 33\%$, which is again nearly invisible. However, it also decays via $\tilde{\nu}_{\ell L} \to \ell\widetilde{W}_1$ at $\sim 66\%$, which provides a detectable decay mode for the sneutrinos. The $\tilde{e}_R$ would like to decay to $bino + lepton$, but in the case of inoAMSB models, the bino-like neutralino is too heavy for this decay to occur. In the case of inoAMSB1 benchmark point, we instead get $\tilde{\ell}_R \to e\widetilde{Z}_1$ at $\sim 78\%$. Since this decay mode is suppressed, some three body decay modes can become comparable. In his case, we find $\tilde{\ell}_R^- \to \ell^-\tau^+\tilde{\tau}_1^-$ at $\sim 13\%$, and $\tilde{\ell}_R^- \to \ell^-\tau^-\tilde{\tau}_1^+$ at $\sim 7\%$.

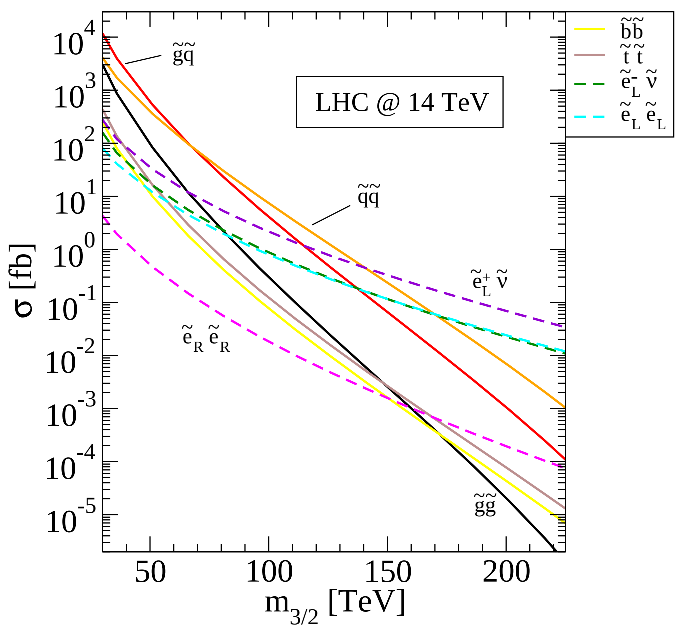

Figure 2.10: Sparticle pair production cross sections at LHC with $\sqrt{s} = 14$ TeV for the inoAMSB model with $\tan\beta = 10$ and $\mu > 0$.

2.4.3 LHC collider events for the inoAMSB models

We use Isajet 7.80 [29] for the simulation of signal and background events at the LHC. A toy detector simulation is employed with calorimeter cell size $\Delta\eta \times \Delta\phi = 0.05 \times 0.05$ and $-5 < \eta < 5$. The hadronic calorimeter (HCAL) energy resolution is taken to be $80\%/\sqrt{E} + 3\%$ for $|\eta| < 2.6$ and forward calorimeter (FCAL) is $100\%/\sqrt{E} + 5\%$ for $|\eta| > 2.6$. The electromagnetic (ECAL) energy resolution is assumed to be $3\%/\sqrt{E} + 0.5\%$. We use the UA1-like jet finding algorithm GETJET with jet cone size $R = 0.4$ and require that $E_T(jet) > 50$ GeV and $|\eta(jet)| < 3.0$. Leptons are considered isolated if they have $p_T(e \ or \ \mu) > 20$ GeV and $|\eta| < 2.5$ with visible activity within a cone of $\Delta R < 0.2$ of $\Sigma E_T^{cells} < 5$ GeV. The strict isolation criterion helps reduce multi-lepton backgrounds from heavy quark ($c\bar{c}$ and $b\bar{b}$) production.

We identify a hadronic cluster with $E_T > 50$ GeV and $|\eta(j)| < 1.5$ as a b-jet if it contains a B hadron with $p_T(B) > 15$ GeV and $|\eta(B)| < 3$ within a cone of $\Delta R < 0.5$ about the jet axis. We adopt a b-jet tagging efficiency of 60%, and assume that light quark and gluon jets can be mis-tagged as b-jets with a probability 1/150 for $E_T < 100$ GeV, 1/50 for $E_T > 250$ GeV, with a linear interpolation for 100 GeV$< E_T < 250$ GeV [49].

We have generated 2M events for case inoAMSB1 from Table 2.1. In addition, we have generated background events using Isajet for QCD jet production (jet-types include g, u, d, s, c and b quarks) over five p_T ranges as shown in Table 2.2. Additional jets are generated via parton showering from the initial and final state hard scattering subprocesses. We have also generated backgrounds in the $W + jets$, $Z + jets$, $t\bar{t}(172.6)$ and $WW,\ WZ,\ ZZ$ channels at the rates shown in the same Table. The $W + jets$ and $Z + jets$ backgrounds use exact matrix elements for one parton emission, but rely on the parton shower for subsequent emissions.

For our initial selection of signal events, we first require the following minimal set of cuts labeled **C1**:

- $n(jets) \geq 2$,
- $E_T^{\rm miss} > max\ (100 \text{ GeV}, 0.2M_{eff})$

- $E_T(j1,\ j2) > 100,\ 50$ GeV,

- transverse sphericity $S_T > 0.2$,

where $M_{eff} = E_T^{\rm miss} + E_T(j1) + E_T(j2) + E_T(j3) + E_T(j4)$.

Since sparticle production in inoAMSB models is dominated by $\tilde{q}\tilde{g}$ and $\tilde{q}\tilde{q}$ reactions, followed by $\tilde{q} \to q\widetilde{Z}_i$ or $q'\widetilde{W}_j$, we expect at least two very hard jets in each signal event. In Fig. 2.11, we plot out the distribution in a). hardest and b). second hardest jet p_T for the signal case inoAMSB1 along with the summed SM background (denoted by gray histograms). In the case of $p_T(j_1)$, background is dominant for lower p_T values $\lesssim$ 400 GeV, while signal emerges from background for higher p_T values. In the case of $p_T(j_2)$, signal emerges from background already around 250-300 GeV. The rather hard jet p_T distributions are characteristic of squark pair production, followed by 2-body squark decay into a hard jet.

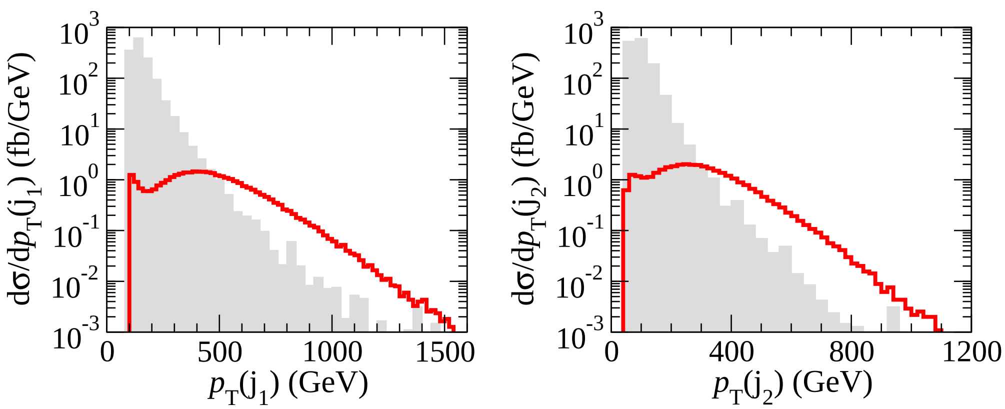

Figure 2.11: Distribution in p_T of a). the hardest and b). second hardest jets from the inoAMSB1 model, and summed SM background (gray histogram), for LHC collisions at $\sqrt{s} = 14$ TeV.

In Fig. 2.12, we show the distributions in a). $E_T^{\rm miss}$ and b). $A_T = \sum E_T$ (where the sum extends over all jets and isolated leptons) expected from inoAMSB1 along with SM background. In this case, the $E_T^{\rm miss}$ distribution from SUSY emerges from background at around 400-500 GeV, illustrating the rather hard $E_T^{\rm miss}$ distribution expected from $\tilde{g}\tilde{q}$ and $\tilde{q}\tilde{q}$ pair production, followed by 2-body decays. The A_T signal distribution actually exhibits two components: a soft peak around 400 GeV which comes from chargino, neutralino and slepton pair production, and a hard peak at much higher values coming from gluino and squark pair production. The low peak is buried under background, while the higher peak emerges from background at around 1400 GeV.

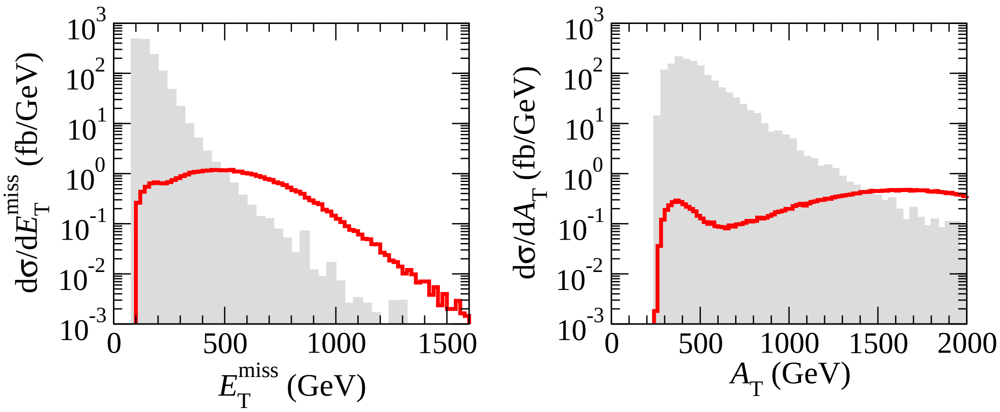

Figure 2.12: Distribution in *a*). $E_T^{\rm miss}$ and *b*). A_T from the inoAMSB1 model, and summed SM background (gray histogram), for LHC collisions at $\sqrt{s} = 14$ TeV.

Fig. 2.13 shows the distribution in *a*). jet multiplicity n_j and *b*). isolated lepton (both es and μs) multiplicity n_ℓ from the inoAMSB1 benchmark, compared to SM background after C1 cuts. While the signal is dominated by $\tilde{q}\tilde{q}$ and $\tilde{q}\tilde{g}$ pair production, the jet multiplicity actually exhibits a broad peak around $n_j \sim 2-5$. Nominally, we would expect dijet dominance from squark pair production. But additional jets from cascade decays and initial state radiation help broaden the distribution. The broadness of the distribution also depends on our jet E_T cut, which requires only that $E_T(jet) > 50$ GeV. In the case of isolated lepton multiplicity, we see that background dominates signal for $n_\ell = 0,\ 1$ and 2. However, BG drops more precipitously as n_ℓ increases, so that for $n_\ell = 3$ or 4, signal now dominates background [50]. In these cases, even with minimal cuts, an isolated $3\ell + \geq 2$ jets$+E_T^{\rm miss}$ signal should stand out well above background.

2.4.3.1 LHC cascade decay events including HITs: a smoking gun for models with wino-like neutralinos

Of course, a distinctive property of models like inoAMSB (and also mAMSB and HCAMSB) with a wino-like $\widetilde{Z}_1$ state is that the chargino is very long lived [51]: of order $\sim 10^{-10}$ sec. Thus,

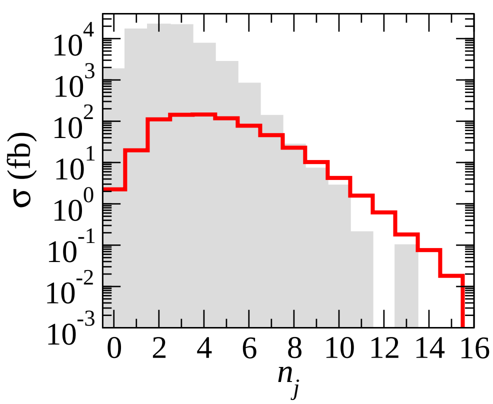

Figure 2.13: Distribution in a). $n(jets)$ and b). $n(leptons)$ from the inoAMSB1 model, and summed SM background (gray histogram), for LHC collisions at $\sqrt{s} = 14$ TeV.

once we have obtained cascade decay signal events in any of the multi-jet plus multi-lepton plus $E_T^{\rm miss}$ channels, we may in addition look for the presence of a highly-ionizing track (HIT) from the long-lived chargino. The presence of HITs in the SUSY collider events would be indictative of models such as inoAMSB, mAMSB or HCAMSB, where $M_2 \ll M_1$ and M_3, so that the lightest neutralino is a nearly pure wino state and where $m_{\widetilde{W}_1} \simeq m_{\widetilde{Z}_1}$.

2.4.4 The reach of LHC in the inoAMSB model line

We would next like to investigate the reach of the CERN LHC for SUSY in the inoAMSB context. To this end, we will adopt the inoAMSB model line with variable $m_{3/2}$ but fixed $\tan\beta = 10$ and $\mu > 0$. The sparticle mass spectra versus $m_{3/2}$ was shown previously in Fig. 2.3

Motivated by the previous signal and background distributions, we will require the following cuts $C2$ [52]:

- $n(jets) \geq 2$
- $S_T > 0.2$
- $E_T(j1),\ E_T(j2),\ E_T^{\rm miss} > E_T^c$,

where E_T^c can be variable. Parameter space points with lower sparticle masses will benefit from lower choices of E_T^c, while points with heavier sparticle masses– with lower cross sections but higher energy release per event– will benefit from higher choices of E_T^c. In addition, in the zero-leptons channel we require $30^\circ < \Delta\phi(\vec{E}_T^{miss}, \vec{E}_T(j_c)) < 90^\circ$ between the $\vec{E}_T^{miss}$ and the nearest jet in transverse opening angle. For all isolated leptons ℓ, we require $p_T(\ell) > 20$ GeV. We separate the signal event channels according to the multiplicity of isolated leptons: we exhibit the 0ℓ, opposite-sign (OS) dilepton, 3ℓ and 4ℓ channels. Here, we do not here require "same flavor" on the OS dilepton events. We suppress the 1ℓ and same-sign dilepton SS channels for brevity, and because the reach is better in the channels shown.

The resultant cross sections after cuts $C2$ for SM backgrounds along with signal point inoAMSB1 are listed in Table 2.2 for $E_T^c = 100$ GeV. For each BG channel, we have generated

process	0ℓ	OS	SS	3ℓ	4ℓ
QCD(p_T: 0.05-0.10 TeV)	–	–	–	–	–
QCD(p_T: 0.10-0.20 TeV)	755.1	–	–	–	–
QCD(p_T: 0.20-0.40 TeV)	803.8	621.1	109.6	36.5	–
QCD(p_T: 0.40-1.00 TeV)	209.8	304.7	72.6	29.0	2.6
QCD(p_T: 1.00-2.40 TeV)	2.2	5.3	1.7	1.5	0.2
$t\bar{t}$	1721.4	732.6	273.8	113.3	6.6
$W + jets; W \to e, \mu, \tau$	527.4	22.6	8.4	1.3	$--$
$Z + jets; Z \to \tau\bar{\tau},\ \nu s$	752.9	11.1	1.3	0.2	$--$
WW, ZZ, WZ	3.4	0.3	0.25	$--$	$--$
summed SM BG	4776.1	1697.8	467.7	181.9	9.4
inoAMSB1	112.7	85.7	27.6	36.0	7.5

Table 2.2: Estimated SM background cross sections (plus the inoAMSB1 benchmark point) in fb for various multi-lepton plus jets $+E_T^{\rm miss}$ topologies after cuts C2 with $E_T^c = 100$ GeV.

~ 2 million simulated events. With the hard cuts $C2$, we are unable to pick up BG cross sections in some of the multi-lepton channels. We will consider a signal to be observable at an assumed value of integrated luminosity if *i*) the signal to background ratio, $S/BG \geq 0.1$, *ii*) the signal has a minimum of five events, and *iii*) the signal satifies a statistical criterion $S \geq 5\sqrt{BG}$ (a 5σ effect).

Using the above criteria, the 100 fb^{-1} reach of the LHC can be computed for each signal channel. In Fig. 2.14, we show the signal rates versus $m_{3/2}$ for the inoAMSB model line for $E_T^c = 100$ (solid blue), 300 (dot-dash red) and 500 GeV (dashed purple). The 100 fb^{-1} LHC reach is denoted by the horizontal lines for each E_T^c value. From frame *a*)., for the multi-jet$+E_T^{\rm miss}$$+0\ell$ signal, we see the LHC reach in the 0ℓ channel extends to $m_{3/2} \sim 40,\ 93$ and 110 TeV for $E_T^c = 100,\ 300$ and 500 GeV, respectively, for the inoAMSB model line. This corresponds to a reach in $m_{\tilde{g}}$ of 1.1, 2.0 and 2.4 TeV.

Frames *b*)., *c*). and *d*). show the reach in the multi-jet$+E_T^{\rm miss}$$+\ OS$, 3ℓ and 4ℓ channels, respectively. While the reach is qualitatively similar in all channels, the best reach comes from the 3ℓ channel, where the 100 fb^{-1} LHC can detect inoAMSB models up to $m_{3/2} \sim 118$ TeV (corresponding to a reach in $m_{\tilde{g}}$ of 2.6 TeV), using $E_T^c = 500$ GeV. The 100 fb^{-1} LHC reach for all cases is summarized in Table 2.3.

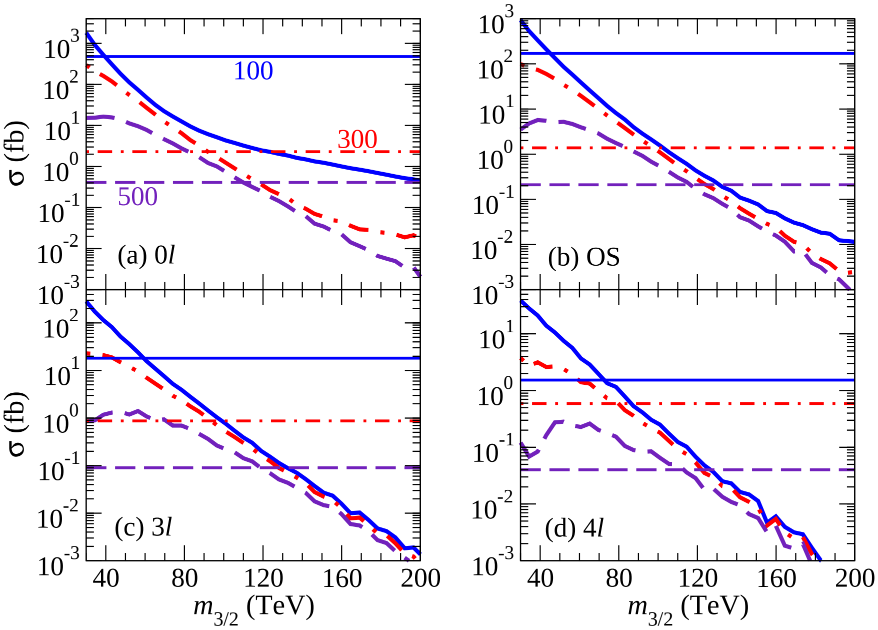

Figure 2.14: Cross section for multi-jet plus $E_T^{\rm miss}$ events with a). $n(\ell) = 0$, b). OS isolated dileptons c). isolated 3ℓs and d). isolated 4ℓs at the LHC after cuts $C2$ listed in the text with $E_T^c = 100$ GeV (blue solid), $E_T^c = 300$ GeV (red dot-dashed) and $E_T^c = 500$ GeV (purple dashes), versus $m_{3/2}$, from the inoAMSB model line points with $\tan\beta = 10$ and $\mu > 0$. We also list the 100 fb^{-1} 5σ, 5 event, $S > 0.1\ BG$ limit with the horizontal lines.

E_T^c (GeV)	0ℓ	OS	3ℓ	4ℓ
100	40	57	60	75
300	93	95	98	80
500	110	115	118	110

Table 2.3: Estimated reach of 100 fb^{-1} LHC for $m_{3/2}$ (TeV) in the inoAMSB model line in various signal channels.

2.4.4.1 Cascade decays including HITs plus a multi-bump $m(\ell^+\ell^-)$ distribution: a smoking gun for inoAMSB models

Next, we examine the distribution in $m(\ell^+\ell^-)$ for cascade decay events containing: ≥ 2 high p_T jets, large $E_T^{\rm miss}$ and a pair of same flavor/opposite-sign (SF/OS) dileptons. This distribution has for long been touted as being very useful as a starting point for reconstructing sparticle masses in SUSY cascade decay events, because it may contain a kinematic mass edge from $\widetilde{Z}_2 \to \tilde{\ell}^{\pm}\ell^{\mp}$ or $\widetilde{Z}_2 \to \ell^+\ell^-\widetilde{Z}_1$ decays. In the case of the inoAMSB1 benchmark model, where $m_{\tilde{\ell}_{L,R}} < m_{\widetilde{Z}_2}$– and a substantial mass gap between $m_{\tilde{\ell}_L}$ and $m_{\tilde{\ell}_R}$ is featured– we expect *two* distinct, well-separated mass edges: one from $\widetilde{Z}_2 \to \tilde{\ell}_L\ell$ and one from $\widetilde{Z}_2 \to \tilde{\ell}_R\ell$ decays. In addition, a peak at $m(\ell^+\ell^-) \sim M_Z$ is expected, since real Z bosons can be emitted from cascade decays including $\widetilde{Z}_3 \to Z\widetilde{Z}_1$, $\widetilde{Z}_4 \to Z\widetilde{Z}_1$ and $\widetilde{W}_2 \to Z\widetilde{W}_1$ (in the case of benchmark model inoAMSB1, these decays occur with branching fractions 25%, 6% and 29%, respectively).

In Fig. 2.15, we show the $m(\ell^+\ell^-)$ distribution from inoAMSB1 (red histogram) in frame *a*). Here, we require cuts $C1$, along with $E_T^{\rm miss} > 300$ GeV and $A_T > 900$ GeV, which completely suppresses SM backgrounds. Indeed, we see clearly a Z boson peak at M_Z, along with two distinct mass edges occuring at $m(\ell^+\ell^-) = m_{\widetilde{Z}_2}\sqrt{1-\frac{m_{\tilde{\ell}}^2}{m_{\widetilde{Z}_2}^2}}\sqrt{1-\frac{m_{\widetilde{Z}_1}^2}{m_{\tilde{\ell}}^2}} = 182$ GeV, and 304 GeV. The 182 GeV edge comes from $\widetilde{Z}_2$ decays through $\tilde{\ell}_R$, while the 304 GeV edge comes from $\widetilde{Z}_2$ decays through $\tilde{\ell}_L$. We also show the same distribution for the mAMSB1 (green) and HCAMSB1 (blue) cases from Table 2.1. The mAMSB plot contains two mass edges as well. However, since in mAMSB we expect $m_{\tilde{\ell}_L} \simeq m_{\tilde{\ell}_R}$, these edges nearly overlap, and are essentially indistinguishable. In the case of HCAMSB models, the bino-like neutralino is the $\widetilde{Z}_4$ and is quite heavy, while $\widetilde{Z}_2$ and $\widetilde{Z}_3$ are mainly higgsino-like. The higgsino-like states decay strongly to vector bosons, as does $\widetilde{W}_2$, giving rise to a continuum $m(\ell^+\ell^-)$ distribution which contains a Z peak [18]. Thus, while the presence of SUSY cascade decay events at LHC containing HITs would point to AMSB-like models, the different $m(\ell^+\ell^-)$ distributions which are expected would allow one to differentiate between the mAMSB, HCAMSB and inoAMSB cases!

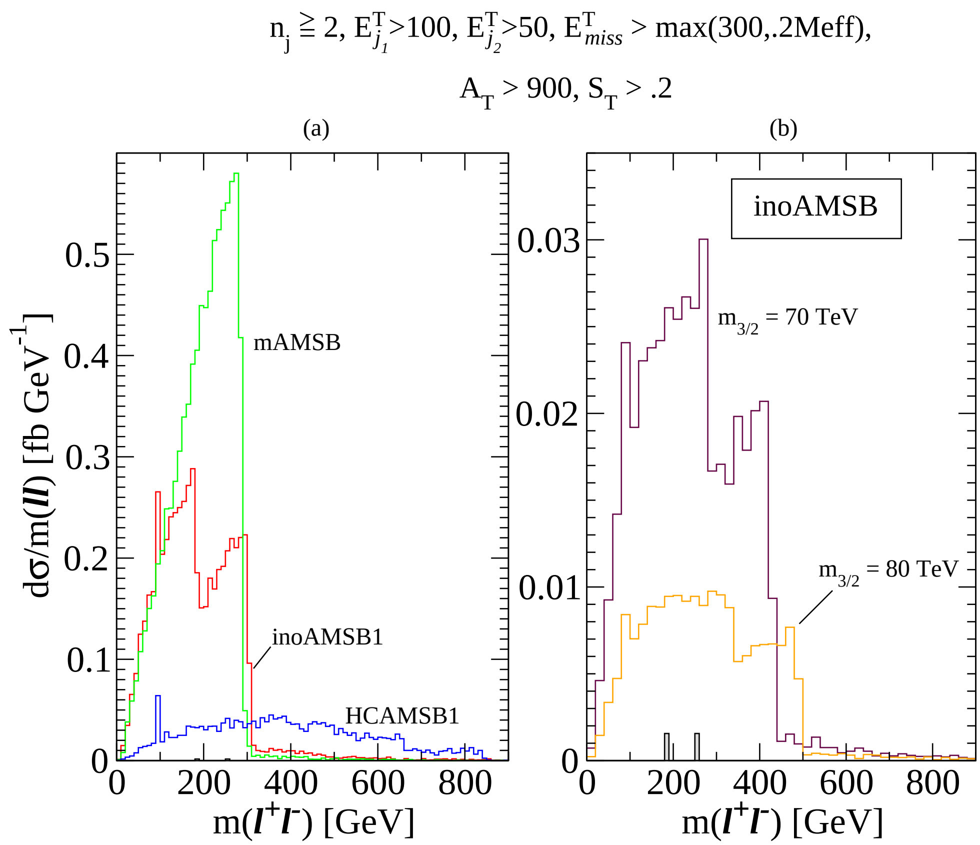

Figure 2.15: Invariant mass distribution for SF/OS dileptons from a). mAMSB1, HCAMSB1 and inoAMSB1 after requiring cut set $C1$ plus $E_T^{\rm miss} > 300$ GeV and $A_T > 900$ GeV. In frame b), we show the same distribution, except taking inoAMSB with $m_{3/2} = 70$ and 80 TeV.

In frame *b*)., we show inoAMSB models with $m_{3/2} = 70$ and 80 GeV. These distributions also show the expected double edge plus Z peak structure that was found for inoAMSB1, although now the mass edges have migrated to higher $m(\ell^+\ell^-)$ values.

2.5 Discussion and conclusions

In this paper, we have examined the phenomenology of supersymmetric models with the boundary conditions $m_0 \sim A_0 \sim 0$ at M_{GUT}, while gaugino masses assume the form as given in AMSB. We call this model gaugino-AMSB, or inoAMSB or short. Such boundary conditions can arise in type IIB string models with flux compactifications. They are very compelling in that off-diagonal flavor violating and also CP violating terms are highly suppressed, as in the case of no-scale supergravity or gaugino-mediated SUSY breaking models. However, since gaugino masses assume the AMSB form at M_{GUT}, the large $U(1)_Y$ gaugino mass M_1 pulls slepton masses to large enough values through renormalization group evolution that one avoids charged LSPs (as in NS or inoMSB model) or tachyonic sleptons (as in pure AMSB models).

The expected sparticle mass spectrum is very distinctive. Like mAMSB and HCAMSB, we expect a wino-like lightest neutralino $\widetilde{Z}_1$, and a quasi-stable chargino $\widetilde{W}_1$ which could leave observable highly ionizing tracks in a collider detector. The spectrum is unlike mAMSB in that a large mass splitting is expected between left- and right- sleptons. We also investigated what happens if the string scale M_s is much lower than M_{GUT}. In this case, the entire spectrum become somewhat expanded, and if $M_s \lesssim 10^{14}$ GeV, then the left-sneutrino becomes the LSP, which is excluded by double beta decay experiments.

We also investigated in detail some aspects of LHC collider signatures. Since $m_{\tilde{q}} < m_{\tilde{g}}$ in inoAMSB models, we expect dominant $\tilde{q}\tilde{q}$ and $\tilde{q}\tilde{g}$ production at LHC, followed by 2-body $\tilde{q}$ and $\tilde{g}$ decays. This leads to collider events containing at least two very high p_T jets plus $E_T^{\rm miss}$ as is indicative from squark pair production.

While squark and gluino cascade decay events should be easily seen at LHC (provided $m_{3/2} \lesssim$ 110 TeV), the signal events should all contain visible HITs, which would point to a model with

$m_{\widetilde{W}_1} \simeq m_{\widetilde{Z}_1}$, as occurs in anomaly-mediation where $M_2 < M_1,\ M_3$ at the weak scale. We find an LHC reach for 100 fb^{-1} of integrated luminosity out to $m_{3/2} \sim 118$ TeV, corresponding to a reach in $m_{\tilde{g}}$ of about 2.6 TeV.

We also find that the invariant mass distribution of SF/OS dilepton pairs should have a distinctive two-bump structure that is indicative of neutralino decays through both left- and right- sleptons with a large slepton mass splitting. This distribution would help distinguish inoAMSB models from HCAMSB, where a continuum plus a Z-bump distribution is expected, or from mAMSB, where the two mass edges (present only if m_0 is small enough that $m_{\tilde{\ell}_L}$ and $m_{\tilde{\ell}_R}$ are lighter than $m_{\widetilde{Z}_2}$) would be very close together, and probably not resolvable.

Chapter 3

Testing the gaugino AMSB model at the Tevatron via slepton pair production

Chapter Summary

Gaugino AMSB models– wherein scalar and trilinear soft SUSY breaking terms are suppressed at the GUT scale while gaugino masses adopt the AMSB form– yield a characteristic SUSY particle mass spectrum with light sleptons along with a nearly degenerate wino-like lightest neutralino and quasi-stable chargino. The left- sleptons and sneutrinos can be pair produced at sufficiently high rates to yield observable signals at the Fermilab Tevatron. We calculate the rate for isolated single and dilepton plus missing energy signals, along with the presence of one or two highly ionizing chargino tracks. We find that Tevatron experiments should be able to probe gravitino masses into the ~ 55 TeV range for inoAMSB models, which corresponds to a reach in gluino mass of over 1100 GeV.

3.1 Introduction

Searches for supersymmetry (SUSY) at the Fermilab Tevatron collider usually focus on gluino and squark pair production reactions, due to their large strong interaction production rates [53–55], or on observation of chargino-neutralino production and decay to isolated trileptons, due to their low background rates [56–58]. The possibility of observation of slepton pair production at the

Tevatron was examined in Ref. [59] in the context of the MSSM with gaugino mass unification and found to be difficult: the dilepton signature from $p\bar{p} \to \tilde{\ell}^+\tilde{\ell}^- \to \ell^+\ell^- + E_T^{\rm miss}$ (here, $\ell = e$ or μ) is beset with large backgrounds from W^+W^- and $Z \to \tau^+\tau^-$ production, while the $\tilde{\ell}\tilde{\nu}_L \to \ell^\pm + E_T^{\rm miss}$ signal is beset by even larger backgrounds from direct $W^\pm \to \ell^\pm\nu_\ell$ production. However, these past works did not anticipate the Tevatron reaching integrated luminosities in the vicinity of 8-16 fb^{-1}.

In this chapter, we investigate the recently introduced *gaugino AMSB* model (inoAMSB) [3], which arises naturally from some highly motivated string theory constructions. The inoAMSB model gives rise to a characteristic SUSY particle mass spectrum which features 1. a wino-like lightest neutralino $\widetilde{Z}_1$, 2. a nearly mass degenerate quasi-stable chargino $\widetilde{W}_1$, (points 1 and 2 also occur in previous AMSB constructs [10,60,61]), 3. a rather light spectrum of sleptons, arranged in a mass hierarchy $m_{\tilde{\nu}_L} < m_{\tilde{\ell}_L} < m_{\tilde{\ell}_R}$ and 4. a rather heavy spectrum of squarks and gluinos, where $m_{\tilde{g}} \sim m_{\tilde{q}} \sim 7.5 m_{\widetilde{W}_1}$. Given the LEP2 limit on quasi-stable charginos from AMSB models, where $m_{\widetilde{W}_1} > 91.9$ GeV [62], this implies $m_{\tilde{g}} \gtrsim 700$ GeV: quite beyond the reach of Tevatron. However, in inoAMSB models the sleptons can exist with masses as low as ~ 130 GeV. Pair production of inoAMSB sleptons, followed by decays into quasi-stable charginos, should give rise to characteristic isolated single or dilepton plus $E_T^{\rm miss}$ signatures, accompanied by the presence of one or two highly ionizing chargino tracks (HITs) [60].

In a previous work [3], we presented the spectrum of SUSY particle masses which are expected from inoAMSB models, and evaluated prospects for detection at the LHC with $\sqrt{s} = 14$ TeV. A 100 fb^{-1} LHC reach to $m_{\tilde{g}} \sim 2.3$ TeV was found. The gluino and squark cascade decay [63] events would often contain the presence of highly ionizing chargino tracks that could range up to a few *cm* in length. The unique inoAMSB mass spectrum $m_{\widetilde{Z}_2} > m_{\tilde{\ell}_R} > m_{\tilde{\ell}_L} > m_{\widetilde{W}_1, \widetilde{Z}_1}$ leads to a characteristic *double bump* (mass edge) structure in the opposite-sign dilepton invariant mass distribution which could serve to distinguish the inoAMSB model from minimal AMSB (mAMSB) or hypercharged AMSB [18] (HCAMSB).

In Ref. [64],the relic density of dark matter in inoAMSB (and also in mAMSB and HCAMSB) was considered. In all AMSB models with sub-TeV scale $\widetilde{Z}_1$, the thermal abundance of neutralino cold dark matter is well below the WMAP-measured value of $\Omega_{CDM}h^2 = 0.1126 \pm 0.0036$ [42]. However, the possibility of additional neutralino production via moduli [65], gravitino [66] or axino [67] decay can augment the thermal abundance, bringing the expected neutralino abundance into accord with measured values.

In this paper, we calculate signal rates for slepton pair production in inoAMSB models at the Fermilab Tevatron collider. We find a considerable reach for the nearly background free signature of single or OS dilepton plus $E_T^{\rm miss}$ plus one or two HITs [60]; these signal rates ought to allow Tevatron experiments to explore slepton masses from the inoAMSB model into the 200 GeV range for ~ 10 fb^{-1} of integrated luminosity, corresponding to a reach in $m_{3/2}$ of over 50 TeV.

3.2 The gaugino AMSB model

Gaugino Anomaly Mediated Supersymmetry Breaking [3] is a very simple scenario for generating SUSY breaking soft terms in low energy supersymmetric theories. The main assumption is that the high energy theory which generates SUSY breaking is of the sequestered type [10], which effectively means that the classical gaugino and scalar masses and A-terms are highly suppressed relative to the gravitino mass scale. This is in contrast to the situation in usual supergravity (SUGRA) models, where these soft parameters are classically generated at the gravitino mass scale. Nevertheless, in contrast to what is usually advocated in AMSB [10], it has been argued [114] that only *gaugino masses* are generated by Weyl anomalies. In inoAMSB [3] [**?**], the scalar masses are then generated by renormalization group (RG) running as in what is often called gaugino mediation [14] or simple no-scale SUSY breaking models [13]. The inoAMSB model then avoids both the generic FCNC problems of gravity mediated scenarios and also the tachyonic slepton problem of the traditional AMSB construct. It also avoids the presence of tau slepton LSPs which occur in gaugino mediation/no-scale models with gaugino masses unified at a high scale.

This very simple phenomenological model depends on just two parameters: the gravitino mass $m_{3/2}$ which sets the scale for all sparticle masses, and $\tan\beta$, the ratio of the the Higgs vacuum expectation values in the MSSM. In fact, it appears to be the simplest SUSY mediation model that one can conceive of which satisfies all phenomenological constraints.

Furthermore, inoAMSB can be realized within a highly motivated class of string theories [**?**]. The models in question are called the large volume compactification scenario (LVS) of type IIB string theory and were introduced in [2]. The moduli (and the dilaton) of string theory, which appear as 4D fields in the effective action, are stabilized using a combination of fluxes and non-perturbative effects (for reviews see [7]). The Calabi-Yau (CY) manifolds on which the theory is compactified to 4D is of the so-called "Swiss Cheese" type with one large four cycle (which controls the overall size of the internal space) and one or more small cycle. An analysis of the potential for the moduli shows that the volume is exponentially large in the small cycle(s) whose size in turn is stabilized at values larger than the string scale. The effective parameter which controls this is determined by the Euler character of the CY manifold and the (flux dependent) value of the dilaton.

It was shown in [**?**] that in these models, for large enough volume (greater than 10^5 Planck units), FCNC effects are suppressed. Indeed, all classically generated soft SUSY breaking parameters are volume suppressed compared to the gaugino mass soft terms that are generated by anomaly mediation. The latter effect is actually a consequence of the generation of gaugino masses by the Weyl anomaly effect as discussed in [114].

The phenomenology of this class of string theoretic models is effectively controlled by the gravitino mass. But the theory at this point only allows us to estimate an upper bound to the possible size of μ and B terms. So we use the latter after trading it for (as is usual) $\tan\beta$, and regard the former as an output from the experimental value of the Z mass. The parameters of the phenomenological model which comes from these string theory considerations are thus

$$m_{3/2},\ \tan\beta,\ sign(\mu). \tag{3.1}$$

The gravitino mass determines the values of the gaugino masses at the high scale (which will be chosen to be the GUT scale) by the Weyl anomaly formula given in [114]. It turns out that for the scenario in [?], this is exactly the same as what is often given as the AMSB formula for these masses *i.e.*

$$M_i = \frac{b_i g_i^2}{16\pi^2} m_{3/2}, \tag{3.2}$$

with $b_i = (33/5,\ 1,\ -3)$. The initial (high scale) values of the other soft parameters are then taken to be

$$m_0 = A_0 = 0, \tag{3.3}$$

where m_0 is the common soft SUSY breaking scalar mass evaluated at the high scale $\sim M_{string}$ or M_{GUT}, and A_0 is the trilinear soft SUSY breaking (SSB) term.

3.3 Production and decay of inoAMSB sleptons at the Tevatron

We begin by examining the sort of sparticle mass spectra that is expected from the inoAMSB boundary conditions: $m_0 = A_0 = 0$ but with $M_i = \frac{b_i g_i^2}{16\pi^2} m_{3/2}$. We adopt a unified value of the gauge coupling $g_{GUT} = 0.714$ and then for a given value of $m_{3/2}$ compute the GUT scale values of the three gaugino masses M_i for $i = 1 - 3$. We compute the sparticle mass spectra using the Isasugra subprogram of the event generator Isajet [29], along with the option of non-universal gaugino masses. The parameter space is that of Eq. 3.1.

After input of the above parameter set, Isasugra implements an iterative procedure of solving the MSSM RGEs for the 26 coupled renormalization group equations, taking the weak scale measured gauge couplings and third generation Yukawa couplings as inputs, as well as the above-listed GUT scale SSB terms. Isasugra implements full 2-loop RG running in the $\overline{DR}$ scheme, and minimizes the RG-improved 1-loop effective potential at an optimized scale choice $Q = \sqrt{m_{\tilde{t}_L} m_{\tilde{t}_R}}$ (which accounts for leading two-loop terms) [30] to determine the magnitude of μ and the value of m_A. All physical sparticle masses are computed with complete 1-loop corrections, and 1-loop weak scale threshold corrections are implemented for the t, b and τ Yukawa couplings [31]. The off-set of the weak scale boundary conditions due to threshold corrections (which depend on the entire superparticle mass spectrum), necessitates an iterative up-down RG running solution. The resulting superparticle mass spectrum is typically in close accord with other sparticle spectrum generators [32].

In Fig. 3.1, we show the mass spectrum of various sleptons and light gauginos of interest to Tevatron experiments versus $m_{3/2}$ for $\tan\beta = 10$ and $\mu > 0$. Results hardly change if we flip the sign of μ. If $\tan\beta$ is increased, then third generation squark and slepton and heavy Higgs masses decrease, while first/second generation slepton masses of interest here remain nearly the same. We see from Fig. 3.1 that while charginos and neutralinos are predicted to be the lightest MSSM particles, $\tilde{\ell}_L$ and $\tilde{\nu}_L$ are also quite light– as low as ~ 130 GeV– with $m_{\tilde{\nu}_L} < m_{\tilde{\ell}_L}$. Unlike mSUGRA or mAMSB, the $\tilde{\ell}_R$ mass is split from $\tilde{\ell}_L$ and quite a bit heavier: at least 280 GeV in inoAMSB. The $\widetilde{Z}_2$ is bino-like, with $m_{\widetilde{Z}_2} > m_{\tilde{\ell}_R}$.

In Fig. 3.2, we show various slepton pair production cross sections as calculated at NLO [69] using the Prospino program [70, 71].[1] The results are calculated versus $m_{3/2}$ for the same parameters as in Fig. 3.1. We do not present $\widetilde{W}_1\widetilde{W}_1$ or $\widetilde{W}_1\widetilde{Z}_1$ cross sections, since the visible energy from quasi-stable $\widetilde{W}_1 \to \pi\widetilde{Z}_1$ decay is insufficient to trigger on.

From Fig. 3.2, we see that the reactions $p\bar{p} \to \tilde{e}_L^{\pm}\tilde{\nu}_{eL}$, $p\bar{p} \to \tilde{\nu}_{eL}\bar{\tilde{\nu}}_{eL}$ and $p\bar{p} \to \tilde{e}_L\bar{\tilde{e}}_L$ are comparable and can exceed the 1 fb level for $m_{3/2} \lesssim 45$ GeV. They reach a maximum value of ~ 10 fb for $m_{3/2} \sim 33$ TeV. When we sum over $\ell = e,\ \mu$ and τ, then the total slepton pair production is even larger. The $\tilde{e}_R\bar{\tilde{e}}_R$ pair production is much lower in rate, and unobservable at projected Tevatron luminosities. Also, we see that cross sections involving $\widetilde{Z}_2$ production are much smaller, and won't contribute to the observable rates. For $m_{3/2} \gtrsim 60$ TeV, the slepton pair production cross sections drop below the 0.1 fb level, and are likely unobservable at Tevatron.

To determine the slepton pair producton signatures, we must next calculate their branching fractions [73]. Using Isajet, we find the following values:

- $\tilde{\nu}_{\ell L} \to \widetilde{Z}_1\nu_\ell$ 33%,
- $\tilde{\nu}_{\ell L} \to \widetilde{W}_1\ell$ 67%,

[1] Recent works on slepton pair production at hadron colliders including resummation effects are included in Ref. [72].

while

- $\tilde{\ell}_L \to \widetilde{Z}_1 \ell \quad 33\%$,
- $\tilde{\ell}_L \to \widetilde{W}_1 \nu_\ell \quad 67\%$.

Each quasi-stable chargino gives rise to a HIT, which may be visible in the microvertex tracker. By combining branching fractions with slepton pair production, we find the following event topologies.

(1) $\tilde{\ell}_L \tilde{\nu}_{\ell L} \to \ell + 2\ HITs + E_T^{\rm miss} \quad 45\%$,

(2) $\tilde{\ell}_L \tilde{\nu}_{\ell L} \to \ell^+ \ell^- +\ HIT + E_T^{\rm miss}, \quad 22\%$,

(3) $\tilde{\ell}_L \tilde{\nu}_{\ell L} \to \ell + E_T^{\rm miss}, \quad 10\%$,

(4) $\tilde{\nu}_{\ell L} \bar{\tilde{\nu}}_{\ell L} \to \ell^+ \ell^- + 2\ HITs + E_T^{\rm miss}, \quad 45\%$,

(5) $\tilde{\nu}_{\ell L} \bar{\tilde{\nu}}_{\ell L} \to \ell +\ HIT + E_T^{\rm miss}, \quad 44\%$,

(6) $\tilde{\ell}_L \bar{\tilde{\ell}}_L \to \ell +\ HIT + E_T^{\rm miss}, \quad 44\%$,

(7) $\tilde{\ell}_L \bar{\tilde{\ell}}_L \to \ell^+ \ell^- + E_T^{\rm miss}, \quad 10\%$.

The $\ell^+\ell^- + E_T^{\rm miss}$ topology from reaction 7 will likely be swamped by WW and $Z \to \tau^+\tau^-$ backgrounds, while the $\ell^\pm + E_T^{\rm miss}$ topology from reaction 3 will be buried under $W \to \ell\nu_\ell$ background. However, the event topologies including HITs should stand out from SM background, and furthermore, should signal the presence of the quasi-stable chargino. We note here that topologies 1 and 2 are unique to $\tilde{\ell}_L \tilde{\nu}_L$ production, while topology 4 is unique to $\tilde{\nu}_{\ell L} \bar{\tilde{\nu}}_{\ell L}$ production. If a two HIT topology has one of the HITs missed for some reason, it will look like a single HIT event. But the 2 HIT topologies 1 and 4 are unique in that they each contain two quasi-stable chargino tracks. Thus, these topologies will pinpoint the particular superparticle production mechanism. Topologies 5 and 6 arise from both $\tilde{\nu}_L \bar{\tilde{\nu}}_L$ and $\tilde{\ell}_L \bar{\tilde{\ell}}_L$ production.

The first/second generation slepton masses and branching fractions listed above are largely immune to variations in $\tan\beta$, so even if $\tan\beta$ changes over the range $\sim 5-40$ (parameter space maxes out at $\tan\beta \sim 42$; see Fig. 5 of Ref. [3]), the expected signatures are expected to be nearly $\tan\beta$ invariant. As $\tan\beta$ increases, the $\tilde{\tau}_1$ and $\tilde{\nu}_{\tau L}$ masses decrease, leading to a somewhat increased rate for production of one of two tau leptons plus HITs plus $E_T^{\rm miss}$ relative to production of one or two isolated ℓs plus HITs plus $E_T^{\rm miss}$.

3.4 Signal and background after cuts

Once the superparticle mass spectrum and decay branching fractions have been calculated using Isasugra, the output is fed into Herwig [74] for event generation using $p\bar{p}$ collisions at $\sqrt{s} =$ 1.96 TeV. We adopt the AcerDet toy detector simulation program as well [75]. We then generate all superparticle production events. A large component from $\widetilde{W}_1\widetilde{Z}_1$ and $\widetilde{W}_1^+\widetilde{W}_1^-$ production will not provide enough visible energy for triggers, so we focus instead on slepton pair production, where the signal is an opposite-sign/same flavor (OSSF) dilepton pair (e^+e^- or $\mu^+\mu^-$) plus missing E_T (MET).

To gain perspective on the energy scales from slepton pair production, we plot first in Fig. 3.3 the p_T distribution of the hardest (ℓ_1) and softest (ℓ_2) leptons from slepton pair production in inoAMSB with $m_{3/2} = 35$ TeV, $\tan\beta = 10$ and $\mu > 0$. So far, we have imposed no cuts, so the events come from pure slepton pair production with either one or two isolated leptons in the final state. The $p_T(\ell_1)$ distribution spans an approximate range $\sim 30-120$ GeV, with a peak at ~ 65 GeV. The second lepton p_T distribution spans $\sim 10-80$ GeV, with a peak at ~ 20 GeV. We also show the expected MET distribution, which peaks around 60 GeV.

In Fig. 3.4, we show the OSSF dilepton opening angle in the transverse plane. The distribution peaks around $\Delta\phi(\ell^+\ell^-) \sim \pi$, reflecting the fact that the sleptons are produced back-to-back in the transverse direction. However, when the lepton momentum from slepton decay is boosted to the LAB frame, the distribution smears out considerably: while most events occur at large transverse opening angle, there is a significant probability for both detected leptons to appear on the same side of the detector, *i.e.* with $\Delta\phi(\ell^+\ell^-) < \pi/2$.

Following recent CDF/D0 analyses of W and Z production [76,77], we next impose a minimal set of cuts:

- $E_T^{\rm miss} > 25$ GeV,
- at least one isolated lepton (e or μ) with $p_T(\ell) > 25$ GeV and $|\eta(\ell)| < 1$,
- for two lepton events, $p_T(\ell_2) > 25$ GeV and $|\eta(\ell_2)| < 2$,
- for events containing HITs, we require $|\eta(HIT)| < 2$.

Next, keeping $\tan\beta = 10$ and $\mu > 0$, we scan over $m_{3/2}$ values from 30-80 TeV. The rates for various single and OSSF dilepton events, with 0,1, or 2 HITs, are shown in Fig. 3.5. We also compute single and OSSF dilepton background rates from $p\bar{p} \to W^\pm \to \ell\nu_\ell$ production, and W^+W^- and $Z \to \tau^+\tau^-$ production, respectively. The single lepton background from W production is about six orders of magnitude above signal, making a search in this channel hopeless. The WW and $\tau^+\tau^-$ backgrounds are somewhat above the largest OSSF dilepton signal levels.

At this stage, it is important to note that most signal events will contain at least one HIT, which should be well separated in angle from the isolated leptons. The presence of HITs should allow distinguishability of signal from background. The efficiency for HIT identification is detector dependent, and beyond the scope of our theory analysis: here we will assume a HIT identification efficiency of 100%. Long-lived tracks from hyperon production with $\Xi \to \Lambda\pi$ decay have been identified by the CDF collaboration in the SVX detector and used to great effect in their analysis of Ξ_b production and decay [78]. If we require the presence of one or more HITs from quasi-stable charginos, then SM background should be largely negligible. In particular, the $\ell^+\ell^- + 2\ HITs + E_T^{\rm miss}$ signal from sneutrino pair production followed by $\tilde{\nu}_\ell \to \ell\widetilde{W}_1$ decay should provide a smoking gun signature for inoAMSB at the Tevatron. From Fig. 3.5, we see that this cross section ranges up to 2 fb after cuts. With ~ 10 fb^{-1} of integrated luminosity, Tevatron experiments may have a reach for the inoAMSB model in this channel to $m_{3/2} \sim 40 - 50$ TeV. The $1\ell + 2\ HITs + E_T^{\rm miss}$ channel, coming from $\tilde{e}_L\tilde{\nu}_{\ell L}$ production, is generically about a factor 3 higher than the $\ell^+\ell^- + 2\ HITs + E_T^{\rm miss}$ channel, and should provide corroborating evidence. There are also comparable contributions to the $\ell + HIT + E_T^{\rm miss}$ and $\ell^+\ell^- + HIT + E_T^{\rm miss}$ channels. By combining all channels, the 10 fb^{-1} reach of Tevatron for slepton pair production in inoAMSB models should extend to $m_{3/2} \sim 55$ GeV. Augmenting the signal with single tau-jet and ditau-jets plus $HITs + E_T^{\rm miss}$ events will increase the reach even further.

Once an inoAMSB signal for slepton pair production is established, then the next step will be to try to extract sparticle masses from the event kinematics. We will first look at the sneutrino pair production reaction $p\bar{p} \to \tilde{\nu}_{\ell L}\bar{\tilde{\nu}}_{\ell L} \to \ell^+\ell^- + 2\ HITs + E_T^{\rm miss}$, which arises when $\tilde{\nu}_{\ell L} \to \ell\widetilde{W}_1$ decay. Since the $\widetilde{W}_1$ gives essentially all $E_T^{\rm miss}$– aside from the HIT– it would be useful to construct the transverse mass [79] from the $\tilde{\nu}_{\ell L}$ decay:

$$m_T^2(\ell, \vec{\not{E}}_T) = (|\vec{p}_{\ell T}| + |\vec{\not{E}}_T|)^2 - (\vec{p}_{\ell T} + \vec{\not{E}}_T)^2 \tag{3.4}$$

from each signal event, since this quantity is bounded by $m_T(max) = m_{\tilde{\nu}_{\ell L}}\left(1 - m^2_{\widetilde{W}_1}/m^2_{\tilde{\nu}_{\ell L}}\right)$. However, since we do not *a priori* know the value of $p_T(\widetilde{W}_1)$, but only know $\vec{\not{E}}_T \simeq \vec{p}_T(\widetilde{W}_1) + \vec{p}_T(\widetilde{W}_1')$, we must instead use the Cambridge m_{T2} variable [80]:

$$m_{T2} = \underset{\vec{p}_T(\widetilde{W}_1) = \vec{\not{E}}_T - \vec{p}_T(\widetilde{W}_1')}{min} \left[max\left(m_T(\ell_1, \vec{p}_T(\widetilde{W}_1)), m_T(\ell_2, \vec{p}_T(\widetilde{W}_1')) \right) \right] \tag{3.5}$$

which by construction must be bounded by the m_T value which is constructed with the correct lepton and missing E_T vectors.

The distribution in m_{T2} for $\ell^+\ell^- + 2\ HITs + E_T^{\rm miss}$ is shown as the blue histogram in Fig. 3.6. We see as expected a continuum distribution followed by a visible cut-off around $m_T(max) \simeq 73.4$ GeV.

If instead we examine the m_{T2} distribution for $\ell^+\ell^- + 1\ HIT + E_T^{\rm miss}$, then we will mainly pick up $\tilde{\ell}_L^+\tilde{\ell}_L^-$ production, plus some fraction of $\tilde{\nu}_{\ell L}\bar{\tilde{\nu}}_{\ell L}$ events where one of the HITs is missed, perhaps due to having too high $|\eta| > 2$ value. In this case, m_{T2} is bounded by 105.9 GeV, as is illustrated in Fig. 3.6.

3.4.1 Slepton pair production in mAMSB

We note here that Tevatron experiments can be sensitive to slepton pair production in the mAMSB model as well [60]. Light sleptons occur in mAMSB for very low values of the m_0 parameter. We have examined a case in the mAMSB model with $m_0 = 220$ GeV, $m_{3/2} = 35$ TeV, $\tan\beta = 10$ and $\mu > 0$. This mAMSB benchmark gives rise to a spectrum with $m_{\tilde{\tau}_1} = 124$ GeV, $m_{\tilde{\nu}_{\ell L}} = 150$ GeV, $m_{\tilde{\ell}_R} = 160.3$ GeV, $m_{\tilde{\ell}_L} = 174$ GeV and $m_{\widetilde{W}_1,\widetilde{Z}_1} \simeq 99.3$ GeV. The event rates and distributions are rather similar to the inoAMSB model with $m_{3/2} = 35$ TeV. Naively, one might expect $\tau^+\tau^- + HITs + E_T^{\rm miss}$ production to occur at higher rates in mAMSB than in inoAMSB, since in mAMSB, the $\tilde{\tau}_1$ is NLSP, while in inoAMSB, the $\tilde{\nu}_{\ell L}$ is NLSP. However, since $m_{\tilde{\ell}_R}$ is quite a bit lighter in mAMSB than in inoAMSB, production of $\ell^+\ell^- + HITs + E_T^{\rm miss}$ is augmented by $\tilde{\ell}_R^+\tilde{\ell}_R^-$ production. Detailed simulations find a ratio

$$R = \frac{N(\tau^+\tau^- + 2\ HITs + E_T^{\rm miss})}{N(\ell^+\ell^- + 2\ HITs + E_T^{\rm miss})} \tag{3.6}$$

to be 0.16 for inoAMSB while $R = 0.18$ for mAMSB (here, we require $p_T(\tau - jet) > 20$ GeV and $|\eta(\tau - jet)| < 2$). Thus, it looks difficult to distinguish the two models at the Tevatron based on slepton pair production. Distinguishing the two models is straightforward once enough integrated luminosity is accumulated at LHC, since then $\widetilde{Z}_2$s that are produced in gluino and squark cascade decays lead to a double edge structure in the $m(\ell^+\ell^-)$ distribution (reflecting the large $m_{\tilde{\ell}_L}$, $m_{\tilde{\ell}_R}$ mass gap) while the mAMSB model with light sleptons gives only a single mass edge, owing to the near degeneracy of $\tilde{\ell}_R$ and $\tilde{\ell}_L$ [3]. We also emphasize here that slepton pair production only occurs in mAMSB for very low m_0 and $m_{3/2}$ values, and the $m_{\tilde{\ell}_{L,R}} - m_{\widetilde{Z}_1}$ mass gap is quite variable for different m_0 values, while in inoAMSB, this mass gap is essentially a fixed prediction depending only on $m_{3/2}$.

3.5 Conclusions

In this paper, we have examined the possibility of detecting slepton pair production from the gaugino AMSB model at the Fermilab Tevatron, with 10-16 fb^{-1} of integrated luminosity. This model is characterized by a spectrum of very light sleptons, along with a wino-like neutralino and a nearly mass degenerate, quasi-stable chargino; the latter occur in most AMSB-type models. In inoAMSB, the sneutrinos are the lightest sleptons, but they can decay visibly into modes such as $\tilde{\nu}_{\ell L} \to \ell\widetilde{W}_1$. If the highly ionizing chargino tracks (HITs) can be identified, then the $\ell + HITs + E_T^{\rm miss}$ and $\ell^+\ell^- + HITs + E_T^{\rm miss}$ signatures should be nearly background free. Summing over all production reactions and final states containing HITs should give the Fermilab Tevatron a reach in $m_{3/2}$ to ~ 55 TeV, which corresponds to a gluino mass of ~ 1200 GeV. This should be somewhat beyond what LHC can explore with $\sqrt{s} = 7$ TeV and $\sim 1{\rm fb}^{-1}$ of integrated luminosity [81]. If a sizable signal is established, then the distribution in m_{T2} should provide some information on the masses of the sparticles being produced. In particular, the max of the m_{T2} distribution should be somewhat higher for dilepton events with one HIT, as opposed to dilepton events containing two HITs. This reflects the $m_{\tilde{\ell}_L} > m_{\tilde{\nu}_{\ell L}}$ mass hierarchy which is expected from inoAMSB models.

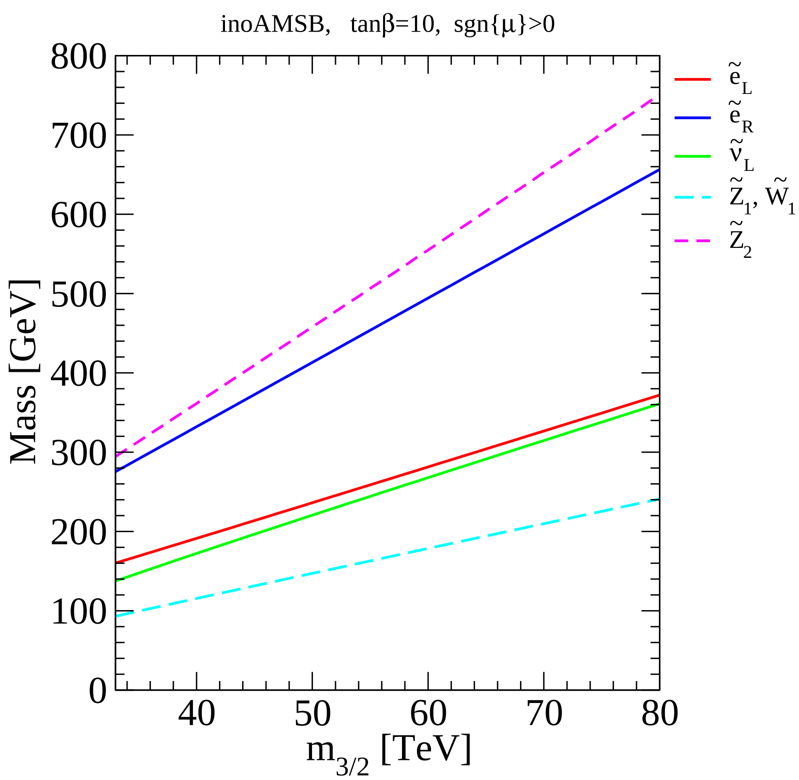

Figure 3.1: Plot of various gaugino and slepton masses in the inoAMSB model versus $m_{3/2}$ for $\tan\beta = 10$ and $\mu > 0$.

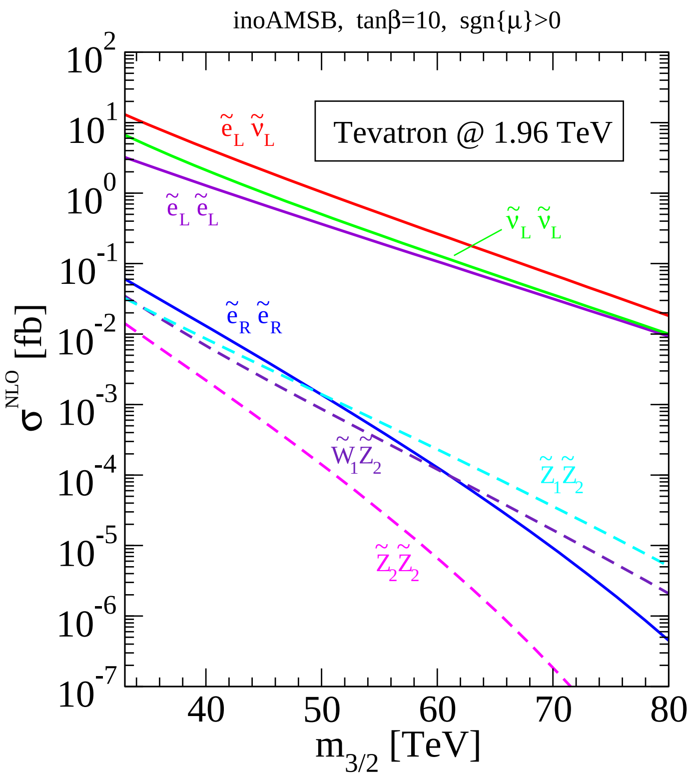

Figure 3.2: Plot of various slepton and gaugino pair production cross sections at the Fermilab Tevatron collider with $\sqrt{s} = 1.96$ TeV for the inoAMSB model. We plot versus $m_{3/2}$ for $\tan\beta = 10$ and $\mu > 0$.

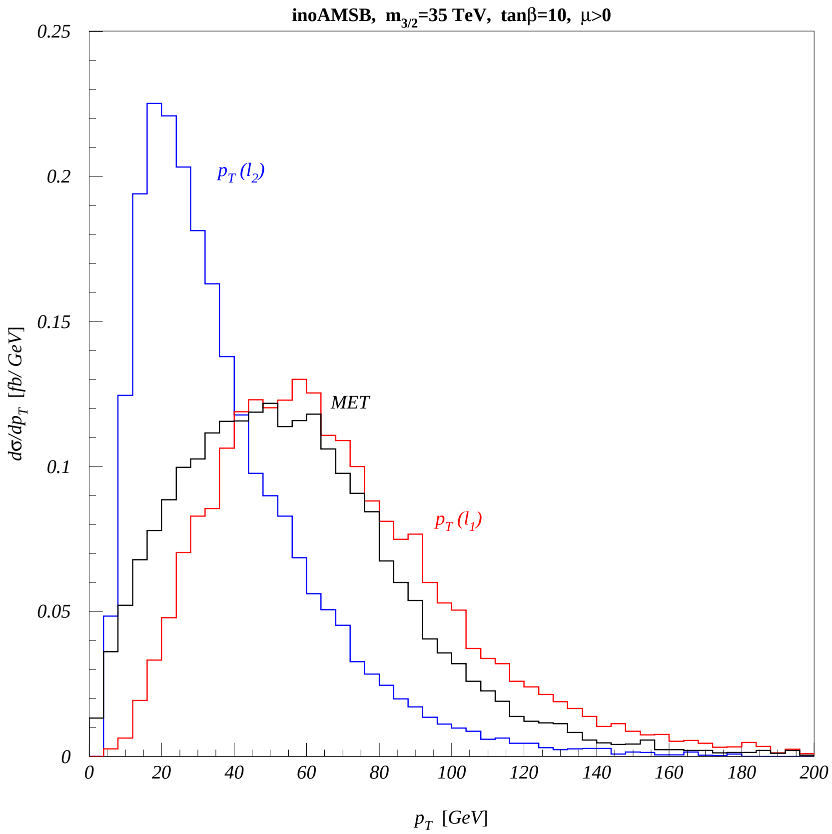

Figure 3.3: Plot of p_T distribution of hardest lepton, second hardest lepton and MET from slepton pair production events with OSSF dileptons at the Fermilab Tevatron for the inoAMSB model. We adopt $m_{3/2} = 35$ TeV, $\tan\beta = 10$ and $\mu > 0$.

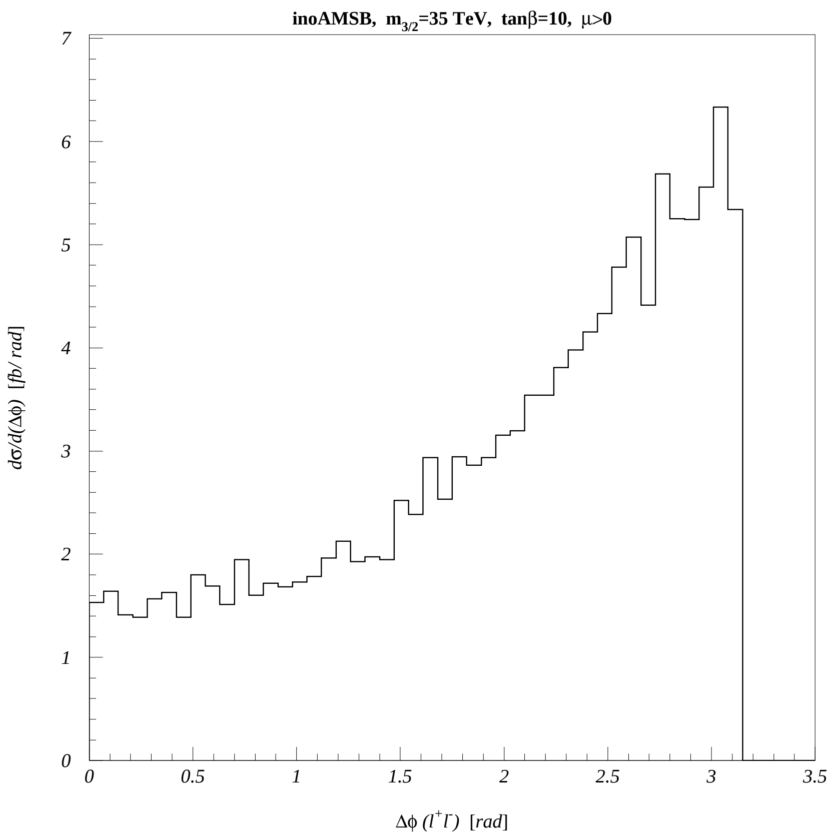

Figure 3.4: Distribution in OSSF dilepton transverse opening angle at the Fermilab Tevatron for the inoAMSB model. We adopt $m_{3/2} = 35$ TeV, $\tan\beta = 10$ and $\mu > 0$.

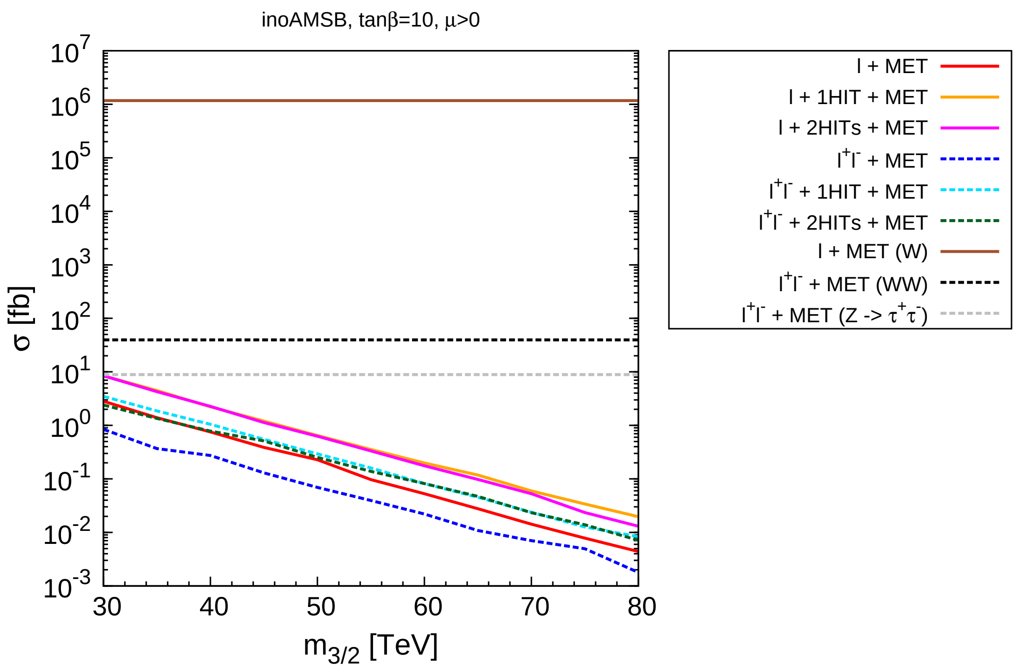

Figure 3.5: Plot of various isolated lepton plus $E_T^{\rm miss}$ event topologies after cuts at the Fermilab Tevatron for the inoAMSB model. Here, $\ell = e$ or μ. We plot signal rate after cuts versus $m_{3/2}$ for $\tan\beta = 10$ and $\mu > 0$.

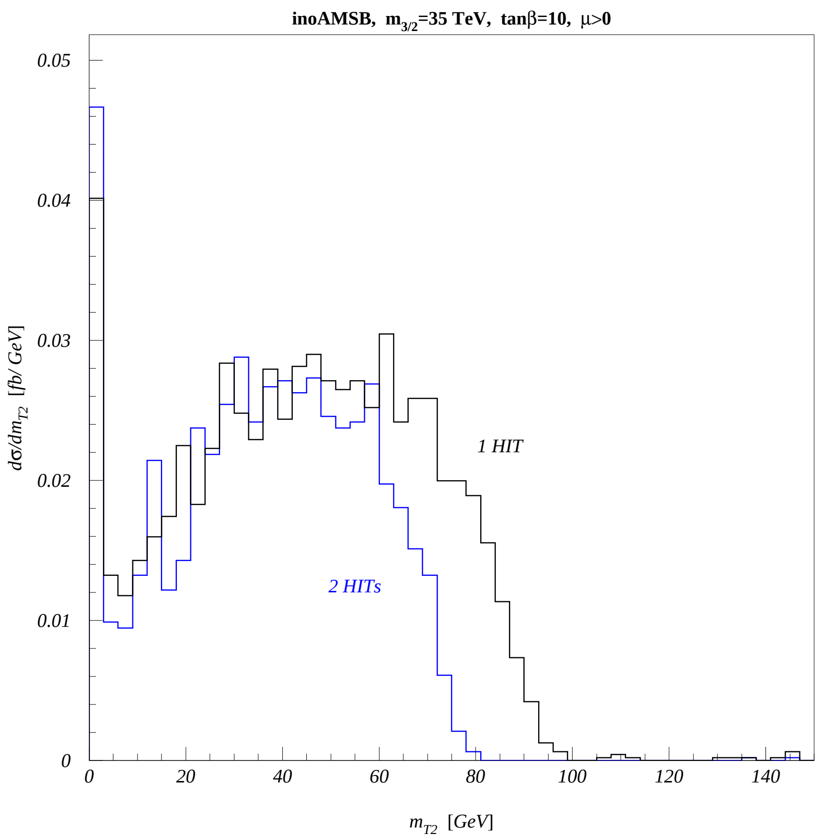

Figure 3.6: Distribution in variable $m_{T2}(\ell^+, \ell^-, E_T^{\rm miss})$ from OSSF slepton pair events at the Tevatron for events containing 1 or 2 HITs. We plot for $m_{3/2} = 35$ TeV, $\tan\beta = 10$ and $\mu > 0$.

Chapter 4

Dark Matter density and the Higgs mass in LVS String Phenomenology

Chapter Summary

The Large Volume Scenario for getting a non-supersymmetric vacuum in type IIB string theory leads, through the Weyl anomaly and renormalization group running, to an interesting phenomenology. However, for gravitino masses below 500 TeV there are cosmological problems and the resulting Higgs mass is well below 124 GeV. Here we discuss the phenomenology and cosmology for gravitino masses which are $\gtrsim 500$ TeV. We find that not only is the cosmological modulus problem alleviated and the right value for dark matter density obtained, but also the Higgs mass is in the 122-125 GeV range. However the spectrum of SUSY particles will be too heavy to be observed at the LHC.

4.1 Introduction

Currently the Large Volume Scenario (LVS) [87] of type IIB string theory compactified on a Calabi-Yau orientifold (CYO) with fluxes[1] is the only viable framework for discussing phenomenology in a top down approach. This is because, apart from the LVS argument (which of course works only in type IIB theory), so far there is no compactification of any string theory that gives a supersymmetry breaking minimum with all moduli stabilized. On the other hand, the problem of getting the MSSM in such constructions has not yet been solved. However, in this class of models, the MSSM is localized in the CYO, so the stabilization problem is essentially decoupled from the problem of finding the MSSM.

[1] For reviews see [7] [8]

By contrast, heterotic string theory models which are MSSM like have been constructed, but the moduli stabilization problem with supersymmetry breaking and a tunable cosmological constant is far from being solved. In fact a major problem in these constructions is that the two issues are not decoupled. Given that in this case there is only one type of flux, it is not at all clear that with current technology a solution can be found.

The case of type IIA strings is somewhere in between the above two cases. While models close to the MSSM have been found (with intersecting D6 branes for instance) and some progress on moduli stabilization in certain special cases has been made (with supersymmetric minima), a viable model whose SUSY breaking phenomenology can be determined is far from being realized.

Thus we are led to the conclusion that, at least for the time being, the only string construction that can yield a viable SUSY breaking phenomenology is LVS. Within LVS, there have been several different versions which in principle could have resulted in a meaningful phenomenology. However, as has been argued by one of us in a recent paper [105], all of these bar one have either theoretical or phenomenological problems. The only model which appears to survive all constraints is that discussed in [24] and [83] and has been named inoAMSB.

In the following we will show that once all the phenomenological (i.e. FCNC) and standard cosmological constraints are imposed, inoAMSB leads to a unique set of predictions. Our basic assumption is the following:

- The MSSM is located on D3 branes at a singularity of a CYO which is of the "Swiss Cheese" type.

Given this assumption, we need to ensure the following theoretical constraints in order to proceed with the LVS argument, which really applies only to the compactified string theory in the four dimensional low energy regime. In other words, we need to justify a 4D $\mathcal{N} = 1$ supergravity (SUGRA) description. Flux compactifications necessarily proceed via the ten dimensional low energy limit of string theory, which in turn needs to result in a four dimensional theory. The constraints follow from the requirement that the superderivative expansion is valid at each stage.

Thus we need:

- The energy scales of the theory $E \ll M_{KK} \ll M_{string}$.
- After SUSY breaking $\sqrt{F}/M_{KK} \ll 1$.

These are the principle theoretical constraints on the LVS construction. In addition there are phenomenological and cosmological constraints apart from the obvious ones, like the necessity for having a highly suppressed cosmological constant (CC). These constraints include:

- Flavor changing neutral currents (FCNC) must be suppressed.
- The gravitino and the lightest modulus of the string theory compactification must be heavy enough so as not to interfere with Big Bang Nucleosynthesis (BBN) in standard cosmology.

In the context of these string constructions the FCNC constraint translates into a lower bound on the internal volume $\mathcal{V}$ [24]. The classical contribution to the soft terms at the UV scale (taken close to the string scale) is highly suppressed (relative to the gravitino mass) by a factor of the volume. However, the gaugino gets a contribution which is only suppressed by a factor of $\left(\frac{\alpha}{4\pi}\right)$, the perturbation expansion parameter of the relevant gauge group. The soft terms at the TeV scale are then generated by RG running essentially by the mechanism of gaugino mediation [**?**] [**?**] and are flavor neutral as usual. So the FCNC constraint comes from comparing the classical off diagonal contribution to the RG generated soft term, giving the relevant lower bound.

For low values of the gravitino mass ($m_{3/2} \lesssim 200\,\mathrm{TeV}$) this lower bound is $\mathcal{V} \gtrsim 10^5$ in string units. The relevant phenomenology is discussed in [83]. However, in this case, we have a cosmological modulus problem since for the lightest modulus we have $m_{modulus} = m_{3/2}/\sqrt{\mathcal{V}} \ll 10\,\mathrm{TeV}$. Also the neutralino contribution to dark matter density is about an order of magnitude too low and the Higgs mass is well below 120 GeV! In this note we look at the same class of models with very high ($\gtrsim 500\,\mathrm{TeV}$) gravitino mass. In this case the FCNC constraints are somewhat ameliorated and the CYO volume lower bound becomes $\mathcal{V} \gtrsim 10^4$. Up to an $\mathcal{O}(1)$ factor, this puts us around the lower bound for the light modulus mass but, importantly, gives the right value for neutralino dark matter. It also gives a Higgs mass in the 122-125 GeV range in agreement with the recent hints from CERN.

At the string scale (assumed to be close to the GUT scale) the SUSY parameters take their values from the convential inoAMSB arguments. The gauginos gain mass through the super-Weyl anomaly and take the following form:

$$M_i = \frac{b_i g_i^2}{16\pi^2} m_{3/2} \qquad b_i = (33/5, 1, -3) \tag{4.1}$$

The scalars are suppressed relative to $m_{3/2}$ and are given by

$$m^2 = +\frac{3}{16}\frac{\hat{\xi}}{|\ln m_{3/2}|}\frac{m_{3/2}^2}{\mathcal{V}} \tag{4.2}$$

where $\hat{\xi} \sim \mathcal{O}(1)$ is related to the Euler character of the CYO. For $m_{3/2} = 500\,\text{TeV} = 5\times 10^{-13}$ ($\mathrm{M_P} = 1$) and $\mathcal{V} = 10^4$ this gives

$$m = \sqrt{\frac{3}{16}\frac{1}{|\ln(5\times 10^{-13})| \times 10^4}}\ 500\ \text{TeV} \approx 407\ \text{GeV} \tag{4.3}$$

The A term is also highly suppressed at the GUT scale while the absolute value of the μ term is an output determined by the mass of the Z boson.

In what follows, we compute 2-loop RGE evolution for various soft masses using ISAJET [118]. We observe that the SUSY particle masses are generically lifted to the TeV scale. Consequently, this diminishes the likelihood of direct production at the LHC. In Table 4.1, we present the SUSY particle masses (physical mass eigenstates) for this model with various values of $m_{3/2}$ and $\tan(\beta)$. In Figure 4.1, we plot the (1-loop) SUSY sparticle mass RGE evolution.

In Figure 4.1, we call attention to the fact that $M_{H_d}^2$ becomes large and negative near the Weak scale. This may seem contrary to the traditional expectation of a small and positive $M_{H_d}^2$. However, as noted in [82] (page 204), for large values of $\tan(\beta)$, the bottom and tau Yukawa couplings make large contributions to the $M_{H_d}^2$ RGE, driving it negative. For $\tan(\beta) \approx 10$, this effect vanishes.

parameter	inoAMSB1	inoAMSB2	inoAMSB3	inoAMSB4
m_0	0 GeV	407 GeV	407 GeV	615 GeV
$m_{3/2}$	$100,000$	$500,000$	$500,000$	$750,000$
A_0	0	50	50	75
$\tan\beta$	10	10	40	20
M_1	956.1	4910.1	4918.4	7481.3
M_2	287.9	1400.0	1399.9	2103.7
μ	1127.5	6465.4	6453.9	6500.3
$m_{\tilde{g}}$	2186.1	9501.9	9502.0	13907.0
$m_{\tilde{u}_L}$	1908.7	8137.9	8139.2	11824.6
$m_{\tilde{u}_R}$	1975.7	8485.5	8492.0	12366.6
$m_{\tilde{t}_1}$	1691.8	7411.1	7135.4	10833.6
$m_{\tilde{t}_2}$	1814.8	7633.6	7488.6	11004.0
$m_{\tilde{b}_1}$	1779.5	7602.0	7154.6	10973.1
$m_{\tilde{b}_2}$	1908.3	8134.8	7332.0	11665.5
$m_{\tilde{e}_L}$	457.8	2202.3	2197.5	3286.8
$m_{\tilde{e}_R}$	809.5	3875.2	3875.2	5789.6
$m_{\widetilde{W}_2}$	1129.8	4599.8	4507.2	6550.3
$m_{\widetilde{W}_1}$	299.7	1474.3	1474.1	2217.1
$m_{\widetilde{Z}_4}$	1143.2	4841.0	4846.4	7372.5
$m_{\widetilde{Z}_3}$	1135.8	4597.8	4508.3	6549.3
$m_{\widetilde{Z}_2}$	936.8	4594.6	4506.2	6548.5
$m_{\widetilde{Z}_1}$	299.4	1472.9	1471.9	2214.0
m_A	1208.9	5050.9	2100.4	6799.9
m_h	116.0	122.1	123.9	124.2
$\Omega_{\widetilde{Z}_1} h^2$	0.007	0.111	0.110	0.111
σ [fb]	439	6.7×10^{-2}	7.1×10^{-2}	2.6×10^{-3}
$\tilde{g},\tilde{q}$ pairs	3%	0%	0%	0%
$\mathrm{EW}-\mathrm{ino}$ pairs	93%	93%	95%	96%
slep. pairs	3%	0.5%	0.4%	0.09%
$\tilde{t}_1\bar{\tilde{t}}_1$	0%	0%	0%	0%

Table 4.1: Masses and parameters in GeV units for four case study points inoAMSB1,2,3,4 using ISAJET 7.79 with $m_t = 172.6$ GeV and $\mu > 0$. We also list the total tree level sparticle production cross section in fb at the LHC with 14 TeV center of mass energy.

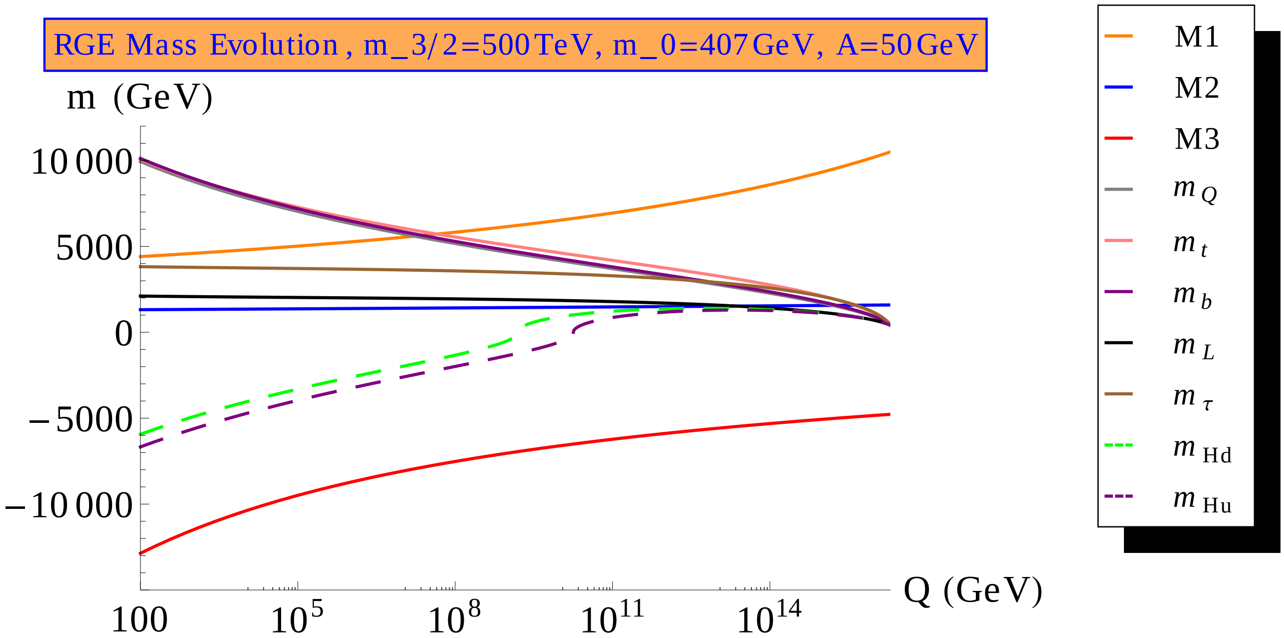

Figure 4.1: SUSY particle mass evolution using 1-loop RGE's, $\mathcal{V} = 10^4$, $m_{3/2} = 500$ TeV, $\tan\beta = 40$, $m_0 = 407$ GeV, $A_0 = 50$ GeV

4.2 Cosmological Issues

4.2.1 Cosmological Modulus Problem

Within inoAMSB models, there exists the potential for conflict with the Cosmological Modulus Problem [106] [89]. Essentially, the sGoldstino, which is a light scalar modulus, can dominate the energy density of the universe and decay during the era of Big Bang Nucleosynthesis, disrupting the consistency of the BBN model. In LVS, the light scalar modulus has a mass given by

$$m_{mod} \sim \frac{m_{3/2}}{\sqrt{\mathcal{V}}} \tag{4.4}$$

For $m_{3/2} = 500\,\text{TeV}$ and $\mathcal{V} = 10^4$, this gives a modulus mass of $m_{mod} \sim 5\,\text{TeV}$, somewhat below the phenomenological bound of 10 TeV. We can satisfy this bound by raising $m_{3/2}$ to 1000 TeV or 1 PeV. This will lift the sparticle spectrum into the $10's$ of TeV's. One might naively assume that the dark matter relic abundance, $\Omega_{DM}h^2$, would violate known bounds. However, as we shall see, this bound is still satisfied.

4.2.2 Dark Matter Relic Abundance

It is a well known problem [84] that AMSB type models generically produce a dark matter relic abundance that is several orders of magnitude lower than the current experimental value ($\Omega_{DM}h^2 \sim 0.11$ [42]). This is attributable to the near degeneracy between the lightest wino and the lightest zino. Their mass difference is typically $\sim \mathcal{O}(100\,\text{MeV})$. This leads to an overabundance of $\widetilde{W}$ at freeze-out and efficient $\widetilde{W}$, $\widetilde{Z}$ co-annihilation. However, when $m_{3/2} = 500\,\text{TeV}$, the mass difference between $\widetilde{W}$ and $\widetilde{Z}$ is $\sim \mathcal{O}(2$ GeV). This suppresses the abundance of $\widetilde{W}$ at freeze-out and hence raises the SUSY contribution to dark matter relic abundance. For $m_{3/2} = 500$ TeV, the value calculated from ISAJET is $\Omega_{DM}h^2 \approx 0.11$.

In Figure 4.2, we plot the dark matter relic abundance as a function of $m_{3/2}$ (with $\tan(\beta) = 10$). We see that the experimental bound is roughly saturated for $m_{3/2} = 500\,\text{TeV}$ and $m_{3/2} = 750\,\text{TeV}$. In particular, for $m_{3/2} \sim 1000\,\text{TeV}$, the experimental bound on dark matter relic abundance is not violated but some other mechanism must account for it.

4.3 Phenomenological Issues

4.3.1 FCNC and Anomalous Magnetic Moment of the Muon

The SUSY particle spectrum determined by this model is also subject to constraints on known Standard Model processes. In particular, the flavor changing neutral current process $b \to s\gamma$ as well as the anomalous magnetic moment of the muon, $\delta a_\mu \equiv (g-2)_\mu$, are influenced by the presence of SUSY particles in their respective loop diagrams. For our model, the calculated values from ISAJET for these quantities are presented in Table 2 along with the corresponding experimental values [90] [97]. From these results we conclude that our model does not violate these phenomenological constraints.

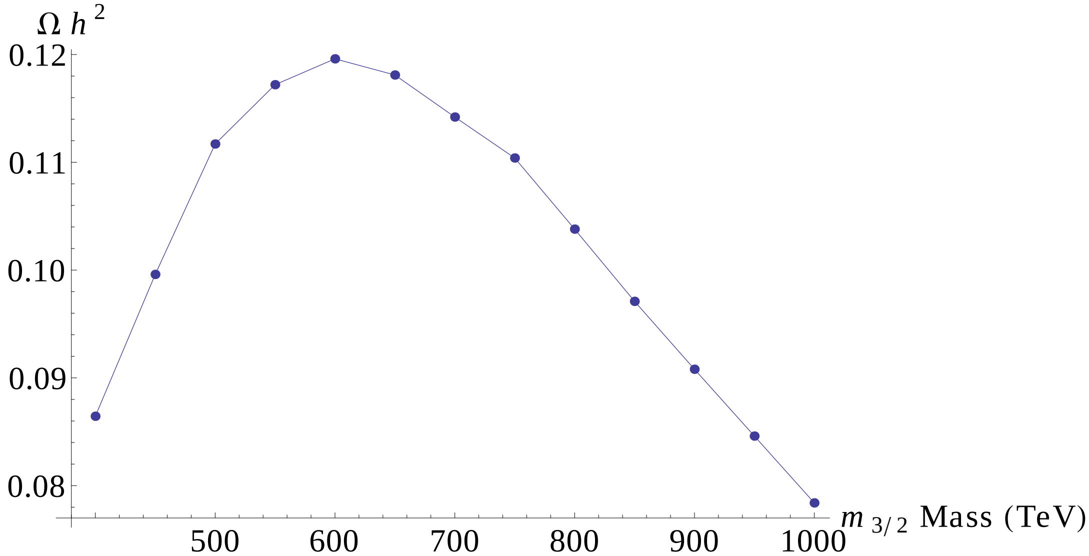

Figure 4.2: Dark matter relic abundance as a function of $m_{3/2}$

	Experimental Value	Estimated Value
$(g-2)_\mu$	$29.5 \pm 8.8 \times 10^{-10}$	0.73×10^{-10}
$BR(b \to s\gamma)$	$3.11 \pm 0.8 \times 10^{-4}$	3.16×10^{-4}

Table 4.2: Phenomenological constraints for inoAMSB with $m_{3/2} = 500$ TeV, $m_0 = 407$ GeV, $A_0 = 50$ GeV, $\tan\beta = 40$ using ISAJET 7.79 with $m_t = 172.6$ GeV and $\mu > 0$.

Note that in Table 4.1 the value of the μ-term is an output determined by the experimentally measured value of the Z mass. In these string theory constructions the value of this term is dependent of the mechanism which is responsible for lifting the LVS minimum to a positive value at the 10^{-3} eV scale. As discussed in [24], one needs to turn on F-terms in either the dilaton or the complex structure directions in order to achieve this.[2] Thus this term will be dependent in a complicated way on the fluxes and in general can be fine tuned to satisfy the Z mass constraint. This fine tuning is of course the little hierarchy problem appearing as a landscape flux choice problem and corresponds to a fine tuning (with $m_{3/2} \sim 500\,\text{TeV} - 800\,\text{TeV}$) of 1 part in $3-4\times 10^3$. Of course this is still much better than the original standard model fine tuning of 1 part in 10^{30}!

[2] For an explicit example see the recent paper [100].

4.4 Prospects for the LHC

The fact that the SUSY particle masses are on the TeV scale will, roughly speaking, suppress the likelihood of their direct detection at the LHC. However, there is one principle difference between this model and the case when $m_{3/2} < 100\,\text{TeV}$. Namely, the near degeneracy between $\widetilde{W}_1$ and $\widetilde{Z}_1$ is noticeably lifted, with $M(\widetilde{W}_1) - M(\widetilde{Z}_1) \approx 2$ GeV. This means that $\widetilde{W}_1^+$ can decay to $\widetilde{Z}_1$ plus quarks. These quarks may be energetic enough to produce jets that meet LHC trigger requirements. However, the likelihood of their production is very small. One can see from the production cross section calculations (given in the bottom rows of Table 4.1), that even for an integrated luminosity of $100\,\text{fb}^{-1}$, the LHC will produce fewer than 10 events. This clearly limits any hope of direct production of SUSY particles at the LHC.

4.5 Conclusion

As we discussed in the introduction, with a rather minimal set of string theory inputs, phenomenological constraints (chiefly the absence of FCNC) and cosmological constraints, we have obtained a very predictive phenomenology. The main output is the correlation between satisfying the light modulus and neutralino dark matter constraint on the one hand (which essentially limits the value of the gravitino mass to a range between 500 TeV and 800 TeV) and the value of the mass of the light Higgs, giving the latter in the range where it may have been observed at the LHC. Unfortunately even the LSP in this scenario is at 1.4 TeV, so that it is unlikely to be observed there. On the other hand, if sub TeV scale superparticles (for instance a light stop) is observed this version of string phenomenology will be ruled out.

It is useful to deconstruct the arguments made here to understand precisely what input or set of inputs would need to be changed, and indeed if one has any room to maneuver whatsoever to get a low mass spectrum. Firstly, let us take a purely phenomenological supergravity approach. From this perspective the essential features of the scenario are a) sequestering i.e. the classical soft masses are highly suppressed compared to the gravitino mass b) the gaugino masses are generated at some high scale close to the GUT scale by the Weyl anomaly [26], i.e. eqn. (4.1). Since the actual value of the classical mass in Table 1 is essentially irrelevant as long as it is highly suppressed compared to the gravitino mass (i.e. $\ll (\frac{\alpha}{4\pi})m_{3/2}$) the rest of the phenomenology and in particular the Higgs mass and the dark matter density follows.

How generic is this phenomenology? Obviously the first requirement is that we start with a sequestered situation, i.e. one in which the classical soft parameters are highly suppressed relative to the gravitino mass. The second requirement is the validity of the Weyl anomaly formulae (4.1). This follows quite generally from the Kaplunovsky-Louis formula for the gaugino mass [26] [114] when, as in a sequestered model, the classical term can be ignored. Then the anomaly term $(b_i/16\pi^2)F^iK_i$ [3] gives the formula (4.1) since $F^iK_i \sim m_{3/2}$ once the CC is tuned to leading order. The string theory input, i.e. type IIB with LVS compactification, is simply a concrete realization of this inoAMSB framework.

The latter is much more general than the type IIB LVS case. Firstly, the no-scale like supergravity action seems to be quite generic in string theory. In the heterotic string for instance, although there is no construction yet with all the moduli stabilized, to the extent that supersymmetry breaking has been investigated, it is clearly of the no-scale type to leading order in the α' and the string loop expansion. The supersymmetry breaking is dominantly in the Kähler modulus direction with the superpotential being independent of this modulus up to non-perturbative terms. Also the gauge coupling function is proportional to the dilaton. Thus as is well-known (see for example [95]), the leading contribution to the soft masses is zero - in other words we have a sequestered situation. Therefore it is likely that once the moduli stabilization problem in the heterotic case is understood, its phenomenology will again be of the inoAMSB type.

[3] K_i and F^i are the derivative of the Kähler potential and the supersymmetry breaking F-term respectively.

Chapter 5

Physical Vacua in IIB Compactifications with a Single Kähler Modulus

Chapter Summary

We search for phenomenologically viable vacua of IIB string flux compactifications on Calabi-Yau orientifolds with a single Kähler modulus. We perform both analytic studies and numerical searches in order to find models with de Sitter vacua and TeV-scale SUSY particle phenomenology.

5.1 Introduction

The search for physically plausible four dimensional vacua represents a preeminent goal of contemporary research in string theory. The challenges endemic to this search originate principally from the fact that string theory is a ten dimensional theory that must be compactified to four dimensions. The process of compactification necessarily introduces moduli fields that, from the standpoint of 4D effective field theory, must be stabilized with acceptable masses and vacuum expectation values. For the case of IIB string theory, the general procedure for addressing these questions by using internal fluxes and non-perturbative terms has recently been developed. For reviews see [7] and [8].

One of the principal drawbacks of an early model, the KKLT scenario [9], is that the moduli are *a priori* stabilized at values producing a negative cosmological constant and that supersymmetry (SUSY) remains unbroken. In order to achieve a de Sitter minimum the authors introduce $\overline{D3}$ branes into the compactified volume. This uplifts the scalar potential to a positive value and breaks supersymmetry. However, from a four dimensional supergravity (SUGRA) perspective, this construction breaks supersymmetry explicitly rather than spontaneously. Furthermore as argued in [98], the logic of incorporating the non-perturbative effects implies that one should first find a classically stable string compactification (with at worst flat directions). The addition of D-bar branes vitiate this requirement, since they lead to a run-away potential for the Kähler modulus, decompactifying the internal manifold. Any phenomenology based on this model then is basically a test of this rather ad hoc uplift term, and so will have little to do with the underlying string theory.

A subsequent model of IIB flux compactification, known as the Large Volume Scenario (LVS) [87], overcomes some of the problems of the KKLT model. In particular while the explicit minimum obtained there still has a negative CC, it breaks SUSY. Furthermore it can be argued that the phenomenological consequences (soft masses, etc.) are not strongly affected by the mechanism by which the CC is ultimately uplifted to positive values [101] [23] [24] [83] [4]. In LVS, the compact volume is a so called Swiss Cheese manifold, with one large Kähler modulus and one (or more) smaller Kähler moduli[1] . All of the moduli fields are again stabilized with a combination of fluxes and non-perturbative effects. However, this model is, in principle, susceptible to violations of constraints on flavor changing neutral currents (FCNC) [24]. This potential violation can be traced back to fact that the model uses more than one Kähler modulus.

Essentially, the general expression for the soft masses in this model contains two terms, one flavor diagonal term coming from the large Kähler modulus, (T_l, $\Re(T_l) \equiv t_l$), and one flavor non-diagonal term coming from the small Kähler modulus, (T_s, $\Re(T_s) \equiv t_s$). The ratio of these two terms is proportional to the ratio of their associated harmonic $(1,1)$ forms ω_l, ω_s (ω_l dual to t_l, ω_s dual to t_s). FCNC suppression then demands that $\omega_s \lesssim 10^{-3} \frac{1}{\ln(m_{3/2})t_b} \omega_l$. This can be achieved if the small Kähler modulus is chosen to be a blow up of a singularity some distance R from the stack of D3 branes and with R being larger than a certain lower bound (for details see [24]).

[1] The standard model fields are located on a stack of D7-branes wrapping an additional cycle which in some models tends to shrink below the string scale, or on a stack of D3 branes located at a singularity. We will assume for the purposes of this paper that the latter is the case here and will ignore this additional cycle and questions associated with its stabilization.

While, in principle, there is no problem achieving this within the LVS construction it is still worthwhile examining whether this additional input discussed above can be avoided. This leads us to examine models that use a single Kähler modulus. We may follow the procedure of [87] and look for minima of the scalar potential in which the complex structure moduli are stabilized at points which are such that the SUSY breaking direction is orthogonal to these moduli. From here, we have the choice of assuming that the axio-dilaton is also stabilized at such a point or that it contributes to the breaking of supersymmetry. [2]

Our strategy is to consider various SUGRA models coming from IIB flux compactification. These models are defined by their Kähler potentials and superpotentials. We stabilize the moduli fields in these models either analytically or numerically and we examine the relevant particle phenomenology in each case. For the numerical results, we use standard minimization functions in Mathematica to locate minima and to evaluate the scalar potential and other quantities. In addition, we use the program STRINGVACUA [113] in order to simplify these calculations but we do not make use of this program's algebraic geometry-based algorithms. We find that it is possible to find minima where supersymmetry is broken and with the scale of the cosmological constant being close to zero. In the simplest case the gravitino and hence soft mass scale is far above the TeV scale. Hence these models, while appearing to be consistent outcomes of type IIB string theory compactified on CY orientifolds with just one Kähler modulus, do not address the hierarchy problem and hence are not relevant for physics at the LHC. Nevertheless these are simple examples of SUSY breaking models with nearly zero cosmological constant coming from string theory. To get models with TeV scale gravitino mass on the other hand requires rather complicated models with several non-perturbative terms. These we analyze numerically and we present an example with 10TeV gravitino mass.

This paper is outlined as follows. In section 2, we investigate a simple SUGRA model in which

[2] It should be noted that this procedure is just a slight extension of that followed in the original LVS paper [87]. Also we would like to stress that this LVS procedure is not the same as the so-called two stage procedure in which the dilaton and complex structure moduli are first integrated out (assuming that the relevant masses are high, and then studying the resulting theory for the light moduli). For some discussion on the validity of the latter see for instance [104] [109] [110] [108] [96].

supersymmetry is broken by the Kähler modulus using non-perturbative and α' corrections. We derive both analytic and numerical results for this model. In addition, we discuss its phenomenology. In section 3, we derive similar results for a model in which supersymmetry is broken by both the Kähler modulus as well as the axio-dilaton. In section 4, we summarize our results. We conclude by examining a natural extension of our first model in the appendix.

5.2 Single Kähler Modulus + α' + Non-Perturbative Term

We begin by examining a model of supergravity coming from IIB string compactifications on Calabi Yau orientifolds with D branes and fluxes[3] . We assume that the MSSM lives on a stack of D3 branes at a singularity. We consider a model with a single Kähler modulus, T, and an axio-dilaton, S, but with many complex structure moduli, U^i, $(i = 1, \ldots, h_{21};\ h_{21} > 1)$. In addition, we include an α' correction [91] and a non-perturbative term coming from either gaugino condensation or instantons. This model is defined by its Kähler and superpotentials given below

$$K = -2\ln\Big(\big(\frac{1}{2}(T+\overline{T})\big)^{3/2} + \frac{\hat{\xi}}{2}\big(\frac{1}{2}(S+\overline{S})\big)^{3/2}\Big) - \ln(S+\overline{S}) - \ln(k(U,\overline{U})), \tag{5.1}$$

$$W = W_{flux}(S,U) + Ae^{-aT}. \tag{5.2}$$

Here[4] $\hat{\xi} = \frac{-\chi\zeta(3)}{2(2\pi)^3}$, $\chi = 2(h_{11} - h_{21})$, U represents all of the U^i and $a = \frac{2\pi}{N}$, where N is the rank of the hidden sector gauge group. Note that since the compactifications that we consider all have $h_{21} > h_{11}$ the parameter $\hat{\xi}$ is positive. We define the complex moduli fields as $T = t + i\tau$ and $S = s + i\sigma$. We will search for minima of this model's scalar potential that break supersymmetry along the T direction.

[3] This particular model was first studied in [86] and [122]. We extend the study of this model by including various analytic and numerical results.

[4] Our notation differs slightly from [87], $\hat{\xi}$ and ξ are interchanged.

5.2.1 Analytic Results

We begin by examining this model (eqns. (5.1),(5.2)) analytically. The scalar potential can be written as

$$V = e^K \left[K^{T\overline{T}} D_T W D_{\overline{T}} \overline{W} + 2\Re\left(K^{S\overline{T}} D_S W D_{\overline{T}} \overline{W}\right) - 3|W|^2\right] + |F^S|^2 + |F^U|^2 \tag{5.3}$$

We follow the approach of the LVS model and look for minima that break supersymmetry in a self-consistent large volume approximation

$$\mathcal{V}|_{min} = t^{3/2}|_{min} \gg \xi \equiv \hat{\xi}\ s^{3/2}|_{min} \tag{5.4}$$

This allows us to approximate the Kähler potential and its derivative as

$$K_T = K_{\overline{T}} \approx \frac{-3}{2t}\left(1 - \frac{\xi}{2t^{3/2}}\right) \qquad K^{T\overline{T}} \approx \frac{4t^2}{3}\left(1 + \frac{\xi}{2t^{3/2}}\right) \tag{5.5}$$

$$e^K = \frac{1}{\left(t^{3/2} + \frac{\xi}{2}\right)^2 k(U,\overline{U})(2s)} \approx \frac{1}{t^3 k(U,\overline{U})(2s)}\left(1 - \frac{\xi}{t^{3/2}}\right) \tag{5.6}$$

Combining these terms together we get for the scalar potential

$$\begin{aligned} V \quad \sim \quad & \frac{1}{t^3 k(U,\overline{U})(2s)}\left[\frac{4t^2}{3}\left(a^2|A|^2 e^{-2at}\right) + 2\Re\left((-aAe^{-aT})(-2t)\overline{W}\right) + \frac{3\xi}{4t^{3/2}}|W|^2\right] \\ & + \mathcal{O}\left(\frac{e^{-2at}}{t^{5/2}}, \frac{e^{-at}}{t^{7/2}}, \frac{1}{t^{9/2}}\right) + 2\Re(K_{S\overline{T}} F^S F^{\overline{T}}) + |F^S|^2 + |F^U|^2 \end{aligned} \tag{5.7}$$

By extremizing the scalar potential only in the T direction, we will find that $V|_{min} \sim \mathcal{O}(\frac{1}{\mathcal{V}^3})$. The terms in eqn. (5.7) that involve F^S and F^U can be approximated as

$$\begin{aligned} |F^S|^2 \sim \mathcal{O}\left(\frac{1}{\mathcal{V}^2}\right) \qquad |F^U|^2 \sim \mathcal{O}\left(\frac{1}{\mathcal{V}^2}\right) \\ 2\Re\left(K_{S\overline{T}} F^S F^{\overline{T}}\right) \sim \mathcal{O}\left(\frac{1}{t^{5/2}} \frac{1}{t^{3/2}} \frac{1}{t^{1/2}}\right) \sim \mathcal{O}\left(\frac{1}{\mathcal{V}^3}\right) \end{aligned} \tag{5.8}$$

Since $|F^S|$ and $|F^T|$ are both positive definite, we see that a large volume minimum with $F^S|_{min} = F^U|_{min} = 0$ obtained by looking at the T minimization conditions will in fact be a minimum of the full potential $V(S,T,U)$ because motion along any of the moduli fields away from the minimum necessarily increases $V(S,T,U)$.

We now proceed to look at the conditions for a minimum with respect to T of V [5]. From eqn. (5.7) we may extract the axion dependence of the scalar potential

$$V(\tau) \sim \frac{1}{t^3 k(U,\overline{U})(2s)} \left(2\Re\left(-aAe^{-aT}\overline{W}_0(-2t)\right)\right) \tag{5.9}$$

We define the complex quantities as follows, $A = |A|e^{i\phi_A}$, $W_0 = |W_0|e^{i\phi_{W_0}}$ ($W_0 \equiv W(S,U)_{\text{flux}}|_{\text{min}}$). The potential's axion dependence now becomes

$$V(\tau) \sim \frac{4ae^{-at}}{t^2} \left(|A||W_0|\cos(a\tau - \phi_A + \phi_{W_0})\right) \tag{5.10}$$

Where we have assumed that $\frac{1}{(2s)(k(U,\overline{U}))}|_{min} \sim \mathcal{O}(1)$. Extremizing with respect to τ,

$$V'(\tau) = \frac{-4a^2e^{-at}}{t^2} \left(|A||W_0|\sin(a\tau - \phi_A + \phi_{W_0})\right) = 0 \tag{5.11}$$

The set of solutions to this equation is

$$a\tau - \phi_A + \phi_{W_0} = n\pi \qquad n \in \mathbb{Z} \tag{5.12}$$

This set of solutions gives us insight into the structure of the Hessian matrix. In order to find minima of the potential, we must find extrema for which the eigenvalues of the Hessian matrix are all positive. From eqn. (5.11) and (5.12) we see that the off-diagonal terms vanish, $\frac{\partial^2 V}{\partial\tau\partial t}|_{min} = \frac{\partial^2 V}{\partial t\partial\tau}|_{min} = 0$. This simplifies the Hessian matrix to the following form

$$\begin{pmatrix} \frac{\partial^2 V}{\partial t^2} & 0 \\ 0 & \frac{\partial^2 V}{\partial \tau^2} \end{pmatrix}$$

From this matrix, we see that both eigenvalues are positive if and only if both $\partial_t^2 V$ and $\partial_\tau^2 V$ are also positive.

We now check the concavity of the potential at the τ extremum,

$$V''(\tau) = \frac{-4a^3e^{-at}}{t^2} \Big(|A||W_0|\cos(a\tau - \phi_A + \phi_{W_0})\Big) \tag{5.13}$$

In order to isolate a minimum, we require $V'' > 0$, therefore

$$a\tau - \phi_A + \phi_{W_0} = (2n+1)\pi \quad n \in \mathbb{Z} \tag{5.14}$$

[5] This is essentially the same procedure as in [87].

Inserting eqn. (5.14) into eqn. (5.10) with $F^S = F^U = 0$, we compute the scalar potential for this model and expand in negative powers of the volume. For large volumes the potential can be safely approximated by

$$V \sim \frac{4}{3}\Big(a^2|A|^2 e^{-2at}\Big)\frac{t^{1/2}}{\mathcal{V}} + 4\Big(a|A|^2 e^{-2at} - a|W_0||A|e^{-at}\Big)\frac{t}{\mathcal{V}^2} + \frac{3|W_0|^2\xi}{4\mathcal{V}^3} + \ldots \tag{5.15}$$

Where we have again assumed that $\frac{1}{(2s)(k(U,\overline{U}))}|_{min} \sim \mathcal{O}(1)$.

From here, the scalar potential can be further simplified with knowledge of the magnitude of W_0. There are two relevant regimes, $|W_0| \sim e^{-at}$ and $|W_0| \gg e^{-at}$ that may lead to the sort of minimum we are looking for. In the first regime we see that the α' correction term (the last term of eqn. (5.15)) can be ignored. This is then essentially the KKLT situation and the corresponding minimum is supersymmetric. The numerical search for minima in this limit confirm that such minima are indeed supersymmetric.

We now investigate the remaining regime, $|W_0| \gg e^{-at}$. In this limit, the scalar potential is exponentially suppressed at large volumes and simplifies to

$$V \sim -\Big(4|W_0|(a|A|e^{-at})\Big)\frac{t}{\mathcal{V}^2} + \frac{3W_0^2\xi}{4\mathcal{V}^3} + \ldots \tag{5.16}$$

We solve for the minimum of this potential by suppressing the term in the derivative that is $\sim \mathcal{O}\left(\frac{W_0 e^{-at}}{t^3}\right)$. This is tantamount to assuming that $at \gtrsim \mathcal{O}(2)$. The extremization condition $(\partial_t V = 0)$ yields the relation

$$|W_0| = \frac{32}{27\xi}\left(a^2|A|e^{-at}\right)t^{7/2} \tag{5.17}$$

This shows that at the minimum of the potential, $|W_0|$ is much larger than e^{-at}, which is consistent with our original assumption. Checking for positive concavity of the minimum and using the same approximation $(at \gtrsim \mathcal{O}(2))$ gives the condition

$$V'' = \frac{27|W_0|^2\xi}{8t^{11/2}}\Big(-a + \frac{11}{2t}\Big) > 0 \tag{5.18}$$

We see from this equation that for $at < 11/2$ this extremum is a minimum (note that this is essentially a condition relating the fluxes and a as is evident from eqn. (5.17)). Therefore, the gravitino mass is bounded from below by

$$m_{3/2} \sim \frac{|W_0|}{t^{3/2}} \gtrsim \frac{e^{-11/2}\left(\frac{11}{2}\right)^2}{\xi} \sim 10^{-3}\ \mathrm{M_P}\ \text{ or }\ 10^{15}\ \mathrm{GeV} \tag{5.19}$$

For $\xi \sim \mathcal{O}(100)$. We may estimate the value of the scalar potential at the minimum by inserting eqn. (5.17) into eqn. (5.16). This yields the following relation

$$\begin{aligned} V|_{min} &= -\Big(4|W_0|\Big(+ \frac{27\xi|W_0|}{32t^{7/2}a}\Big)\Big)t^{-2} + \frac{3|W_0|^2\xi}{4t^{9/2}} \\ &= \frac{3|W_0|^2\xi}{4t^{9/2}}\Big(- \frac{9}{2at} + 1\Big) \end{aligned} \tag{5.20}$$

For $at \sim \mathcal{O}(1)$, $V|_{min} \sim \mathcal{O}\left(\frac{1}{\mathcal{V}^3}\right)$. This is in agreement with our original assertion about the scale of $V|_{min}$, namely, for large volumes, $V|_{min}$ is suppressed relative to the terms in the full potential $V(T,S,U)$ that are proportional to F^S or F^U. Therefore, this is a minimum of the full scalar potential. It is a deSitter minimum for $\frac{9}{2} < at < \frac{11}{2}$. It is important to reiterate that this bound on at is approximate and principally used to make an order of magnitude estimate on the lower bound of $m_{3/2}$. Exact bounds on at necessary for a deSitter minimum require one to numerically solve[6] the conditions $\partial_t V = 0$ and $\partial_t^2 V > 0$.

We may check the stability of this minimum against the well known necessary criteria established in the work of Covi et.al. [102] (see eq. 5.35) as well as [111]. The relevant bound is

$$\tilde{\delta} \equiv \frac{\xi}{16\mathcal{V}} \geq \frac{2V|_{min}}{105 m_{3/2}^2} \tag{5.21}$$

For our model, we maximize $V|_{min}$ and observe that

$$\frac{\xi}{16\mathcal{V}} \geq \frac{2\times 2\times 3|W_0|^2\xi}{105\times 11\times 4t^{9/2}m_{3/2}^2} = \frac{\xi}{385\mathcal{V}} \tag{5.22}$$

Therefore, we confirm that this necessary condition is indeed satisfied.

We may also check whether this minimum is stable under quantum corrections. As discussed in [92] [93] [120], the Kähler potential (eqn. (5.1)) receives corrections at 1-loop of the form

$$K \to K + \frac{1}{T+\overline{T}}\left[\frac{f(A,\overline{A},U,\overline{U})}{S+\overline{S}}\right] + \ldots \tag{5.23}$$

[6] We thank Alexander Westphal and Markus Rummel for discussing this issue. The explicit calculation of the deSitter bounds of at is performed in [119].

Here, $f(A, \overline{A}, U, \overline{U})$ is a function of the open string scalars as defined in [93]. For our model, this translates into a scalar potential of the form

$$V = \left[\frac{c_1(S+\overline{S})^{3/2}}{(T+\overline{T})^{9/2}} + \frac{c_2}{(T+\overline{T})^{10/2}(S+\overline{S})^2} + \frac{c_3(S+\overline{S})^{3/2}}{(T+\overline{T})^{11/2}} + \dots \right] |W_0|^2 \tag{5.24}$$

where $c_i \lesssim \mathcal{O}(10)$. Comparing this with eqn. (5.20), we may identify the 1-loop correction as the term $\sim \mathcal{O}\left(\frac{1}{(T+\overline{T})^{10/2}}\right)$. We see that for $s \sim \mathcal{O}(1)$ the 1-loop correction indeed alters our minimum. In order to suppress this correction we need to choose fluxes such that the value of s is large enough. From eqn. (5.24), we find that for

$$(S+\overline{S}) \gtrsim (T+\overline{T})^{1/7} \tag{5.25}$$

the quantum term in eqn. (5.24) can be ignored and we recover our original minimum. For example, if $t \sim 10$, s must be $\gtrsim 1.4$ to suppress the quantum correction[7] .

We now calculate the classical soft masses using the general expression [114] [95]

$$m^2_{\alpha\overline{\beta}} = V|_{min} K_{\alpha\overline{\beta}} + m^2_{3/2} K_{\alpha\overline{\beta}} - F^A F^{\overline{B}} R_{A\overline{B}\alpha\overline{\beta}} \tag{5.26}$$

For our model this reduces to

$$m^2_{\alpha\overline{\beta}} \sim m^2_{3/2} K_{\alpha\overline{\beta}} - F^T F^{\overline{T}} R_{T\overline{T}\alpha\overline{\beta}} \tag{5.27}$$

The calculation of the Riemann curvature tensor and the F-terms may be adapted from the results derived in [24] which follow from [112] and [102]. We quote the value of the soft mass, m_s^2, (where $m^2_{\alpha\overline{\beta}} \equiv m_s^2 K_{\alpha\overline{\beta}}$) below

$$m_s^2 = \frac{5\xi}{8t^{3/2}} m^2_{3/2} \tag{5.28}$$

We conclude that the soft masses are not tachyonic (since ξ is positive). However, they are fixed at a scale comparable to $m_{3/2}$, i.e. parametrically above the weak scale and are thus of limited phenomenological interest.

[7] Consistency of the two super-covariant derivative expansion when the lightest integrated-out scale is the Kaluza-Klein scale requires $|W_0| < t^{-1/2}$. This implies $t \lesssim \mathcal{O}(10)$.

5.3 Single Kähler Modulus with S and T SUSY breaking

5.3.1 Series Expansion Analysis

We now investigate a class of SUGRA models in which supersymmetry can be broken in both the S and T directions. As in the previous example, we study models coming from IIB compactifications on Calabi Yau orientifolds with matter living on D3 branes at a singularity. We include Wilson lines in the compactification in order the break the gauge group into a direct product group $\Pi_i SU(N_i)$. We assume that these groups condense to give non-perturbative corrections to the superpotential that break supersymmetry. Unlike the previous model, we do not include α' corrections to the Kähler potential. The generic expressions for the Kähler and superpotentials are given below

$$K = -3\ln(T+\overline{T}) - \ln(S+\overline{S}) - \ln(k(U,\overline{U})) \tag{5.29}$$

$$W = A(U) + B(U)S + \sum_i C_i(U,S)e^{-x_i T} \tag{5.30}$$

Here, $x_i \equiv \frac{2\pi}{N_i}$ where N_i is the rank of the ith gauge group and U represents all of the complex structure moduli ($U^a, a = 1, \ldots, h_{21}$). For our analysis we will assume that the exponential prefactors C_i are $\mathcal{O}(1)$ and that their U and S dependence comes from threshold effects and internal fluxes, i.e. $C_i(U,S) = C_i(U)e^{\alpha_i S}$. (See for example [94][8]) Therefore, the superpotential can be written as

$$W = A(U) + B(U)S + \sum_i C_i(U)e^{-x_i T + \alpha_i S} \tag{5.31}$$

Let us now examine a technique for handling this model numerically[9] . Suppose that we identify a minimum of the scalar potential at a point, (S_0, T_0, U_0) in field space. Without loss of generality we assume that this point is real. We expand the superpotential only in fluctuations about the S and T directions. We assume that there is sufficient freedom in the choice of fluxes that once the minimization in these two directions are carried out fluxes can be chosen such that

[8] In this paper the fluxes are used to break the $SU(5)$ gauge group containing the standard model. Here by contrast we are breaking the condensing group which generates the non-perturbative terms in W.

[9] The following method was first outlined in [98].

this remains a minimum with some value of U such that $F^U = 0$. With a sufficient number of 3-cycles this should be always possible. We expand W as

$$W(S,T,U) = \sum_{n,m} a_{nm}(U)(S-S_0)^n(T-T_0)^m \tag{5.32}$$

Comparing this with eqn. (5.30) gives

$$\begin{aligned} a_{nm} &= \frac{1}{n!m!}\partial_S^n \partial_T^m W_0 \\ &= \frac{1}{n!m!}[(A_0 + S_0 B_0)\delta_{n0}\delta_{m0} + B_0 \delta_{n1}\delta_{m0} + \sum_i (-x_i)^m \partial_S^n C_{i0} e^{-x_i T_0}] \\ &\equiv e^{-x_i T_0} S_0^{-n} T_0^{-m} \tilde{a}_{nm} \end{aligned} \tag{5.33}$$

Where $W_0 \equiv W(S_0, T_0, U_0)$. We now redefine the fields as ($\widetilde{S} \equiv S/S_0$, $\widetilde{T} \equiv T/T_0$). We may then write the superpotential as

$$W = e^{-x_i T_0} \sum_{nm} \tilde{a}_{nm}(\widetilde{S}-1)^n(\widetilde{T}-1)^m \equiv e^{-x_i T_0}\widetilde{W} \tag{5.34}$$

This results in an overall scaling of the scalar potential

$$V = \frac{e^{-2x_i T_0}}{T_0^3 S_0}\widetilde{V}(\widetilde{S},\widetilde{T},U,\overline{\widetilde{S}},\overline{\widetilde{T}},\overline{U}) \tag{5.35}$$

where $\widetilde{V}$ is defined in terms of $\widetilde{W}$ and $\widetilde{K} = -3\ln(\widetilde{T}+\overline{\widetilde{T}}) - \ln(\widetilde{S}+\overline{\widetilde{S}}) - \ln(k(U,\overline{U}))$.

Expanding the superpotential in a Taylor series allows us to control the location and value of scalar potential's minimum. Since the Hessian matrix for the scalar potential only depends on terms up to third order in the expanded superpotential, we can arbitrarily tune a minimum of the scalar potential by solving the following system of equations (from eqn. (5.33))

$$\begin{aligned} \tilde{a}_{00} &= e^{x_1 T_0}(A_0 + S_0 B_0) + \sum_i C_{i0} e^{-(x_i - x_1)T_0} \\ \tilde{a}_{10} &= S_0\left[e^{x_1 T_0} B_0 + \sum_i \partial_S C_{i0} e^{-(x_i - x_1)T_0}\right] \\ \tilde{a}_{01} &= T_0 \sum_i (-x_i) C_{i0} e^{-(x_i - x_1)T_0} \\ &\vdots \\ \tilde{a}_{30} &= \frac{S_0}{6}\sum_i \partial_S C_{i0} e^{-(x_i - x_1)T_0} \end{aligned} \tag{5.36}$$

5.3.2 Numerical Example

Following the arguments of the previous section we consider the following SUGRA model

$$K = -3\ln(T+\overline{T}) - \ln(S+\overline{S}) - \ln(k(U,\overline{U})) \tag{5.37}$$

$$W = A_0 + B_0 * S + C_1 e^{-x_1 T + \alpha_1 S} + C_2 e^{-x_2 T + \alpha_2 S} + C_3 e^{-x_3 T + \alpha_3 S} + C_4 e^{-x_4 T + \alpha_4 S} \tag{5.38}$$

We include four non-perturbative terms because expanding the superpotential to third order requires ten independent parameters. If we want to construct a minimum of the scalar potential with the gravitino mass fixed to a certain scale it turns out that unless we include four non-perturbative terms it is too hard to solve for a minimum. We can construct an extremum of the scalar potential with two or three non-perturbative terms but we cannot guarantee that such an extremum is a minimum because we lack enough free parameters to simultaneously solve all ten equations given above (eqn. (5.36)).

For models with two or three non-perturbative terms, requiring the extremum to be a minimum, in principle, defines some region in 3-dimensional parameter space. (e.g. $\{(\tilde{\alpha}_{00}, \tilde{\alpha}_{10}, \tilde{\alpha}_{01})\}$). This region is identified by requiring the eigenvalues of the Hessian to be positive definite. However, general expressions for the eigenvalues are complicated enough to prevent the identification of this region in a computationally tractable manner. Therefore, including four non-perturbative terms and solving the system of equations given above (eqn. (5.36)) is the most reliable technique for identifying a minimum in this class of models.

From these arguments we construct a Minkowski minimum with $m_{3/2} \sim 10$ TeV for the following values of the parameters given in table 5.1. Plots of this minimum along the s, ($\Re(S)$), and t, ($\Re(T)$), directions are given in figures 5.1 and 5.2. This minimum is adapted from the local model identified in [98].

In this example we note that, at the minimum of the potential, $|F_S| \sim 4|F_T|$. In principle we expect $|F_S|$ and $|F_T|$ to be of the same order. In fact, the relatively low scale of $m_{3/2}$ for this model depends on these two F-terms making comparable contributions to the SUSY breaking.

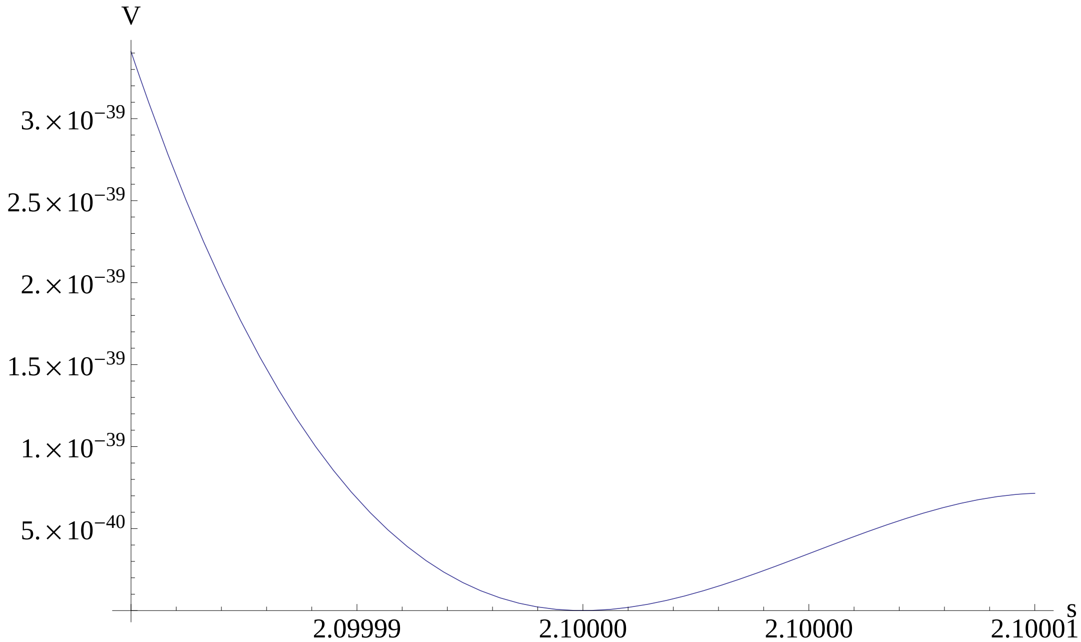

Figure 5.1: Vmin for $<t>= 40$

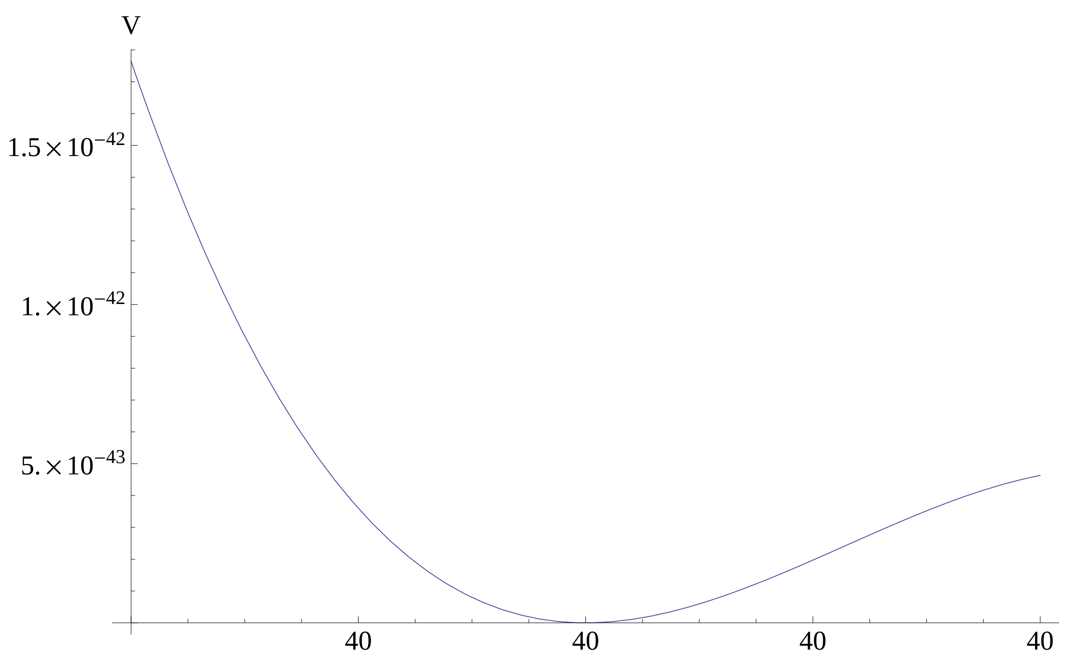

Figure 5.2: Vmin for $<s>= 2.1$

	$A_0 = 1.85 * 10^{-8}$ $B_0 = 1.6 * 10^{-10}$ $C_1 = -3.4$ $x_1 = \frac{2\pi}{30}$ $\alpha_1 = -1.06$ $C_2 = 13.3$ $x_2 = \frac{2\pi}{29}$ $\alpha_2 = -1.1$ $C_3 = -17.7$ $x_3 = \frac{2\pi}{28}$ $\alpha_3 = -1.14$ $C_4 = 8.1$ $x_4 = \frac{2\pi}{27}$ $\alpha_4 = -1.18$
$<t>$	40
$<\tau>$	0
$<s>$	2.1
$<\sigma>$	0
$V_0\|_{min}$	0
$m_{3/2}^2 \equiv e^K \|W\|^2$	1.3×10^{-28}
$\|F^T\|^2 K_{T\overline{T}} \equiv e^K K^{T\overline{T}} \|D_T W\|^2$	3.2×10^{-28}
$\|F^S\|^2 K_{S\overline{S}} \equiv e^K K^{S\overline{S}} \|D_S W\|^2$	6.8×10^{-29}

Table 5.1: Moduli field vev's, F-terms, Gravitino mass and the Cosmological Constant for SKM + 4 Non-Pert Terms at a non-SUSY minimum of the scalar potential (in $M_P = 1$ units).

In the limit of $|F_S| \to 0$ with $|F_T| \neq 0$ we return to the situation described by well-known no-go theorems [111] [102] [98] and there would be no deSitter minimum. When $|F_S|$ is non-zero but subdominant to $|F_T|$ we may plausibly recover a high scale deSitter minimum, analogous to the previous model, with the axio-dilaton playing the role of a subdominant correction to the Kähler modulus. In either case, a low scale deSitter minimum depends crucially on that fact that $|F_S| \sim |F_T|$.

We may calculate the soft masses for this particular example by following the approach of [21]. Namely, we may express the full Kähler potential, including matter fields as

$$K = K_{mod} + Z(T)_{\alpha\overline{\beta}} \Phi^\alpha \overline{\Phi}^{\overline{\beta}} + \ldots \tag{5.39}$$

Where, $Z(T)_{\alpha\overline{\beta}} = \frac{3\delta_{\alpha\overline{\beta}}}{T+\overline{T}}$ and $K_{mod} = -3\ln(T+\overline{T}) - \ln(S+\overline{S}) - \ln(k(U,\overline{U}))$. The soft masses can be calculated from the Kähler potential following the general expression given in eqn. (5.26). The only relevant non-vanishing curvature component is $R_{T\overline{T}\alpha\overline{\beta}} = \frac{1}{3} K_{T\overline{T}} Z_{\alpha\overline{\beta}} + \mathcal{O}(\Phi^2)$. Therefore, for this model, the soft mass expression becomes

$$m_s^2 Z_{\alpha\overline{\beta}} = \left(m_{3/2}^2 - \frac{1}{3} F^T \overline{F}^{\overline{T}} K_{T\overline{T}} \right) Z_{\alpha\overline{\beta}} = \frac{1}{3} F^S \overline{F}^{\overline{S}} K_{S\overline{S}} Z_{\alpha\overline{\beta}} \tag{5.40}$$

Therefore, $m_s^2 \approx 2.2 \times 10^{-29}\ M_P$ or $m_s \approx 4.8$ TeV. Note that as long as $V_0 \ll m_{3/2}^2$ for this class of models, m_s^2 will always be roughly equal to $\frac{1}{3}|F^S|^2$ and hence positive.

It is worth reiterating that this specific model, including all its relevant scales, has been arbitrarily chosen. We are free, in principle, to generate a model with any desired scale by solving the corresponding system of equations (eqn. (5.36)). What we have demonstrated is a general technique for finding such models.

5.4 Conclusion

We have demonstrated that there exists physically plausible vacua coming from IIB string compactifications on Calabi-Yau orientifolds having one Kähler modulus together with fluxes and D-Branes. Such models have natural FCNC suppression due to the fact that they contain only one Kähler modulus[10] . In the simplest model, (eqns. (5.1),(5.2)), an α' correction allows SUSY to be broken along the T, (Kähler modulus), direction. A Minkowski or de Sitter classical minimum is attainable but the soft mass phenomenology is such that it is of no relevance for the hierarchy problem. This is due to the fact that the gravitino mass is fixed at a high scale ($m_{3/2} \gtrsim 10^{-3} \times M_P$).

In the second model, (eqns. (5.37),(5.38)), the gravitino mass can be set to any scale by appropriate choice of fluxes. SUSY is broken in both the S, (axio-dilaton), and T, (Kähler modulus), directions and we expect both fields to contribute comparable F-terms. The classical cosmological constant as well as the location of the minimum in field space can be tuned by solving the appropriate equations coming from the Taylor series expansion of the superpotential (eqn. (5.36)). However, in order to solve these equations in a tractable manner, the superpotential must include at least four non-perturbative terms.

Finally let us observe that while in principle it is possible to find models (as demonstrated by the above numerical example) that can in fact give a phenomenology that is relevant to TeV scale physics, it is hard to obtain generic consequences of the entire class of such models. The phenomenology is clearly quite sensitive to the model parameters (fluxes choices). This is quite

[10] Quantum corrections will not alter this picture due to the large volume suppression, see [99].

unlike the case of LVS models where with a few general assumptions about the location of the MSSM a viable phenomenology is obtained [101] [23] [24] [83] [4]. While the original motivation for this investigation was in fact to remove the requirement on the location on the MSSM cycle, that is needed in the LVS case, to satisfy FCNC constraints, the upshot of our investigation actually strengthens the case for this scenario.

5.5 Appendix: Single Kähler Modulus + α' + RaceTrack

We may naturally extend our first model, (eqns. (5.1),(5.2)) to include the effects of two non-perturbative corrections to the superpotential. This model is given below

$$K = -2\ln\Big(\big(\frac{1}{2}(T+\overline{T})\big)^{3/2} + \frac{\hat{\xi}}{2}\big(\frac{1}{2}(S+\overline{S})\big)^{3/2}\Big) - \ln(S+\overline{S}) - \ln(k(U,\overline{U})) \tag{5.41}$$

$$W = W_{flux}(S,U) + Ae^{-aT} + Be^{-bT} \tag{5.42}$$

Here $\hat{\xi} = \frac{-\chi\zeta(3)}{2(2\pi)^3}$, $\chi = 2(h_{11}-h_{21})$ and $a = \frac{2\pi}{N}$, $b = \frac{2\pi}{M}$, where N and M are the ranks of two hidden sector gauge groups. We may naively believe that is model will yield an improvement on the first model, but as we shall see, this improvement is only minor. Ultimately, the gravitino mass is still fixed near the Planck scale. As before we define the complex moduli fields as $T = t + i\tau$ and $S = s + i\sigma$ and we search for minima of this model's scalar potential that break supersymmetry along the T direction.

5.5.1 Analytic Results

As with our first model, we may identify minima of the full scalar potential, $V(S,T,U)$, by minimizing $V(T)$ with $F^S|_{min} = F^U|_{min} = 0$. Our analytic results are essentially a straight forward generalization of the simpler model. We present them here with a modicum of redundancy.

Taking the large volume approximations (eqns. (5.4),(5.5),(5.6)) we get a full expression for the scalar potential

$$\begin{aligned} V \quad \sim \quad & \frac{1}{t^3 k(U,\overline{U})(2s)}\Big[\frac{4t^2}{3}\big(a^2|A|^2e^{-at} + b^2|B|^2e^{-2bt} + 2\Re\big(aAe^{-aT}b\overline{B}e^{-b\overline{T}}\big)\big) \\ & +2\Re\big((-aAe^{-aT} - bBe^{-bT})(-2t)\overline{W}\big) + \frac{3\xi}{4t^{3/2}}|W|^2\Big] \end{aligned} \tag{5.43}$$

From eqn. (5.43) we may extract the axion dependence of the scalar potential

$$V(\tau) = \frac{1}{t^3 k(U,\overline{U})(2s)}\Big(2\Re\big(-aAe^{-aT}\overline{W}_0(-2t) - aAe^{-aT}\overline{B}e^{-b\overline{T}}(-2t) - bBe^{-bT}\overline{W}_0(-2t) - bBe^{-bT}\overline{A}e^{-a\overline{T}}(-2t) + \frac{4t^2}{3}aAe^{-aT}b\overline{B}e^{-b\overline{T}}\big)\Big) \tag{5.44}$$

We define the complex quantities as follows, $A = |A|e^{i\phi_A}$, $B = |B|e^{i\phi_B}$, $W_0 = |W_0|e^{i\phi_{W_0}}$, $(W_0 \equiv W_{flux}|_{min})$. The potential's axion dependence now becomes

$$V(\tau) = \frac{1}{t^3}\Big(4ta|A||W_0|e^{-at}\cos(a\tau - \phi_A + \phi_{W_0}) + 4tb|B||W_0|e^{-bt}\cos(b\tau - \phi_B + \phi_{W_0}) (\frac{8}{3}t^2ab + 4at + 4bt)|A||B|e^{-(a+b)t}\cos((a-b)\tau - \phi_A + \phi_B)\Big) \tag{5.45}$$

Where we have again assumed $\frac{1}{k(U,\overline{U})(2s)} \sim \mathcal{O}(1)$. Extremizing with respect to τ,

$$V'(\tau) = \frac{1}{t^3}\Big(-4ta^2|A||W_0|e^{-at}\sin(a\tau - \phi_A + \phi_{W_0}) - 4tb^2|B||W_0|e^{-bt}\sin(b\tau - \phi_B + \phi_{W_0}) - (a-b)(\frac{8}{3}t^2ab + 4at + 4bt)|A||B|e^{-(a+b)t}\sin((a-b)\tau - \phi_A + \phi_B)\Big) = 0 \tag{5.46}$$

The only set of solutions to this equation that is independent of $|A|$,$|B|$ and $|W_0|$ is

$$a\tau - \phi_A + \phi_{W_0} = n\pi \quad b\tau - \phi_B + \phi_{W_0} = m\pi \quad n, m \in \mathbb{Z} \tag{5.47}$$

We now check the concavity of the potential at the τ extremum,

$$V''(\tau) = \frac{1}{t^3}\Big(-4ta^3|A||W_0|e^{-at}\cos(a\tau - \phi_A + \phi_{W_0}) - 4tb^3|B||W_0|e^{-bt}\cos(b\tau - \phi_B + \phi_{W_0}) - (a-b)^2(\frac{8}{3}t^2ab + 4at + 4bt)|A||B|e^{-(a+b)t}\cos((a-b)\tau - \phi_A + \phi_B)\Big) \tag{5.48}$$

In order to isolate a minimum, we require $V'' > 0$. This condition, in turn, depends on the value of t, a, b, $|A|$, $|B|$ and $|W_0|$. In the limit where $|W_0| \gg e^{-at}$, V'' can be made positive if

$$a\tau - \phi_A + \phi_{W_0} = (2n+1)\pi \quad b\tau - \phi_B + \phi_{W_0} = (2m+1)\pi \quad n, m \in \mathbb{Z} \tag{5.49}$$

Inserting eqn. (5.49) into eqn. (5.45), we compute the scalar potential for this model and expand in negative powers of the volume. For large volumes the potential can be safely approximated by

$$
\begin{aligned}
V \sim\ & \frac{4}{3}\Big(b^2|B|^2e^{-2bt}+a^2|A|^2e^{-2at}+2ab|A||B|e^{-(a+b)t}\Big)\frac{t^{1/2}}{\mathcal{V}} \\
&+4\Big(b|B|^2e^{-2bt}+a|A|^2e^{-2at}+|A||B|(a+b)e^{-(a+b)t}-|W_0|(a|A|e^{-at}+b|B|e^{-bt})\Big)\frac{t}{\mathcal{V}^2} \\
&+\frac{3|W_0|^2\xi}{4\mathcal{V}^3}+\dots
\end{aligned}
\tag{5.50}
$$

From here, the scalar potential can be further simplified with knowledge of the magnitude of W_0. Again, there are two relevant regimes; assuming $a \sim b$, $|W_0| \sim e^{-at}$ and $|W_0| \gg e^{-at}$. As in the simpler model, minima in the first regime ($a \sim b$, $|W_0| \sim e^{-at}$) are supersymmetric. One may see this by examining the potential in this regime. With the benefit of foresight, we first assume that $|W_0| \approx (at)e^{-at}$. In this limit, the scalar potential is volume suppressed yielding

$$
\begin{aligned}
V \sim\ & \frac{4}{3}\Big(b^2|B|^2e^{-2bt}+a^2|A|^2e^{-2at}+2ab|A||B|e^{-(a+b)t}\Big)\frac{t^{1/2}}{\mathcal{V}} \\
&+4\Big(-|W_0|(a|A|e^{-at}+b|B|e^{-bt})\Big)\frac{t}{\mathcal{V}^2}
\end{aligned}
\tag{5.51}
$$

One can solve for the minimum of the scalar potential. At this minimum, $|W_0|$ is

$$
|W_0| = \frac{2}{3}\left(\frac{b^3|B|^2e^{-2bt}+a^3|A|^2e^{-2at}+(a+b)ab|A||B|e^{-(a+b)t}}{a^2|A|e^{-at}+b^2|B|e^{-bt}}\right)t \sim \mathcal{O}\left((at)e^{-at}\right) \tag{5.52}
$$

This is consistent with our original assumption, $|W_0| \approx (at)e^{-at}$. As in the simpler model, this minimum is supersymmetric. One can see this by examining the F-term flatness equation.

$$
D_T W = \partial_T W + K_T W = -aAe^{-aT} - bBe^{-bT} - \frac{3t^{1/2}W}{2t^{3/2}+\xi} = 0 \tag{5.53}
$$

Therefore, at the minimum,

$$
|W_0| \sim (at)e^{-at} \tag{5.54}
$$

This is the same order of magnitude estimate that we initially assumed. The numerical search for minima in this limit confirm that all such minima are indeed supersymmetric.

We now investigate the remaining regime, $|W_0| \gg e^{-at}$. In this limit, the scalar potential is exponentially suppressed at large volumes and simplifies to

$$
V \sim -\Big(4|W_0|(a|A|e^{-at}+b|B|e^{-bt})\Big)\frac{t}{\mathcal{V}^2}+\frac{3W_0^2\xi}{4\mathcal{V}^3}+\dots \tag{5.55}
$$

Solving for the minimum and assuming that $at \sim bt \gtrsim \mathcal{O}(2)$ (as in the earlier model) gives the condition

$$|W_0| = \frac{32}{27\xi}\Big((a^2|A|e^{-at} + b^2|B|e^{-bt})\Big)t^{7/2} \tag{5.56}$$

This shows that at the minimum of the potential, $|W_0| \gg e^{-at}$, which is consistent with our original assumption. Checking for positive concavity of the minimum gives

$$V'' = \frac{27|W_0|^2\xi}{8t^{11/2}}\left(-a + \frac{11}{2t}\right) - \frac{4|W_0|b^2}{t^2}(b-a)|B|e^{-bt} > 0 \tag{5.57}$$

We see from this equation that for $at \lesssim \mathcal{O}(7)$ this extremum is a minimum (this is an approximate upper bound based on the assumption that $a \sim b$). This should be compared with the upper bound obtained in our first model ($at < 11/2$). We see that there is only marginal improvement our first model. The gravitino mass is bounded from below by

$$m_{3/2} \sim \frac{|W_0|}{t^{3/2}} \gtrsim 5 \times 10^{-4}\ \mathrm{M_P} \ \text{ or } \ 5 \times 10^{14}\ \mathrm{GeV} \tag{5.58}$$

Where, as before, $\xi \sim \mathcal{O}(100)$. We may estimate the value of the scalar potential at the minimum by inserting the extremization equation (eqn. (5.56)) into eqn. (5.55). This yields the following relation

$$\begin{aligned} V|_{min} &= -\left(4|W_0|\left(+\frac{27\xi|W_0|}{32t^{7/2}a} - \frac{b^2}{a}|B|e^{-bt} + b|B|e^{-bt}\right)\right)t^{-2} + \frac{3|W_0|^2\xi}{4t^{9/2}} \\ &= \frac{3|W_0|^2\xi}{4t^{9/2}}\left(-\frac{9}{2at} + 1\right) - \frac{4|W_0|}{t^2}|B|be^{-bt}\left(1 - \frac{b}{a}\right) \end{aligned} \tag{5.59}$$

In principle, $V|_{min}$ can be fine-tuned to zero. Due to the transcendental nature of eqn. (5.59), this has to be done numerically. We also note that, as with the first model, this model is, in principle, susceptible to destabilization via 1-loop quantum corrections (à la eqn. (5.24)). However, with sufficiently large values of s, this correction can be suppressed and the classical minimum maintained.

Chapter 6

A QCD Axion from a IIB Local Model in the Large Volume Scenario

Chapter Summary

We examine a model for the QCD axion within IIB string theory. The matter content is that of the Next-to-Minimal Supersymmetric Standard Model and the string moduli are stabilized using the Large Volume Scenario. We investigate the resulting particle spectrum and argue that, under certain conditions, this model can be made to satisfy the known phenomenological constraints from cosmology and particle physics.

6.1 Introduction

Since its inception in 1978, the axion model has provided an elegant solution to the Strong CP problem (for review see for instance [115]). Within this model, the axion is taken to be a pseudo-Goldstone boson of an additional $U(1)$ global symmetry known as Pecci-Quinn symmetry. This symmetry is broken at some scale f_a that is assumed to be high (i.e. $f_a \gg M_{Weak}$). In conventional axion models, known constraints from cosmology restrict f_a to be within the window 10^9 GeV $\lesssim f_a \lesssim 10^{12}$ GeV.

The upper bound on f_a comes as somewhat of a disappointment for GUT-scale model building because these models generically prefer $f_a \sim M_{GUT}$. In fact, axions are ubiquitous within string theory, but in most instances f_a is of the order of the string scale. Fortunately, several authors [88] [85] have noted that in supersymmetric extensions of the axion model the conventional upper bound on f_a can be circumvented. Essentially, the bound of $f_a \lesssim 10^{12}$ GeV comes from constraints on the dark matter relic abundance of the universe. However, the decays of the axion superparters, the saxion and the axino, can dilute the axion's contribution to the dark matter relic abundance and hence allow for a higher scale f_a.

The increased upper bound on f_a improves the likelihood of constructing a realistic QCD axion model within string theory. However, any honest attempt to do so likely requires one to address the challenges endemic to most string theory model building. These challenges include successful moduli stabilization, the presence of a chiral matter sector containing the Standard Model and low-scale supersymmetry breaking. Recently, much progress has been made in overcoming these challenges in IIB string theory. In particular, the issue of moduli stabilization and SUSY-breaking can be achieved in the Large Volume Scenario (LVS) [87]. Additionally, a chiral matter sector can be introduced by local D-Brane models at a singularity. These models are then embedded within a global Calabi-Yau Orientifold (CYO) whose moduli are stabilized along to lines of LVS.

In the present paper, we will examine an effective supergravity Lagrangian coming from such a local model [101] [23]. In particular, we will assume that chiral matter fields come from a D7-Brane wrapping a 4-cycle that shrinks below the string scale. This local model will be embedded in a CYO with the requisite number of Kähler moduli and non-perturbative effects to ensure moduli stabilization and low-scale SUSY breaking. Additionally, we will assume that the matter content is that of the Next-to-Minimal Supersymetric Standard Model (NMSSM) [107]. This assumption will allow us to exploit several benefits over the traditional Minimal Supersymmetric Standard Model (MSSM). These benefits will be described in detail later.

Many aspects of the phenomenology resulting from local models within LVS have been analysed in detail (see for instance [24] [83]). In particular, the nature and scale of the soft-terms as well as the scales of the stabilized Kähler moduli have been determined. Essentially, gauginos gain mass predominately through the Weyl anomaly whereas the remaining soft terms emerge from Renormalization Group running. In this paper, we assume these soft-terms take this form and we instead focus on the phenomenology of an effective supergravity model. We incorporate the soft-terms and Kähler moduli vev's when necessary. This paper is outlined as follows. In section 2, we introduce our supergravity model and examine its field content. In section 3, we determine the relevant mass scales of the axion supermultiplet and other important quantities. In section 4, we discuss the important phenomenological constraints from cosmology and determine under what conditions they can be satisfied. In section 5, we provide concluding remarks.

6.2 The SUSY Lagrangian

Following the analysis of [101] [23], we consider a Calabi Yau Orientifold of so-called "Swiss cheese" type, i.e. with one big Kähler modulus, T_b, one small Kähler modulus, T_s, and at least two shrinking modulus, (T and B_2). We assume that the presence of non-perturbative effects (e.g. Euclidean D3 instantons or gaugino condensation) can be used to stabilize T_b and T_s such that the resulting volume of the CYO is exponentially large. Additionally, we assume that fluxes can be chosen in order to stabilize the complex structure moduli and the axio-dilation as is done in GKP-KKLT type models (For review see [7] [8]). The chiral matter fields will be introduced via D-branes wrapping the T cycle. The B_2 modulus is needed for a consistant orientifold action, with the B_2 cycle being exchanged with the T cycle under orientifolding.

After fixing the complex structure moduli and the axio-dilalon, but before fixing the volume moduli, the Kähler potential takes the following form (see [101] eq. 3.11)

$$\begin{aligned} K &= -2\ln\left(\left(T_b+\overline{T_b}\right)^{3/2}-\left(T_s+\overline{T_s}\right)^{3/2}+\xi\right)+\frac{\left(T+\overline{T}+MV\right)^2}{\mathcal{V}} \\ &\quad +\frac{\left(B_2+\overline{B_2}+qV'\right)^2}{\mathcal{V}}+\frac{\Phi^i\overline{\Phi}^i}{\mathcal{V}^{2/3}}\left(1+\mathcal{O}\left(T+\overline{T}\right)^{\lambda}+\dots\right) \end{aligned} \tag{6.1}$$

Here, λ is a positive parameter, $\xi \equiv \frac{-\chi\xi(3)}{4(2\pi)^2} <s>^{3/2}$, $\xi > 0$ and Φ^i represents the chiral matter fields. M and q are the $U(1)$ charges of T and B_2 respectively.

After stabilizing the volume moduli, as well as the B_2 moduli, one can absord the volume factor into the remaining terms as follows

$$T \to \frac{T}{\sqrt{\mathcal{V}}}, \quad M \to \frac{M}{\sqrt{\mathcal{V}}} \quad \Phi_i \to \frac{\Phi_i}{\mathcal{V}^{1/3}} \tag{6.2}$$

The Kähler potential then reduces to the following form

$$K = \left(T + \overline{T} + MV\right)^2 + \Phi_i^\dagger e^{Q_i V} \Phi_i \tag{6.3}$$

Here, we adopt the conventional Pecci Quinn charges for the chiral fields ($Q_H = 1$, $Q_S = -2$, ...). For simplicity, we have suppressed the Standard Model gauge couplings that conventially appear inside an MSSM-like Kähler potential. We instead focus on the $U(1)_{PQ}$ SUSY gauge couplings and term involving the T modulus. As stated before, the T modulus is charged under an anomalous $U(1)$. The vector superfield, V, transform under this $U(1)$ in such a way as to cancel the anomaly. Namely, the superfields transform as $\delta T = -M\Lambda$, $\delta\overline{T} = -M\Lambda^\dagger$ and $\delta V = \Lambda + \Lambda^\dagger$. This is a 4D example of the Green Schwartz Mechanism. The now non-anamolous $U(1)$ will later be recognized as the Pecci-Quinn symmetry $U(1)_{PQ}$.

We assume that the superpotential is that of a restricted (Pecci-Quinn Symmetric) version of the NMSSM. (This is often refered to as PQNMSSM). In principle, this matter content must be defined by an appropriate del Pecco surface (see for example [103]). We assume there is no obstruction to constructing such a surface. The superpotential is given by

$$W = ySH_u \cdot H_d + W_{MSSM} \tag{6.4}$$

Where S is the NMSSM singlet chiral superfield and y is a complex cubic interaction constant (Yukawa type). By W_{MSSM}, we imply all terms present in the MSSM superpotential *except* an explicit μ-term. Throughout this paper, the symbol S refers to this singlet field and *not* to the axio-dilaton. In fact, the axio-dilaton will not appear in most calculations, so there should be no confusion. For simplicity we have suppressed any higher order terms involving S that are typical of the most general version of the NMSSM.

Combining the Kähler and superpotentials (eqns. (6.3)(6.4)) together we arrive at the full Lagrangian

$$\mathcal{L} = \frac{1}{4}\left[f\mathcal{W}^\alpha\mathcal{W}_\alpha + \overline{f\mathcal{W}}_{\dot\alpha}\overline{\mathcal{W}}^{\dot\alpha}\right]_F + \left[(T + \overline{T} + MV)^2 + \Phi_i^\dagger e^{Q_i V}\Phi_i\right]_D + [W + h.c.]_F \tag{6.5}$$

Here, the f term is the gauge coupling function to be defined later with α and $\dot{\alpha}$ as spinor indicies. M is naively expected to be on the order of the string scale (e.g. $M \sim 10^{16}$ GeV).

We have suppressed many of the standard MSSM terms in the Lagrangian. We will incorporate these terms when the need arrises. In particular we will be carefull to add F and D-terms for the Higgs fields in order to compute the potential for the scalar fields.

6.2.1 The Field Content

In order to examine the Lagrangrian (eqn. (6.5)), we first expand the superfields in terms of their field content. We define the superfields in terms of the following vector and chiral supermultiplets

$$V \equiv (A_\mu, \lambda, D) \quad \Phi_i \equiv (\phi_i, \psi_i, \mathcal{F}_i) \tag{6.6}$$

For the specific case of the T and S chiral fields, the supermultiplets are

$$T \equiv (\phi, \psi, \mathcal{F}) \qquad S \equiv (s, \psi_S, \mathcal{F}_S) \qquad \phi \equiv \frac{\tau + ia}{\sqrt{2}} \qquad s \equiv \frac{\rho + i\chi}{\sqrt{2}} \tag{6.7}$$

The superfield expansions and integrations are given in Appendix A.1. Here, we qoute the results. The contribution to the Lagrangian coming from the Kähler potential is

$$\begin{aligned}\mathcal{L}_K \quad = \quad & -\frac{1}{2}\partial^\mu\tau\partial_\mu\tau + M\tau D + 2i\left(\psi^\dagger\gamma^\mu\partial_\mu\psi + \sqrt{2}M\psi\lambda\right) + 2|\mathcal{F}|^2 - (\partial_\mu a + MA_\mu)^2 \\ & +|\mathcal{F}_i|^2 - (\mathcal{D}^\mu\phi_i)^\dagger\mathcal{D}_\mu\phi_i + \frac{1}{2}\left(Q_iD\right)|\phi_i|^2 + i\partial_\mu\psi_i^\dagger\overline{\sigma}^\mu\psi_i + \frac{1}{2}Q_iA^\mu\psi_i^\dagger\overline{\sigma}^\mu\psi_i \\ & -\frac{i}{\sqrt{2}}Q_i(\phi_i\lambda^\dagger\psi_i^\dagger - \phi_i^\dagger\lambda\psi)\end{aligned} \tag{6.8}$$

Where $\mathcal{D}_\mu = \left(\partial_\mu + i\frac{Q_i}{2}A_\mu\right)$ and $\lambda = \binom{\lambda}{\lambda^\dagger}$.

We now examine the SUSY field strength tensor. Near the singulary, the gauge coupling function becomes [101]

$$f = S + \kappa T \tag{6.9}$$

In this case, (and this case alone), S is the axio-dilaton (instead of the NMSSM singlet) and T is a Kähler modulus defined in eqn. (6.44). Here κ is a loop correction parameter with $\dim[\kappa] = -1$.

We assume that the axio-dilaton field S is stabilized by a particular choice of fluxes such that we may replace S with its vev, $<S>$, which takes the value $<S>=\frac{1}{g^2}$.

As calculated in Appendix A.1, the SUSY field strength is given by

$$\begin{aligned}\frac{1}{4}\left[(S+\kappa T)\mathcal{W}^\alpha\mathcal{W}_\alpha+h.c.\right]_F &= \kappa g^2\left(\mathcal{F}\lambda^2+\overline{\mathcal{F}\lambda}^2\right)+2^{3/2}\kappa g^2\left(\sigma^{\mu\nu}\psi\lambda F_{\mu\nu}\right)\\ &+4\kappa g^2\left(\frac{\tau}{2}\lambda^\dagger\gamma^\mu\partial_\mu\lambda-\frac{\tau}{8}F_{\mu\nu}^2+\frac{a}{16}\widetilde{F}_{\mu\nu}F^{\mu\nu}\right)\\ &+2D^2+4\left(\lambda^\dagger\gamma^\mu\partial_\mu\lambda-\frac{1}{4}F_{\mu\nu}^2\right)\end{aligned} \tag{6.10}$$

6.2.2 Scalar Potential Considerations

We are interested in computing the terms contributing to the potential of the full Lagrangian eqn. (6.5). Two of these terms come from solving the F and D-term equations of motion. This is done in Appendix A and we quote the results. The F-term potential is

$$V_F(h_u,h_d,s)=|y(h_u^+h_d^- - h_u^0h_d^0)|^2+|ys|^2\left(|h_u^0|^2+|h_u^+|^2-|h_d^0|^2-|h_d^-|^2\right)^2 \tag{6.11}$$

Where we have defined the Higgs doublet superfields by the following supermultiplets

$$H_u\equiv(h_u,\psi_u,\mathcal{F}_u)\qquad H_d\equiv(h_d,\psi_d,\mathcal{F}_d) \tag{6.12}$$

Similiarly, the D-term potential is given by

$$V_D=-\frac{1}{2}\Big(2M^2\tau^2+g^2\frac{1}{4}Q_i^2|\phi_i|^4+g^2\frac{1}{2}\sum_{j\neq i}Q_iQ_j|\phi_i|^2|\phi_j|^2+gM\sqrt{2}\tau|\phi_i|^2Q_i\Big) \tag{6.13}$$

In addition to the F and D-term potentials, we include general soft terms. The potential for the soft terms that are relevant to our calculation is given below

$$V_{Soft}=\left(yA_S(h_u^+h_d^- - h_u^0h_d^0)s+h.c.\right)+m_{H_u}^2|h_u^0|^2+m_{H_d}^2|h_d^0|^2 \tag{6.14}$$

Here, the yA_Shh term plays the role of the b-term in convential MSSM models. As described in [24], the soft Higgs masses are generated through RG evolution.

6.3 Sparticle Masses

We assume the h_u^0 and h_d^0 are stabilized at non-zero vev's (EWSB) by a double-well potential within the W_{MSSM} contribution to the full Lagrangian. After EWSB, the potential the scalar fields can be expanded as

$$h_u = v_u + \frac{h_{uR} + ih_{uI}}{\sqrt{2}} \quad h_d = v_d + \frac{h_{dR} + ih_{dI}}{\sqrt{2}} \quad \phi = v_\tau + \frac{\tau + ia}{\sqrt{2}} \quad s = v_s + \frac{\rho + i\chi}{\sqrt{2}} \tag{6.15}$$

The full potential for the Higgs, T and S scalar fields can now be written combining the F and D-term potentials (eqns. (6.11)(6.13)) with general soft terms (eqn. (6.14)).

$$\begin{aligned} V(h_u, h_d, \phi, s) &= V_F + V_D + V_{soft} \\ &= |y(h_u^+ h_d^- - h_u^0 h_d^0)|^2 + |ys|^2 \left(|h_u^0|^2 + |h_u^+|^2 + |h_d^0|^2 + |h_d^-|^2\right) \\ &\quad + \frac{g_1^2 + g_2^2}{8} \left(|h_u^0|^2 + |h_u^+|^2 - |h_d^0|^2 - |h_d^-|^2\right)^2 \\ &\quad + \frac{g^2 Q_H^2}{8} \left(|h_u^0|^2 + |h_u^+|^2 + |h_d^0|^2 + |h_d^-|^2\right)^2 \\ &\quad + \frac{g_2^2}{2} |(h_u^+ h_d^{0*} + h_u^0 h_d^{-*})|^2 + \frac{1}{\sqrt{2}} \tau g M Q_H \left(|h_u^0|^2 + |h_u^+|^2 + |h_d^0|^2 + |h_d^-|^2\right) \\ &\quad + \frac{1}{\sqrt{2}} \tau g M Q_S |s|^2 + M^2 \tau^2 + \frac{1}{8} Q_S^2 |s|^4 \\ &\quad + \frac{1}{2} g^2 Q_S Q_H |s|^2 \left(|h_u^0|^2 + |h_u^+|^2 + |h_d^0|^2 + |h_d^-|^2\right) \\ &\quad + \left(y A_S (h_u^+ h_d^- - h_u^0 h_d^0) s + h.c.\right) + m_{H_u}^2 |h_u^0|^2 + m_{H_d}^2 |h_d^0|^2 \end{aligned} \tag{6.16}$$

Here we have defined g_1, g_2 and g as the $U(1)_Y$, $SU(2)$ and $U(1)_{PQ}$ gauge couplings respectively. We may combine these into one coupling defined as

$$g_x^2 \equiv \frac{g_1^2 + g_2^2}{2} \tag{6.17}$$

We may also extremize V along the various directions in field space and insert the vev's for each respective field. We assume the following vev's

$$<s> \equiv v_s \quad <\phi> \equiv v_\tau \quad <h_u^0> \equiv v_u \quad <h_d^0> \equiv v_d \quad <h_u^+> = 0 \quad <h_d^-> = 0 \tag{6.18}$$

Suppressing the charged Higgs fields reduces the potential to

$$
\begin{aligned}
V(h_u, h_d, \phi, s) &= V_F + V_D + V_{soft} \\
&= |y(h_u^0 h_d^0)|^2 + |ys|^2 \left(|h_u^0|^2 + |h_d^0|^2\right) + \frac{g_X^2}{4}\left(|h_u^0|^2 - |h_d^0|^2\right)^2 \\
&\quad + \frac{g^2 Q_H^2}{4}\left(|h_u^0|^2 + |h_d^0|^2\right)^2 + \frac{1}{\sqrt{2}}\tau g M Q_H \left(|h_u^0|^2 + |h_d^0|^2\right) \\
&\quad + \frac{1}{\sqrt{2}}\tau g M Q_S |s|^2 + M^2\tau^2 + \frac{1}{4} g^2 Q_S^2 |s|^4 \\
&\quad + \frac{1}{2} g^2 Q_S Q_H |s|^2 \left(|h_u^0|^2 + |h_d^0|^2\right) \\
&\quad + \left(-y A_S (h_u^0 h_d^0) s + h.c.\right) + m_{H_u}^2 |h_u^0|^2 + m_{H_d}^2 |h_d^0|^2
\end{aligned} \tag{6.19}
$$

Extremizing with respect to the remaining scalar fields and inserting vev's yields

$$
\begin{aligned}
\partial_{h_u} V = 0 &\rightarrow 2|y|^2 v_d^2 + \left(2|y|^2 + g^2 Q_S Q_H\right) v_s^2 + g_X^2\left(v_u^2 - v_d^2\right) + (gQ_H v)^2 + v_\tau g M Q_H + 2m_{H_u}^2 = 2|y||A_S|\frac{v_s v_d}{v_u} \\
\partial_{h_d} V = 0 &\rightarrow 2|y|^2 v_u^2 + \left(2|y|^2 + g^2 Q_S Q_H\right) v_s^2 + g_X^2\left(v_d^2 - v_u^2\right) + (gQ_H v)^2 + v_\tau g M Q_H + 2m_{H_d}^2 = 2|y||A_S|\frac{v_s v_u}{v_d} \\
\partial_\tau V = 0 &\rightarrow \frac{1}{\sqrt{2}} g M Q_H v^2 + 2M^2 v_\tau + \frac{1}{\sqrt{2}} g M Q_S v_s^2 = 0 \\
\partial_s V = 0 &\rightarrow g^2 Q_S^2 v_s^2 + v_\tau g M Q_S + \left(2|y|^2 + g^2 Q_S Q_H\right) v^2 = 2|y||A_S|\frac{v_u v_d}{v_s}
\end{aligned} \tag{6.20}
$$

As stated before, $Q_S = -2$ and $Q_H = 1$. We now add and subtract the first two equations of eqn. (6.20). From $\partial_{h_u} V + \partial_{h_d} V$ we get (note $\mu_{eff} \equiv y v_s$)

$$
\begin{aligned}
B\mu_{eff} \equiv A_S y v_s &= \frac{1}{2}\sin(2\beta)\left[m_{H_u}^2 + m_{H_d}^2 + 2\mu_{eff}^2\right] \\
&\quad + \frac{1}{2}\sin(2\beta)\left[g^2 Q_S Q_H v_s^2 + (|y|^2 + g^2 Q_H^2) v^2 + v_\tau g M Q_H\right]
\end{aligned} \tag{6.21}
$$

We have introduced the angle β using the convential definintion

$$
v_d = v\cos(\beta) \qquad v_u = v\sin(\beta) \qquad v_u^2 + v_d^2 \equiv v^2 \tag{6.22}
$$

From $\partial_{h_u} V - \partial_{h_d} V$ we get

$$
\mu_{eff}^2 = \frac{m_{H_d}^2 - m_{H_u}^2 \tan^2(\beta)}{\tan^2(\beta) - 1} - \frac{M_Z^2}{2} - \frac{g^2 v^2}{4} - \frac{g^2}{2} Q_S Q_H v_s^2 + v_\tau g M Q_H \tag{6.23}
$$

Here, $M_Z^2 = \left(\frac{g_1^2 + g_2^2}{2}\right) v^2$. For $g = 0$, we recover the MSSM results for μ and $B\mu$.

6.3.1 Scalar Masses

We will construct two vectors, one containing all CP-even scalars and one containing all CP-odd scalars. The CP even and odd scalar vectors are given below

$$E^T = (h_{dR}, h_{uR}, \rho, \tau) \quad O^T = (h_{dI}, h_{uI}, \chi, a) \tag{6.24}$$

We gather all bilinear terms into the the following matrices

$$-\frac{1}{2}E_a(M_E^2)^{ab}E_b \qquad -\frac{1}{2}O_a(M_O^2)^{ab}O_b \tag{6.25}$$

Using the minimization equations (eqn. (6.20)) we may simplify the CP-even mass matrix to

$$(M_E^2)^{ab} = \begin{pmatrix} g_X^2 v_d^2 + yA_S v_s \frac{v_u}{v_d} & (2|y|^2 - g_X^2 + g^2)v_u v_d - yA_S v_s & (2|y|^2 - 2g^2)v_d v_s - yA_S v_u & gMQ_H v_d \\ & g_X^2 v_u^2 + yA_S v_s \frac{v_d}{v_u} & (2|y|^2 - 2g^2)v_u v_s - yA_S v_d & gMQ_H v_u \\ & & g^2 Q_S^2 v_s^2 + yA_S \frac{v_u v_d}{v_s} & gMQ_S v_s \\ & & & M^2 \end{pmatrix}$$

We suppress the lower triangular terms because the matrix is symmetric. In order to determine the physical mass eigenstates we must diagonalize this matrix. However, analytic expressions for the eigenvalues of this matrix are prohibitively complicated. We can make progress by examining the characteristic equation and estimating the scales of the resulting roots. We know that there are three relevant energy scales in our model. These are;

$$M \gg v_s \gg v \tag{6.26}$$

In this limit, the characteristic equation for this mass matrix can be approximated as

$$\lambda^4 - M^2\lambda^3 + AM^2 v_s^2 \lambda^2 + BM^2 v_s^4 \lambda + CM^2 v_s^6 = 0 \tag{6.27}$$

Where A,B, and C are unknown real coefficients in the set $\{-10, 10\}$. These coefficients depend on the couplings in the model as well as functions of β. We may examine the analytic expression for the roots of eqn. (6.27) and utilize the scale hierarchy (eqn (6.26)). In this limit, the roots corresponding to saxions can be approximated by

$$\begin{aligned}
\lambda_{1,2} &= \frac{M^2}{4} + \frac{1}{2}\sqrt{\frac{M^4}{4} + C_1 M^2 v_s^2} \pm \frac{1}{2}\sqrt{M^4 + C_2 M^2 v_s^2} \\
&\sim \frac{M^2}{4} + \frac{M^2}{4}\left(1 + \frac{2C_1 v_s^2}{M^2}\right) \pm \frac{M^2}{2}\left(1 + \frac{C_2 v_s^2}{2M^2}\right) \\
&\sim M^2,\ v_s^2
\end{aligned} \tag{6.28}$$

Where C_1 and C_2 are order 1 coefficients that are linear combinations of A, B, and C. Therefore, there are two physical saxions, one (s_1) at a high mass scale and one (s_2) at a low mass. These are given by

$$m_{s_1}^2 = \lambda_1 \sim M^2 \qquad m_{s_2}^2 = \lambda_2 \sim v_s^2 \tag{6.29}$$

The remaining two CP-even eigenstates correspond to Higgs bosons. The mass of the the lightest of these can be constrained by rotating the upper left 2×2 submatrix of CP-even mass matrix. After doing this, one finds that one the diagonal elements represents an upper bound on the Higgs mass. This is given by

$$m_h^2 < M_Z^2 \left[\cos^2(2\beta) + \frac{|y|^2 + \frac{1}{2}g^2}{g_X^2}\sin^2(2\beta)\right] \tag{6.30}$$

For $g \to 0$ we recover the convential NMSSM bound. This bound suggests that for $|y|^2 + \frac{1}{2}g^2$ slightly bigger than g_X^2, the classical Higgs mass may be lifted over its value within the MSSM. In light of the recent hints of a Higgs mass of roughly $123 - 125$ GeV at the LHC, this classical lifting may be seen as a welcomed result.

In a similiar fashion to the CP-even scalars, we compute the CP-odd mass matrix from eq. (6.19)

$$(M_O^2)^{ab} = \begin{pmatrix} yv_sA_S\tan(\beta) & yv_sA_S & yv_uA_S & 0 \\ & yv_sA_S/\tan(\beta) & yv_dA_S & 0 \\ & & yA_S\frac{v_uv_d}{v_s} & 0 \\ & & & 0 \end{pmatrix}$$

After diagonalizing this matrix we find three zero eigenvalues and one non-zero eigenvalue which we give below

$$M_A^2 = B\mu_{eff}\left(\frac{2}{\sin(2\beta)} + \frac{v^2}{v_s^2}\frac{\sin(2\beta)}{2}\right) \tag{6.31}$$

6.3.2 Fermion Masses

In order to calculate the axino mass, we first identify all fermion bilinears in the full Lagrangian. We consider a fermion vector of the form

$$\Psi = (\psi, \lambda, B, W, \psi_d, \psi_u, \psi_S)^T \tag{6.32}$$

Where ψ is the T modulus fermion, λ Pecci-Quinn U(1) fermion, B and W are the Bino and Wino, ξ_u and ξ_d are the up and down higginos respectively and ψ_S is the NMSSM singlet fermion. The neutralino bilinears take the form

$$\mathcal{L}_{neut} = -\frac{1}{2}\left(\Psi\right)_a^T (M_f)^{ab}\Psi_b \tag{6.33}$$

We present all the terms in Appendix A. After S, H_u and H_d acquire vevs the mass matrix becomes

$$(M_f)^{ab} = \begin{pmatrix} 0 & M & 0 & 0 & 0 & 0 & 0 \\ & 0 & 0 & 0 & gQ_H v_d & gQ_H v_u & gQ_S v_s \\ & & M_1 & 0 & \frac{-1}{\sqrt{2}}g_1 v_d & \frac{1}{\sqrt{2}}g_1 v_u & 0 \\ & & & M_2 & \frac{1}{\sqrt{2}}g_2 v_d & \frac{-1}{\sqrt{2}}g_2 v_u & 0 \\ & & & & 0 & -yv_s & -yv_u \\ & & & & & 0 & -yv_d \\ & & & & & & 0 \end{pmatrix}$$

The bottom left half has been suppressed because the matrix is necessarily symmetric. We have also introduced gaugino mass terms, M_1 and M_2, into the scalar potential. The gauginos gain mass at the GUT scale through the Weyl anomaly and their electroweak scale values are determined through RGE evolution.

Due to the fact that the characteristic equation for the fermion mass matrix is seventh order, analytic expressions, even approximate ones, are not known. One must resort to numerical studies to identify the mass spectrum for these fermions.

6.3.3 Physical Couplings

After determining the physical mass eigenstates of our model, we wish to compute the Pecci-Quinn scale f_a. This will determine the couplings strengths of the axion supermultiplet to matter. In principle, we can acheive this by comparing the full Lagrangian (6.5) in the mass eigenstate basis with the effective PQMSSM Lagrangian given in Baer et.al. [85]. For saxion $s(x)$ and axino $\tilde{a}(x)$, the effective interaction Lagrangian is

$$\mathcal{L}_{eff,s,\tilde{a}} = \frac{\alpha_s}{8\pi}\frac{s(x)}{f_a}\left(F_{\mu\nu}F^{\mu\nu} + 2i\bar{\tilde{g}}\gamma^\mu D_\mu \tilde{g}\right) + i\frac{\alpha_s}{16\pi}\frac{\bar{\tilde{a}}(x)}{f_a}\gamma_5[\gamma^\mu,\gamma^\nu]\tilde{g}F_{\mu\nu} + \mathcal{O}(\alpha_s^{3/2}) \tag{6.34}$$

here $F_{\mu\nu}$ is the $SU(3)$ field strength tensor and $\tilde{g}$ are the associated gluinos. The effective Lagrangian for the axion, $a(x)$, is given by

$$\mathcal{L}_{eff,a} = \frac{\alpha_s}{8\pi}\frac{a(x)}{f_a}F_{\mu\nu}\widetilde{F}^{\mu\nu} \tag{6.35}$$

Comparing these expressions with those in Appendix A.2 we may make the following identifications

$$\hat{\chi}(x) \leftrightarrow a(x) \qquad \hat{\eta}(x) \leftrightarrow \tilde{a}(x) \qquad \hat{\rho}(x) \leftrightarrow s(x) \qquad \frac{1}{8\pi f_a} \sim \frac{1}{M} \tag{6.36}$$

6.4 Cosmological Considerations

For $f_a \sim M_{GUT}$ the cosmological phenomenology has been discussed in detail by Banks et.al. [88], Baer et.al. [85] and others (e.g.). The conclusion derived in these works is that the conventional upper bound on f_a coming from models with only an axion can be circumvented if one includes the supersymmetric partners of the axion, namely the saxion and the axino. In what follows, we discuss the cosmological constraints on all of these particles necessary for a high scale f_a. The relevant parameters in this analysis are axion decay constant f_a, the saxion mass m_s and axino mass $m_{\tilde{a}}$. These are have been determined elsewhere in the paper. We reiterate them below.

$$f_a \sim M \sim 10^{15} \leftrightarrow 10^{16}\ \text{GeV} \qquad m_s \sim v_s \sim 500\ \text{GeV} \leftrightarrow 50\ \text{TeV} \qquad m_{\tilde{a}} \sim 10\ \text{GeV} < m_{\tilde{Z}_1} \tag{6.37}$$

6.4.1 Saxion Dominated Epoch

The presence of a saxion can have both adverse and advantageous effects on the cosmology of this model. Due to its weak couplings (suppressed by f_a), the saxion will thermally decouple early in the history of the universe. At a certain temperature , T_s, the saxion field will coherently oscillate about the minimum of its potential and hence contribute to the energy density of the universe. Due to the fact that the saxion's energy density scales as R^{-3}, it may come to dominate the energy density of the universe. The temperatures at which the saxion dominated epoch begins and ends are denoted as T_{sb} and T_{se} respectively, and they are defined by the following relations;

$$\rho_s(T_{sb}) = \rho_\gamma(T_{sb}) \qquad \Gamma_s = H(T_{se}) \tag{6.38}$$

Where ρ_s is the saxion energy density, ρ_γ is the photon energy density and Γ_s is the saxion decay width given by

$$\Gamma_s(s \to gg) = \frac{\alpha_s m_s^3}{32\pi^3 (f_a)^2} \tag{6.39}$$

6.4.2 BBN Constraints

Since the decay rate of the saxion scales as $\Gamma_s \propto \frac{1}{f_a^2}$, large f_a can give rise the long-lived saxions. If the saxion decays hadronically after $T = 5$ MeV the successful predictions of Big Bang Nucleosynthesis (BBN) will be disrupted. This places a bound on T_{se}, i.e. the end of the saxion dominated era. This bound results in the following condition

$$T_{se} > 5\text{ MeV} \implies m_s \gtrsim 0.1\text{TeV}\left(\frac{f_a}{10^{12}\text{GeV}}\right)^{2/3} \tag{6.40}$$

From eq.(6.40) we see that for $f_a \sim 10^{16}$ GeV, $m_s \gtrsim 50$ TeV. However, from eq.(6.23) we know that $m_s \sim v_s \sim M_{H_u}$. This leaves us with one of two options. Either we retain a high scale f_a ($f_a \sim 10^{16}$) and require $M_{H_u} \sim 50$ TeV. However, from eq.(6.23) we see that this results in a fine tuning between M_{H_u} and μ_{eff} of one part in 10^6. One the other hand, if we decrease f_a to 10^{15} GeV, the lower bound on m_s becomes $m_s \gtrsim 10$ TeV. This results in a fine-tuning of roughly one part in 10^4. This is an improvement in fine-tuning but it comes at the cost of giving up gauge unification.

6.4.3 Dark Matter Overabundance

If one ignores the saxion and axino fields then the relic dark matter density contribution from the axion field scales as follows

$$\Omega_a h^2 \sim f(\theta_i) \left(\frac{f_a}{10^{12}\ \mathrm{GeV}} \right)^{7/6} < 0.1123 \tag{6.41}$$

where $f(\theta_i)$ is the initial axion field amplitude. From this bound we derive that either $f_a \lesssim 10^{12}$ GeV or $f(\theta_i) \ll 0$. However, as pointed out by Baer, one need also consider the possibly that saxions can decay and inject entropy into the universe thereby diluting the axion relic density. Once this dilution is factored in, the axion dark matter relic density becomes

$$\Omega_a h^2 = 1.4 * \theta_i^2 f(\theta_i) \frac{1}{(g_*(T_a))^{14/11}} \left(\frac{f_a}{10^{12}} \right) \frac{T_{se}}{T_{sb}^{4/11}} \tag{6.42}$$

Where θ_i is the initial axion misalignment angle and g_* is the number of massless degrees of freedom ($g_* \approx 229$). Since $T_{se} \propto 1/f_a$ and $T_{sb} \propto f_a^2$ we see that $\Omega_a h^2$ decreases with increased f_a and is minimized for $T_{se} = 5$ MeV, which is the bound for BBN.

6.5 Conclusion

In this work, we have examined the potential for realizing a QCD axion with IIB string theory. Our approach has been to assume that the moduli fields are stablized along the lines of the Large Volume Scenario and the matter fields arise from D-branes wrapping a shrinking cycle. Without constructing the local model explicitly, we considered the matter content to be that of the NMSSM. A QCD axion emerges from a linear combination of the CP-odd scalar fields in the NMSSM and and Standard Model Cycle supermultiplets respectively.

A generic feature of this model is that the Pecci-Quinn scale, f_a, is typically on the GUT scale. As detailed in section 4, this high scale value f_a can still be made to satisfy cosmological contraints. Essentially, the saxion and axino decays inject enough entropy into the universe to dilute the axion's contribution to the dark matter relic abundance.

6.6 Appendix

6.6.1 Superfield Expansions

Working in the Wess Zumino gauge, we may expand the superfields as follows (we use the conventions of Wess and Bagger [121])

$$V = -\tilde{a}\sigma^{\mu}\overline{\theta}A_{\mu} + i\tilde{a}\tilde{a}\overline{\theta}\lambda^{\dagger} - i\overline{\theta\theta}\tilde{a}\lambda + \frac{1}{2}\tilde{a}\tilde{a}\overline{\theta\theta}D \tag{6.43}$$

$$T = \phi + i\tilde{a}\sigma^{\mu}\overline{\theta}\partial_{\mu}\phi + \frac{1}{4}\tilde{a}\tilde{a}\overline{\theta\theta}\partial^2\phi + \sqrt{2}\tilde{a}\psi + \frac{i}{\sqrt{2}}\tilde{a}\tilde{a}\overline{\theta}\overline{\sigma}^{\mu}\partial_{\mu}\psi + \tilde{a}\tilde{a}\mathcal{F} \tag{6.44}$$

where $\phi = \frac{\tau + ia}{2}$. For completeness, we give the chiral matter field expansion

$$\Phi_i = \phi_i + i\tilde{a}\sigma^{\mu}\overline{\theta}\partial_{\mu}\phi_i + \frac{1}{4}\tilde{a}\tilde{a}\overline{\theta\theta}\partial^2\phi_i + \sqrt{2}\tilde{a}\psi_i + \frac{i}{\sqrt{2}}\tilde{a}\tilde{a}\overline{\theta}\overline{\sigma}^{\mu}\partial_{\mu}\psi_i + \tilde{a}\tilde{a}\mathcal{F}_i \tag{6.45}$$

The contribution to the full Lagrangian from the Kähler potential can be expanded via superspace integration

$$\begin{aligned}
\mathcal{L}_K &= \int d^4\tilde{a}K = \int d^4\tilde{a}\left[\left(T + \overline{T} + MV\right)^2 + \Phi_i^{\dagger}e^{Q_iV}\Phi_i\right] \\
&= \frac{1}{2}\tau\left(\partial^2\tau + 2MD\right) + 2i\left(\psi^{\dagger}\overline{\sigma}^{\mu}\partial_{\mu}\psi + \sqrt{2}M\psi^{\dagger}\lambda^{\dagger}\right) + 2i\left(\psi\sigma^{\mu}\partial_{\mu}\psi^{\dagger} - \sqrt{2}M\psi\lambda\right) \\
&\quad +2|\mathcal{F}|^2 - (\partial_{\mu}a + MA_{\mu})^2 + |\mathcal{F}_i|^2 - \left(\partial^{\mu} - i\frac{Q_i}{2}A^{\mu}\right)\phi_i^{\dagger}\left(\partial_{\mu} + i\frac{Q_i}{2}A_{\mu}\right)\phi_i \\
&\quad +\frac{1}{2}\left(Q_iD\right)|\phi_i|^2 + i\partial_{\mu}\psi_i^{\dagger}\overline{\sigma}^{\mu}\psi_i + \frac{1}{2}Q_iA^{\mu}\psi_i^{\dagger}\overline{\sigma}^{\mu}\psi_i - \frac{i}{\sqrt{2}}Q_i(\phi_i\lambda^{\dagger}\psi_i^{\dagger} - \phi_i^{\dagger}\lambda\psi)
\end{aligned} \tag{6.46}$$

We may combine the Weyl spinors λ and ψ into Majorana spinors (following [116])

$$\lambda = \begin{pmatrix}\lambda \\ \lambda^{\dagger}\end{pmatrix} \qquad \psi = \begin{pmatrix}\psi \\ \psi^{\dagger}\end{pmatrix} \tag{6.47}$$

Making this identification and integrating by parts yields

$$\begin{aligned}
\frac{1}{4}\left[(S+\kappa T)\mathcal{W}^\alpha\mathcal{W}_\alpha + (\overline{S}+\kappa\overline{T})\overline{\mathcal{W}}_{\dot\alpha}\overline{\mathcal{W}}^{\dot\alpha}\right]_F &= \frac{\kappa}{4}\left(\mathcal{F}\lambda^2+\overline{\mathcal{F}\lambda}^2\right) \\
&\quad +\frac{\kappa}{\sqrt{2}}\Big(D\psi\lambda + D\overline{\psi\lambda} + \sigma^{\mu\nu}\psi\lambda F_{\mu\nu} + \overline{\sigma}^{\mu\nu}\overline{\psi\lambda}F_{\mu\nu}\Big) \\
&\quad +\kappa\left(\frac{\tau}{2}\lambda\sigma^\mu\partial_\mu\overline{\lambda} + \frac{\tau}{2}\lambda\overline{\sigma}^\mu\partial_\mu\overline{\lambda} - \frac{\tau}{8}F^2_{\mu\nu} + \frac{a}{16}\widetilde{F}_{\mu\nu}F^{\mu\nu}\right) \\
&\quad +\frac{1}{2g^2}D^2 + \frac{1}{g^2}\left(\lambda\sigma^\mu\partial_\mu\overline{\lambda} + \lambda\overline{\sigma}^\mu\partial_\mu\overline{\lambda} - \frac{1}{4}F^2_{\mu\nu}\right) \\
&= \kappa g^2\left(\mathcal{F}\lambda^2+\overline{\mathcal{F}\lambda}^2\right) + 2^{3/2}\kappa g^2\Big(D\psi\lambda + \sigma^{\mu\nu}\psi\lambda F_{\mu\nu}\Big) \\
&\quad +4\kappa g^2\left(\frac{\tau}{2}\lambda^\dagger\gamma^\mu\partial_\mu\lambda - \frac{\tau}{8}F^2_{\mu\nu} + \frac{a}{16}\widetilde{F}_{\mu\nu}F^{\mu\nu}\right) \\
&\quad +2D^2 + 4\left(\lambda^\dagger\gamma^\mu\partial_\mu\lambda - \frac{1}{4}F^2_{\mu\nu}\right) \qquad (6.48)
\end{aligned}$$

Where in the last two lines we have used the Majorana spinors defined in eq. (6.47). We have also canonically normalized the vector supermultiplet $(A^\mu, \lambda, D) \to 2g(A^\mu, \lambda, D)$.

For our model, the superpotential is given by (eq. (6.4))

$$W = ySH_u\cdot H_d + W_{MSSM} = yS\left(H_u^+H_d^- - H_u^0H_d^0\right) + W_{MSSM} \qquad (6.49)$$

The F-term for the $ySH_u\cdot H_d$ component of W is given below

$$\begin{aligned}
\left[yS\left(H_u^+H_d^- - H_u^0H_d^0\right)\right]_F &= y\left(\mathcal{F}_Sh_u^+h_d^- + \mathcal{F}_u^+sh_d^- + \mathcal{F}_d^-sh_u^+u - \psi_S\psi_u^+h_d^- - \psi_d^-\psi_Sh_u^+ - \psi_d^-\psi_u^+h_S\right) \\
&\quad -y\left(\mathcal{F}_Sh_u^0h_d^0 + \mathcal{F}_u^0sh_d^0 + \mathcal{F}_d^0sh_u^0 - \psi_S\psi_u^0h_d^0 - \psi_d^0\psi_Sh_u^0 - \psi_d^0\psi_u^0h_S\right) \qquad (6.50)
\end{aligned}$$

Solving the F-term equations of motion for h_u, h_d and s gives the following potential

$$V(h_u,h_d,s)_F = |y(h_u^+h_d^- - h_u^0h_d^0)|^2 + |ys|^2\left(|h_u^0|^2+|h_u^+|^2-|h_d^0|^2-|h_d^-|^2\right)^2 \qquad (6.51)$$

From the full Lagrangian (eq. (6.5)) we collect all the terms proportional to D. They are given below

$$\begin{aligned}
\left[\left(T+\overline{T}+MV\right)^2\right]_D &\to 2\sqrt{2}\tau MD \\
\left[\phi_i^\dagger e^{2gQ_iV}\phi_i\right]_D &\to g|\phi_i|^2Q_iD \\
\frac{1}{4}\Big[f\mathcal{W}^\alpha\mathcal{W}_\alpha + \overline{f\mathcal{W}}_{\dot\alpha}\overline{\mathcal{W}}^{\dot\alpha}\Big]_F &\to 2D^2 \qquad (6.52)
\end{aligned}$$

We may therefore write the terms in the Lagrangian proportional to D as

$$\mathcal{L}_D = 2\sqrt{2}\tau M D + g|\phi_i|^2 Q_i D + 2D^2 \tag{6.53}$$

For our model (eq. (6.53)) the D-Lagrangian becomes

$$\begin{aligned}\mathcal{L}_D = -V_D &= \frac{-4\left(\sqrt{2}\tau M + g\frac{1}{2}|\phi_i|^2 Q_i\right)^2}{4\,(2)} \\ &= -\frac{1}{2}\Big(2M^2\tau^2 + g^2\frac{1}{4}Q_i^2|\phi_i|^4 + g^2\frac{1}{2}\sum_{j\neq i} Q_i Q_j |\phi_i|^2|\phi_j|^2 + gM\sqrt{2}\tau|\phi_i|^2 Q_i\Big)\end{aligned} \tag{6.54}$$

6.6.2 The Physical Couplings

We now examine the following Lagrangian

$$\mathcal{L} = -\frac{1}{4g^2}F_{\mu\nu}^2 - \frac{1}{2}\left(k\partial_\mu a + MA_\mu\right)^2 + \mathcal{A}_i a \mathrm{Tr}[F_i \wedge F_i] - \left(\mathcal{D}^\mu S\right)^\dagger\left(\mathcal{D}_\mu S\right) + V(|S|) + \gamma S\psi\overline{\psi} \tag{6.55}$$

The potential $V(|S|)$ is double-well Higgs-like potential given by eq. (6.16) and the covariant derivative is given by $\mathcal{D}_\mu = \partial_\mu + iegA_\mu$ (where $e \equiv Q_S$). We may absorb the constant k into the Stuekelberg pseudoscalar field a, ($a \to \frac{a}{k}$). The Lagrangian then becomes

$$\mathcal{L} = -\frac{1}{4g^2}F_{\mu\nu}^2 - \frac{1}{2}\left(\partial_\mu a + MA_\mu\right)^2 + \frac{\mathcal{A}_i a}{k}\mathrm{Tr}[F_i \wedge F_i] - \left(\mathcal{D}^\mu S\right)^\dagger\left(\mathcal{D}_\mu S\right) + V(|S|) + \gamma S\psi\overline{\psi} \tag{6.56}$$

We may perform a Cartesian split on S, (NMSSM singlet field) and expanded about the minimum v, $v \equiv <S>$.

$$S(x) = \frac{1}{\sqrt{2}}\left(v + \rho(x) + i\chi(x)\right) \tag{6.57}$$

The Stuekelberg kinetic term can be expanded as follows

$$\mathcal{L}_{SK} = -\frac{1}{2}\left(\partial_\mu a + MA_\mu\right)^2 = -\frac{1}{2}(\partial a)^2 - M\partial_\mu a A^\mu - \frac{M^2A^2}{2} \tag{6.58}$$

Similarly, the Higgs kinetic term can be expanded (using the Cartesian split) as

$$\begin{aligned}\mathcal{L}_{HK} &= -\frac{1}{2}\left[\left(\partial^\mu - ievA^\mu\right)\left(v + \rho - i\chi\right)\left(\partial_\mu + ievA_\mu\right)\left(v + \rho + i\chi\right)\right] \\ &= -\frac{1}{2}\partial^\mu\rho\partial_\mu\rho - \frac{1}{2}\partial^\mu\chi\partial_\mu\chi - \frac{1}{2}e^2A^2\left(v^2 + \rho^2 + \chi^2 + 2v\rho\right) \\ &\quad -\frac{1}{2}\left(2e\partial_\mu\chi A^\mu(v+\rho) - 2e\partial_\mu\rho A^\mu\chi\right)\end{aligned} \tag{6.59}$$

Neglecting interaction terms and the ρ kinetic term gives

$$\mathcal{L}_{HK,\chi} = -\frac{1}{2}(\partial\chi)^2 - ev\partial_\mu\chi A^\mu - \frac{e^2v^2A^2}{2} \tag{6.60}$$

Adding this term together with the Stuekelberg kinetic term gives

$$\mathcal{L}_{SK} + \mathcal{L}_{HK,\chi} = -\frac{1}{2}(\partial a)^2 - M\partial_\mu a A^\mu - \frac{M^2A^2}{2} - \frac{1}{2}(\partial\chi)^2 - ev\partial_\mu\chi A^\mu - \frac{e^2v^2A^2}{2} \tag{6.61}$$

In order to diagonalize this Lagrangian we multiply by factors of 1 and add and subtract equivalent terms

$$\begin{aligned}\mathcal{L}_{SK} + \mathcal{L}_{HK,\chi} \quad = \quad & -\frac{1}{2}\frac{M^2+e^2v^2}{M^2+e^2v^2}(\partial a)^2 - \frac{1}{2}\frac{M^2+e^2v^2}{M^2+e^2v^2}(\partial\chi)^2 - M\partial_\mu a A^\mu - ev\partial_\mu\chi A^\mu \\ & -\frac{(M^2+e^2v^2)A^2}{2} + \frac{Mev\partial\chi\partial a}{M^2+e^2v^2} + \frac{1}{2}\frac{e^2v^2(\partial\chi)^2}{M^2+e^2v^2} + \frac{1}{2}\frac{M^2(\partial a)^2}{M^2+e^2v^2} \\ & -\frac{Mev\partial\chi\partial a}{M^2+e^2v^2} - \frac{1}{2}\frac{e^2v^2(\partial\chi)^2}{M^2+e^2v^2} - \frac{1}{2}\frac{M^2(\partial a)^2}{M^2+e^2v^2}\end{aligned} \tag{6.62}$$

Rearranging terms

$$\begin{aligned}\mathcal{L}_{SK} + \mathcal{L}_{HK,\chi} \quad = \quad & -\frac{(M^2+e^2v^2)}{2}\Big[A^2 + \frac{e^2v^2(\partial\chi)^2}{(M^2+e^2v^2)^2} + \frac{M^2(\partial a)^2}{(M^2+e^2v^2)^2} + 2A^\mu\frac{ev\partial_\mu\chi}{(M^2+e^2v^2)} \\ & +2A^\mu\frac{M\partial_\mu a}{(M^2+e^2v^2)} + 2\frac{Mev\partial\chi\partial a}{(M^2+e^2v^2)^2}\Big] - \frac{1}{2}\frac{M^2+e^2v^2}{M^2+e^2v^2}(\partial a)^2 - \frac{1}{2}\frac{M^2+e^2v^2}{M^2+e^2v^2}(\partial\chi)^2 \\ & +\frac{Mev\partial\chi\partial a}{M^2+e^2v^2} + \frac{1}{2}\frac{e^2v^2(\partial\chi)^2}{M^2+e^2v^2} + \frac{1}{2}\frac{M^2(\partial a)^2}{M^2+e^2v^2} \\ = \quad & -\frac{(M^2+e^2v^2)}{2}\left(A_\mu + \frac{ev\partial_\mu\chi}{M^2+e^2v^2} + \frac{M\partial_\mu a}{M^2+e^2v^2}\right)^2 \\ & -\frac{1}{2}\frac{M^2(\partial\chi)^2 + e^2v^2(\partial a)^2 - 2Mev\partial\chi\partial a}{M^2+e^2v^2}\end{aligned} \tag{6.63}$$

We now rotate to an orthonormal basis ($\hat{\chi}$, $\hat{a}$) via the rotation

$$\begin{bmatrix}\hat{\chi} \\ \hat{a}\end{bmatrix} = \frac{1}{\sqrt{M^2+e^2v^2}}\begin{bmatrix}M & -ev \\ ev & M\end{bmatrix} \times \begin{bmatrix}\chi \\ a\end{bmatrix} \tag{6.64}$$

We may redefine the vector field via a gauge transformation as

$$\begin{aligned}A_\mu \quad & \to \quad A_\mu + \frac{ev\partial_\mu\chi}{M^2+e^2v^2} + \frac{M\partial_\mu a}{M^2+e^2v^2} \\ & \to \quad A_\mu + \frac{\partial_\mu\hat{a}}{\sqrt{M^2+e^2v^2}}\end{aligned} \tag{6.65}$$

Also

$$(\partial\hat{\chi})^2 = \left(\frac{M\partial\chi - ev\partial a}{\sqrt{M^2+e^2v^2}}\right)^2 = \frac{M^2(\partial\chi)^2 + e^2v^2(\partial a)^2 - 2Mev\partial\chi\partial a}{M^2+e^2v^2} \tag{6.66}$$

Therefore the kinetic Lagrangian simplifies to

$$\mathcal{L}_{SK} + \mathcal{L}_{HK,\chi} = -\frac{(M^2+e^2v^2)}{2}A^2 - \frac{1}{2}(\partial\hat{\chi})^2 \tag{6.67}$$

We may re-express the full Lagrangian (eq. (6.56)) in terms of $\hat{\chi}$. Suppressing terms proportional to $\hat{a}$ yields

$$\mathcal{L}_{\hat{\chi}} = -\frac{1}{4g^2}F_{\mu\nu}^2 - \frac{(M^2+e^2v^2)}{2}A_\mu^2 - \frac{1}{2}(\partial_\mu\hat{\chi})^2 - \frac{\mathcal{A}_i ev}{k\sqrt{M^2+e^2v^2}}\hat{\chi}\mathrm{Tr}[F_i\wedge F_i] + \gamma\frac{iM\hat{\chi}}{\sqrt{M^2+e^2v^2}}\psi\overline{\psi} \tag{6.68}$$

The remaining terms in the Lagrangian are

$$\mathcal{L}_{\hat{a}} = \frac{\mathcal{A}_i M}{k\sqrt{M^2+e^2v^2}}\hat{a}\mathrm{Tr}[F_i\wedge F_i] + \gamma\frac{iev\hat{a}}{\sqrt{M^2+e^2v^2}}\psi\overline{\psi} \tag{6.69}$$

In order to preserve supersymmetry between the components of the axion supermultiplet we must also rotate the saxion (τ) and axino (λ) fields with the real scalar (ρ) and fermionic (ψ_S) components of the S respectively. As with the axi-higgs, we make the following orthogonal transformation

$$\begin{bmatrix}\hat{\rho}\\ \hat{\tau}\end{bmatrix} = \frac{1}{\sqrt{M^2+e^2v^2}}\begin{bmatrix}M & -ev\\ ev & M\end{bmatrix}\times\begin{bmatrix}\rho\\ \tau\end{bmatrix} \tag{6.70}$$

equivalently

$$\begin{bmatrix}\rho\\ \tau\end{bmatrix} = \frac{1}{\sqrt{M^2+e^2v^2}}\begin{bmatrix}M & ev\\ -ev & M\end{bmatrix}\times\begin{bmatrix}\hat{\rho}\\ \hat{\tau}\end{bmatrix} \tag{6.71}$$

The kinetic and interaction terms in the full Lagrangian (eq. (6.5)) that contain τ are

$$\begin{aligned}
\mathcal{L}_\tau &= \mathcal{L}_{K,\tau} + \frac{1}{4}\left[f\mathcal{W}^\alpha\mathcal{W}_\alpha + \overline{f\mathcal{W}}_{\dot{\alpha}}\overline{\mathcal{W}}^{\dot{\alpha}}\right]_{F,\tau} \\
&= -\frac{1}{2}\partial^\mu\tau\partial_\mu\tau + \left(\frac{\tau}{2}\overline{\lambda}\gamma^\mu\partial_\mu\lambda - \frac{\tau}{8}F_{\mu\nu}^2\right) \\
&= \frac{1}{2}\left(\frac{ev}{\sqrt{M^2+e^2v^2}}\right)\partial^\mu\hat{\rho}\partial_\mu\hat{\rho} - \frac{1}{2}\left(\frac{M}{\sqrt{M^2+e^2v^2}}\right)\partial^\mu\hat{\tau}\partial_\mu\hat{\tau} \\
&\quad - \left(\frac{ev}{\sqrt{M^2+e^2v^2}}\right)\hat{\rho}\left(+\frac{1}{2}\overline{\lambda}\gamma^\mu\partial_\mu\lambda - \frac{1}{8}F_{\mu\nu}^2\right) \\
&\quad + \left(\frac{M}{\sqrt{M^2+e^2v^2}}\right)\hat{\tau}\left(\frac{1}{2}\overline{\lambda}\gamma^\mu\partial_\mu\lambda - \frac{1}{8}F_{\mu\nu}^2\right)
\end{aligned} \tag{6.72}$$

Similarly, the elements of the full Lagrangian containing ρ are

$$\begin{aligned}
\mathcal{L}_\rho &= -\frac{1}{2}\partial^\mu\rho\partial_\mu\rho - \frac{1}{2}e^2A^2\rho^2 - ve^2A^2\rho - e\partial_\mu\chi A^\mu\rho + e\partial_\mu\rho A^\mu\chi + \mathcal{F}_u h_d\rho + \mathcal{F}_d h_u\rho \\
&= -\frac{1}{2}\left(\frac{M}{\sqrt{M^2+e^2v^2}}\right)\partial^\mu\hat{\rho}\partial_\mu\hat{\rho} - \frac{1}{2}\left(\frac{ev}{\sqrt{M^2+e^2v^2}}\right)\partial^\mu\hat{\tau}\partial_\mu\hat{\tau} + \text{interaction terms} \quad (6.73)
\end{aligned}$$

We may write an effective Lagrangian for $\hat{\rho}$ as

$$\begin{aligned}
\mathcal{L}_{\hat{\rho}} &= -\frac{1}{2}\left(\frac{M}{\sqrt{M^2+e^2v^2}}\right)\partial^\mu\hat{\rho}\partial_\mu\hat{\rho} - \left(\frac{ev}{\sqrt{M^2+e^2v^2}}\right)\hat{\rho}\left(\xi D + \frac{\kappa}{4}D^2 + \frac{1}{2}\bar{\lambda}\gamma^\mu\partial_\mu\lambda - \frac{1}{8}F_{\mu\nu}^2\right) \\
&\quad + \text{interaction terms} \quad (6.74)
\end{aligned}$$

Chapter 7

Conclusion

In this dissertation we have studied several theoretical and phenomenological issues related to IIB string theory. We have seen that, to date, the Large Volume Scenario for stabilizing string moduli fields represents the best known mechanism for connecting string theory with TeV-scale physics. The method of supersymmetry breaking coming from LVS is known as inoAMSB, and as we have seen, this method has several desirable phenomenological features. Aside from being the simplest of all known models of supersymmetry breaking, inoAMSB has the potential to address many important issue in contemporary physics including the origin of electroweak symmetry, the Higgs mass and dark matter. We have also seen that many interesting physical models, such as the axion of Quantum Chromodynamics, can be made to fit comfortably within this string framework.

Future work in this field would follow naturally along two lines, one more theoretical and one more phenomenological. As in chapter 4, one could investigate moduli stabilization in deeper detail. By examining more exotic string constructions, one might be able to create a scenario that could potentially surpass LVS. Alternatively, one could continue to further study the phenomenological issues of IIB string theory. Ultimately, one would like to prove that the Standard Model itself can be embedded within a moduli stabilization scenario like LVS. Clearly, there remain interesting and important questions to be addressed by future research.

Bibliography

[1] S. B. Giddings, S. Kachru and J. Polchinski, *Phys. Rev.* **D 66** (2002) 106006.

[2] V. Balasubramanian, P. Berglund, J. P. Conlon and F. Quevedo, *J. High Energy Phys.* **03** (2005) 007.

[3] H. Baer, S. de Alwis, K. Givens, S. Rajagopalan and H. Summy, JHEP **1005**, 069 (2010) [arXiv:1002.4633 [hep-ph]].

[4] Howard Baer, Senarath Alwis, Kevin Givens, Shibi Rajagopalan, and Warintorn Sreethawong. Testing the gaugino AMSB model at the Tevatron via slepton pair production. JHEP, 1101:005, 2011. 14 pages including 6 .eps figures.

[5] Senarath de Alwis and Kevin Givens. Dark Matter density and the Higgs mass in LVS String Phenomenology. 2012.

[6] Senarath de Alwis and Kevin Givens. Physical Vacua in IIB Compactifications with a Single Kaehler Modulus. JHEP, 1110:109, 2011.

[7] M. Grana, Phys. Rept. **423**, 91 (2006) [arXiv:hep-th/0509003].

[8] M. R. Douglas and S. Kachru, Rev. Mod. Phys. **79**, 733 (2007) [arXiv:hep-th/0610102].

[9] S. Kachru, R. Kallosh, A. Linde and S. Trivedi, *Phys. Rev.* **D 68** (2003) 046005.

[10] L. Randall and R. Sundrum, *Nucl. Phys.* **B 557** (1999) 79; G. Giudice, M. Luty, H. Murayama and R. Rattazzi, *J. High Energy Phys.* **12** (1998) 027.

[11] S. P. de Alwis, *Phys. Rev.* **D 77** (2008) 105020 arXiv:0801.0578.

[12] See H. Baer and X. Tata, *Weak Scale Supersymmetry: From Superfields to Scattering Events*, (Cambridge University Press, 2006)

[13] J. R. Ellis, C. Kounnas and D. V. Nanopoulos, Nucl. Phys. B **247** (1984) 373; J. R. Ellis, A. B. Lahanas, D. V. Nanopoulos and K. Tamvakis, Phys. Lett. B **134** (1984) 429; G. A. Diamandis, J. R. Ellis, A. B. Lahanas and D. V. Nanopoulos, Phys. Lett. B **173** (1986) 303; For a review, see A. Lahanas and D. V. Nanopoulos, *Phys. Rept.* **145** (1987) 1.

[14] D. E. Kaplan, G. D. Kribs and M. Schmaltz, *Phys. Rev.* **D 62** (2000) 035010; Z. Chacko, M. A. Luty, A. E. Nelson and E. Ponton, *J. High Energy Phys.* **01** (2000) 003.

[15] F. Gabbiani, E. Gabrielli, A. Masiero and L. Silvestrini, *Nucl. Phys.* **B 477** (1996) 321.

[16] M. Schmaltz and W. Skiba, *Phys. Rev.* **D 62** (2000) 095005 and *Phys. Rev.* **D 62** (2000) 095004; H. Baer, A. Belyaev, T. Krupovnickas and X. Tata, *Phys. Rev.* **D 65** (2002) 075024; A. De Simone, J. J. Fan, M. Schmaltz and W. Skiba, *Phys. Rev.* **D 78** (2008) 095010.

[17] R. Dermisek and A. Mafi, *Phys. Rev.* **D 65** (2002) 055002; for associated phenomenology, see H. Baer, C. Balazs, A. Belyaev, R. Dermisek, A. Mafi and A. Mustafayev, *J. High Energy Phys.* **0205** (2002) 061 and Nucl. Instrum. Meth. A **502** (2003) 560.

[18] R. Dermisek, H. Verlinde and L-T. Wang, *Phys. Rev. Lett.* **100** (2008) 131804; H. Baer. R. Dermisek, S. Rajagopalan and H. Summy, *J. High Energy Phys.* **0910** (2009) 078.

[19] J. Wess and J. Bagger, *Supersymetry and Supergravity*, (Princeton University Press, 1992).

[20] S. J. Gates, M. T. Grisaru, M. Rocek and W. Siegel, *Superspace, or one thousand and one lessons in supersymmetry*, Front. Phys. **58** (1983) 1.

[21] S. P. de Alwis, *J. High Energy Phys.* **0903** (2009) 023 arXiv:0806.2672.

[22] R. Blumenhagen, S. Moster and E. Plauschinn, JHEP **0801**, 058 (2008) [arXiv:0711.3389 [hep-th]].

[23] R. Blumenhagen, S. Moster, and E. Plauschinn, *J. High Energy Phys.* **0801** (2008) 058.

[24] S.P. de Alwis. Classical and Quantum SUSY Breaking Effects in IIB Local Models. JHEP, 1003:078, 2010.

[25] J. Bagger, T. Moroi, and E. Poppitz, *J. High Energy Phys.* **04** (2000) 009, hep-th/9911029.

[26] V. Kaplunovsky and J. Louis, *Nucl. Phys.* **B 422** (1994) 57.

[27] N. Arkani-Hamed and H. Murayama, *J. High Energy Phys.* **0006** (2000) 030.

[28] K. Kohri, T. Moroi and A. Yotsuyanagi, *Phys. Rev.* **D 73** (2006) 123511; for an update, see M. Kawasaki, K. Kohri, T. Moroi and A. Yotsuyanagi, *Phys. Rev.* **D 78** (2008) 065011; see also J. Pradler and F. D. Steffen, *Phys. Lett.* **B 648** (2007) 224.

[29] F. Paige, S. Protopopescu, H. Baer and X. Tata, hep-ph/0312045.

[30] H. E. Haber, R. Hempfling and A. Hoang, *Z. Phys.* **C75** (1997) 539.

[31] D. Pierce, J. Bagger, K. Matchev and R. Zhang, *Nucl. Phys.* **B 491** (1997) 3.

[32] G. Belanger, S. Kraml and A. Pukhov, *Phys. Rev.* **D 72** (2005) 015003.

[33] H.N. Brown *et al.* (Muon $g-2$ collaboration), *Phys. Rev. Lett.* **86** (2001) 2227.

[34] H. Baer, C. Balazs, J. Ferrandis and X. Tata, *Phys. Rev.* **D 64** (2001) 035004.

[35] T. Gherghetta, G. Giudice and J. Wells, *Nucl. Phys.* **B 559** (1999) 27; J. L. Feng, T. Moroi, L. Randall, M. Strassler and S. Su, *Phys. Rev. Lett.* **83** (1999) 1731; J. L. Feng and T. Moroi, *Phys. Rev.* **D 61** (2000) 095004; F. Paige and J. Wells, hep-ph/0001249; A. Datta and K. Huitu, *Phys. Rev.* **D 67** (2003) 115006; S. Asai, T. Moroi, K. Nishihara and T. T. Yanagida,

Phys. Lett. **B 653** (2007) 81; S. Asai, T. Moroi and T. T. Yanagida, *Phys. Lett.* **B 664** (2008) 185; H. Baer, J. K. Mizukoshi and X. Tata, *Phys. Lett.* **B 488** (2000) 367; A. J. Barr, C. Lester, M. Parker, B. Allanach and P. Richardson, *J. High Energy Phys.* **0303** (2003) 045.

[36] LEPSUSYWG, note LEPSUSYWG/02-04.1.

[37] S. P. Ahlen *et al.*, *Phys. Lett.* **B 195** (1987) 603; D. Caldwell *et al.*, *Phys. Rev. Lett.* **61** (1988) 510 and *Phys. Rev. Lett.* **65** (1990) 1305; D. Reusser *et al.*, *Phys. Lett.* **B 235** (1991) 143; T. Falk, K. Olive and M. Srednicki, *Phys. Lett.* **B 339** (1994) 248.

[38] H. Baer and M. Brhlik, *Phys. Rev.* **D 55** (1997) 3201.

[39] M. Misiak *et al.*, *Phys. Rev. Lett.* **98** (2007) 022002.

[40] E. Barberio *et al.* (Heavy Flavor Averaging Group), hep-ex/0603003.

[41] H. Baer, M. Brhlik, D. Castano and X. Tata, *Phys. Rev.* **D 58** (1998) 015007.

[42] E. Komatsu et al. Seven-Year Wilkinson Microwave Anisotropy Probe (WMAP) Observations: Cosmological Interpretation. Astrophys.J.Suppl., 192:18, 2011.

[43] T. Moroi and L. Randall, *Nucl. Phys.* **B 570** (2000) 455.

[44] L. F. Abbott and P. Sikivie, *Phys. Lett.* **B 120** (1983) 133; J. Preskill, M. Wise and F. Wilczek, *Phys. Lett.* **B 120** (1983) 127; M. Dine and W. Fischler, *Phys. Lett.* **B 120** (1983) 137; M. Turner, *Phys. Rev.* **D 33** (1986) 889.

[45] K. Rajagopal, M. Turner and F. Wilczek, *Nucl. Phys.* **B 358** (1991) 447; L. Covi, J. E. Kim and L. Roszkowski, *Phys. Rev. Lett.* **82** (1999) 4180; L. Covi, H. B. Kim, J. E. Kim and L. Roszkowski, *J. High Energy Phys.* **0105** (2001) 033; for recent reviews, see L. Covi and J. E. Kim, arXiv:0902.0769 and F. Steffen, *Eur. Phys. J.* **C 59** (2009) 557.

[46] H. Baer, A. Box and H. Summy, *J. High Energy Phys.* **0908** (2009) 080; H. Baer and A. Box, arXiv:0910.0333 (2009).

[47] Prospino, by W. Beenakker, R. Hopker and M. Spira, arXiv:hep-ph/9611232.

[48] H. Baer, C. H. Chen, F. Paige and X. Tata, *Phys. Rev.* **D 49** (1994) 3283.

[49] R. Kadala, J. K. Mizukoshi and X. Tata, *Eur. Phys. J.* **C 56** (2008) 511.

[50] H. Baer, H. Prosper and H. Summy, *Phys. Rev.* **D 77** (2008) 055017; H. Baer, A. Lessa and H. Summy, *Phys. Lett.* **B 674** (2009) 49; H. Baer, V. Barger, A. Lessa and X. Tata, *J. High Energy Phys.* **0909** (2009) 063.

[51] H. C. Cheng, B. Dobrescu and K. Matchev, *Nucl. Phys.* **B 543** (1999) 47.

[52] H. Baer, C. H. Chen, F. Paige and X. Tata, *Phys. Rev.* **D 52** (1995) 2746 and *Phys. Rev.* **D 53** (1996) 6241; H. Baer, A. Belyaev, T. Krupovnickas and X. Tata, *Phys. Rev.* **D 65** (2002) 075024.

[53] H. Baer and E. Berger, *Phys. Rev.* **D 34** (1986) 1361; H. Baer, X. Tata and J. Woodside, *Phys. Rev.* **D 41** (1990) 906; H. Baer, C. Kao and X. Tata, *Phys. Rev.* **D 48** (1993) 2978; H. Baer, C. H. Chen, C. Kao and X. Tata, *Phys. Rev.* **D 52** (1995) 1565; H. Baer, C. H. Chen, F. Paige and X. Tata, *Phys. Rev.* **D 54** (1996) 5866; H. Baer, C. H. Chen, M. Drees, F. Paige and X. Tata, *Phys. Rev.* **D 58** (1998) 075008; H. Baer, A. Mustafayev, S. Profumo and X. Tata, *Phys. Rev.* **D 75** (2007) 035004; H. Baer, S. Kraml, A. Lessa, S. Sekmen and H. Summy, *Phys. Lett.* **B 685** (2010) 72.

[54] T. Aaltonen *et al.* (CDF Collaboration), *Phys. Rev. Lett.* **102** (2009) 121801.

[55] V. M. Abazov *et al.* (D0 Collaboration), *Phys. Lett.* **B 660** (2008) 449.

[56] H. Baer and X. Tata, *Phys. Rev.* **D 47** (1993) 2739; H. Baer, C. Kao and X. Tata, *Phys. Rev.* **D 48** (1993) 5175; V. Barger, C. Kao and T. J. Li, *Phys. Lett.* **B 433** (1998) 328; H. Baer, M. Drees, F. Paige, P. Quintana and X. Tata, *Phys. Rev.* **D 61** (2000) 095007; V. Barger and C. Kao, *Phys. Rev.* **D 60** (1999) 115015; K. Matchev and D. Pierce, *Phys. Lett.* **B 467** (1999) 225; H. Baer, T. Krupovnickas and X. Tata, *J. High Energy Phys.* **0307** (2003) 020.

[57] T. Aaltonen *et al.* (CDF Collaboration), *Phys. Rev. Lett.* **101** (2008) 251801.

[58] V. M. Abazov *et al.* (D0 Collaboration), *Phys. Lett.* **B 680** (2009) 34.

[59] H. Baer, C. H. Chen, F. Paige and X. Tata, *Phys. Rev.* **D 49** (1994) 3283.

[60] T. Gherghetta, G. Giudice and J. Wells, *Nucl. Phys.* **B 559** (1999) 27.

[61] J. L. Feng, T. Moroi, L. Randall, M. Strassler and S. f. Su, Phys. Rev. Lett. **83** (1999) 1731 [arXiv:hep-ph/9904250]; J. L. Feng and T. Moroi, *Phys. Rev.* **D 61** (2000) 095004; A. Datta and K. Huitu, *Phys. Rev.* **D 67** (2003) 115006; S. Asai, T. Moroi, K. Nishihara and T. T. Yanagida, *Phys. Lett.* **B 653** (2007) 81; S. Asai, T. Moroi and T. T. Yanagida, *Phys. Lett.* **B 664** (2008) 185; H. Baer, J. K. Mizukoshi and X. Tata, *Phys. Lett.* **B 488** (2000) 367; A. J. Barr, C. Lester, M. Parker, B. Allanach and P. Richardson, *J. High Energy Phys.* **0303** (2003) 045.

[62] LEPSUSYWG, note LEPSUSYWG/02-04.1.

[63] H. Baer, J. Ellis, G. Gelmini, D. V. Nanopoulos and X. Tata, *Phys. Lett.* **B 161** (1985) 175; G. Gamberini, *Z. Phys.* **C30** (1986) 605; H. Baer, V. Barger, D. Karatas and X. Tata, *Phys. Rev.* **D 36** (1987) 96.

[64] H. Baer, R. Dermisek, S. Rajagopalan and H. Summy, JCAP**1007** (2010) 014.

[65] T. Moroi and L. Randall, *Nucl. Phys.* **B 570** (2000) 455; P. Grajek, G. Kane, D. Phalen, A. Pierce and S. Watson, *Phys. Rev.* **D 79** (2009) 043506; G. Kane, R. Lu and S. Watson, *Phys. Lett.* **B 681** (2009) 151; D. Feldman, G. Kane, R. Lu and B. Nelson, *Phys. Lett.* **B 687** (2010) 363.

[66] K. Kohri, M. Yamaguchi and J. Yokoyama, *Phys. Rev.* **D 72** (2005) 083510; T. Asaka, S. Nakamura and M. Yamaguchi, *Phys. Rev.* **D 74** (2006) 023520; M. Endo, F. Takahashi and T. T. Yanagida, *Phys. Rev.* **D 76** (2007) 083509.

[67] K.-Y. Choi, J. E. Kim, H. M. Lee and O. Seto, *Phys. Rev.* **D 77** (2008) 123501.

[68] V. S. Kaplunovsky and J. Louis, Phys. Lett. B **306**, 269 (1993) [arXiv:hep-th/9303040]. V. Kaplunovsky and J. Louis, *Nucl. Phys.* **B 422** (1994) 57 [arXiv:hep-th/9402005]. S. P. de Alwis, *Phys. Rev.* **D 77** (2008) 105020 [arXiv:0801.0578].

[69] H. Baer, B. Harris and M. H. Reno, *Phys. Rev.* **D 57** (1998) 5871.

[70] W. Beenakker, M. Klasen, M. Kramer, T. Plehn, M. Spira and P. M. Zerwas, Phys. Rev. Lett. **83** (1999) 3780 [Erratum-ibid. **100** (2008) 029901] [arXiv:hep-ph/9906298].

[71] Prospino, by W. Beenakker, R. Hopker and M. Spira, arXiv:hep-ph/9611232.

[72] G. Bozzi, B. Fuks and M. Klasen, *Phys. Lett.* **B 609** (2005) 339, *Phys. Rev.* **D 74** (2006) 015001, *Nucl. Phys.* **B 777** (2007) 157 and *Nucl. Phys.* **B 794** (2008) 46.

[73] H. Baer, A. Bartl, D. Karatas, W. Majerotto and X. Tata, *Int. J. Mod. Phys.* **A 4** (1989) 4111.

[74] G. Corcella *et al.* (Herwig collaboration), hep-ph/0210213.

[75] E. Richter-Was, arXiv:hep-ph/0207355.

[76] V. M. Abazov *et al.* (D0 Collaboration), *Phys. Rev. Lett.* **103** (2009) 141801.

[77] T. Aaltonen *et al.* (CDF Collaboration), *Phys. Rev.* **D 77** (2008) 112001.

[78] T. Aaltonen *et al.* (CDF Collaboration), *Phys. Rev. Lett.* **99** (2007) 052002.

[79] W. L. van Neerven, J. A. M. Vermaseren and K. Gaemers, W. L. van Neerven, J. A. M. Vermaseren and K. J. F. Gaemers, NIKHEF-H/82-20 (1982); J. Smith, W. L. van Neerven and J. A. M. Vermaseren, Phys. Rev. Lett. **50** (1983) 1738; V. Barger, A. D. Martin and R. J. N. Phillips, *Z. Phys.* **C21** (1983) 99

[80] C. G. Lester and D. J. Summers, *Phys. Lett.* **B 463** (1999) 99; A. Barr, C. Lester and P. Stephens, J. Phys. G **29**, 2343 (2003) [arXiv:hep-ph/0304226]; A. J. Barr and C. G. Lester, arXiv:1004.2732 [hep-ph].

[81] H. Baer, V. Barger, A. Lessa and X. Tata, *J. High Energy Phys.* **1006** (2010) 102.

[82] H. Baer and X. Tata. Weak scale supersymmetry: From superfields to scattering events. 2006.

[83] Howard Baer, Senarath de Alwis, Kevin Givens, Shibi Rajagopalan, and Heaya Summy. Gaugino Anomaly Mediated SUSY Breaking: phenomenology and prospects for the LHC. JHEP, 1005:069, 2010.

[84] Howard Baer, Radovan Dermisek, Shibi Rajagopalan, and Heaya Summy. Neutralino, axion and axino cold dark matter in minimal, hypercharged and gaugino AMSB. JCAP, 1007:014, 2010.

[85] Howard Baer and Andre Lessa. Some necessary conditions for allowing the PQ scale as high as M_{GUT} in SUSY models with an axino or neutralino LSP. JHEP, 1106:027, 2011.

[86] Vijay Balasubramanian and Per Berglund. Stringy corrections to Kahler potentials, SUSY breaking, and the cosmological constant problem. JHEP, 11:085, 2004.

[87] Vijay Balasubramanian, Per Berglund, Joseph P. Conlon, and Fernando Quevedo. Systematics of Moduli Stabilisation in Calabi-Yau Flux Compactifications. JHEP, 03:007, 2005.

[88] T. Banks, M. Dine, and M. Graesser. Supersymmetry, axions and cosmology. Phys.Rev., D68:075011, 2003.

[89] Tom Banks, David B. Kaplan, and Ann E. Nelson. Cosmological implications of dynamical supersymmetry breaking. Phys.Rev., D49:779–787, 1994.

[90] R. Barate et al. A Measurement of the inclusive $b \to s\gamma$ branching ratio. Phys.Lett., B429:169–187, 1998.

[91] Katrin Becker, Melanie Becker, Michael Haack, and Jan Louis. Supersymmetry breaking and alpha'-corrections to flux induced potentials. JHEP, 06:060, 2002.

[92] Marcus Berg, Michael Haack, and Boris Kors. String loop corrections to Kaehler potentials in orientifolds. JHEP, 11:030, 2005.

[93] Marcus Berg, Michael Haack, and Boris Kors. On volume stabilization by quantum corrections. Phys. Rev. Lett., 96:021601, 2006.

[94] Ralph Blumenhagen. Gauge Coupling Unification in F-Theory Grand Unified Theories. Phys. Rev. Lett., 102:071601, 2009.

[95] A. Brignole, Luis E. Ibanez, and C. Munoz. Soft supersymmetry-breaking terms from supergravity and superstring models. 1997.

[96] Leonardo Brizi, Marta Gomez-Reino, and Claudio A. Scrucca. Globally and locally supersymmetric effective theories for light fields. Nucl.Phys., B820:193–212, 2009.

[97] H.N. Brown et al. Improved measurement of the positive muon anomalous magnetic moment. Phys.Rev., D62:091101, 2000.

[98] R. Brustein and S. P. de Alwis. Moduli potentials in string compactifications with fluxes: Mapping the discretuum. Phys. Rev., D69:126006, 2004.

[99] C. P. Burgess, Anshuman Maharana, and F. Quevedo. Uber-naturalness: unexpectedly light scalars from supersymmetric extra dimensions. JHEP, 05:010, 2011.

[100] Michele Cicoli, Anshuman Maharana, F. Quevedo, and C.P. Burgess. De Sitter String Vacua from Dilaton-dependent Non-perturbative Effects. 2012.

[101] Joseph P. Conlon, Anshuman Maharana, and Fernando Quevedo. Towards Realistic String Vacua. JHEP, 05:109, 2009.

[102] Laura Covi et al. de Sitter vacua in no-scale supergravities and Calabi-Yau string models. JHEP, 06:057, 2008.

[103] Mirjam Cvetic, James Halverson, and Paul Langacker. Singlet Extensions of the MSSM in the Quiver Landscape. JHEP, 1009:076, 2010.

[104] S. P. de Alwis. Effective potentials for light moduli. Phys. Lett., B626:223–229, 2005.

[105] S.P. de Alwis. Constraints on LVS Compactifications of IIB String Theory. 2012.

[106] B. de Carlos, J.A. Casas, F. Quevedo, and E. Roulet. Model independent properties and cosmological implications of the dilaton and moduli sectors of 4-d strings. Phys.Lett., B318:447–456, 1993.

[107] Ulrich Ellwanger, Cyril Hugonie, and Ana M. Teixeira. The Next-to-Minimal Supersymmetric Standard Model. Phys.Rept., 496:1–77, 2010.

[108] Diego Gallego. On the Effective Description of Large Volume Compactifications. JHEP, 1106:087, 2011.

[109] Diego Gallego and Marco Serone. An Effective Description of the Landscape - I. JHEP, 01:056, 2009.

[110] Diego Gallego and Marco Serone. An Effective Description of the Landscape - II. JHEP, 0906:057, 2009.

[111] Marta Gomez-Reino and Claudio A. Scrucca. Locally stable non-supersymmetric Minkowski vacua in supergravity. JHEP, 0605:015, 2006.

[112] Mariana Grana, Thomas W. Grimm, Hans Jockers, and Jan Louis. Soft Supersymmetry Breaking in Calabi-Yau Orientifolds with D-branes and Fluxes. Nucl. Phys., B690:21–61, 2004.

[113] James Gray, Yang-Hui He, Anton Ilderton, and Andre Lukas. STRINGVACUA: A Mathematica Package for Studying Vacuum Configurations in String Phenomenology. Comput. Phys. Commun., 180:107–119, 2009.

[114] Vadim S. Kaplunovsky and Jan Louis. Model independent analysis of soft terms in effective supergravity and in string theory. Phys. Lett., B306:269–275, 1993.

[115] Jihn E. Kim and Gianpaolo Carosi. Axions and the Strong CP Problem. Rev.Mod.Phys., 82:557–602, 2010.

[116] Boris Kors and Pran Nath. A Supersymmetric Stueckelberg U(1) extension of the MSSM. JHEP, 0412:005, 2004.

[117] Markus A. Luty. 2004 TASI lectures on supersymmetry breaking. pages 495–582, 2005.

[118] Frank E. Paige, Serban D. Protopopescu, Howard Baer, and Xerxes Tata. ISAJET 7.69: A Monte Carlo event generator for pp, anti-p p, and e+e- reactions. 2003.

[119] Markus Rummel and Alexander Westphal. A sufficient condition for de Sitter vacua in type IIB string theory. 2011.

[120] Gero von Gersdorff and Arthur Hebecker. Kaehler corrections for the volume modulus of flux compactifications. Phys. Lett., B624:270–274, 2005.

[121] J. Wess and J. Bagger. Supersymmetry and Supergravity. Princeton University Press, 2nd edition, 1992.

[122] Alexander Westphal. de Sitter String Vacua from Kahler Uplifting. JHEP, 03:102, 2007.